Probing interactions of the BRCT protein family with damaged chromatin

by

Ayodeji N Kulepa

A thesis submitted in partial fulfillment of the requirements for the degree of

Master of Science

Department of Biochemistry
University of Alberta

ABSTRACT

The DNA damage response (DDR) is critical for maintaining genomic integrity and prevention of genotoxic consequences leading to carcinogenesis. The DDR signaling cascade results either in the activation of the repair pathway, or initiation of apoptosis if the repair is not possible. Many hereditary and sporadic forms of human cancers have been linked to mutations in key DDR genes such as tumor protein p53, Ataxia telangiectasia-mutated kinase (ATM) and Breast cancer1 (BRCA1). In the early stages of DDR, the histone variant H2AX is phosphorylated at serine 139 to form γH2AX. This modification leads to the recruitment of Mediator of DNA damage checkpoint protein 1 (MDC1) which specifically interacts with the pSxxY-COOH motif of γH2AX through its BRCT domain. The structural dynamics underlying the interaction of MDC1 with the chromatin remains to be deciphered. We have recombinantly expressed and purified histone octamers with H2AX and aimed to phosphorylate the C-terminal tail. This will help provide insights into the MDC1-nucleosome interaction.

Another BRCT domain protein, BRCA1 is a widely known tumor suppressor protein involved in the homologous recombination (HR) pathway for repair of DNA double-strand breaks (DSB). Mutations in the phosphopeptide binding domain of BRCA1 are associated with increased breast cancer risks and lead to defects in the DDR, sensitizing cells to radiation and many DNA-targeting cancer therapies. The finding that BRCA1 mutations impact HR and sensitize cells to the single strand

break repair enzyme poly (ADP) ribose polymerase (PARP) has led to promising approaches to develop BRCA1 BRCT inhibitor for combinatorial therapy with PARP inhibitors. This approach can be used to target cancerous cells with the wild-type BRCA1 and prevent HR repair of DNA lesions from radio and chemotherapy treatments. Our collaborators recently developed a potential BRCA1 BRCT inhibitor that might lead to new avenues for anticancer therapy development. The inhibitor is a peptide which binds specifically to the BRCA1 BRCT domain on the same surface as the phosphorylated peptides. We tested the ability of this inhibitor to block binding of BRCA1 BRCT to a model binding peptide containing the pSer-x-x-Phe motif. Specificity is also tested by the ability of this inhibitor to block interactions between a related BRCT protein MDC1 and its peptide target pSer-x-x-Tyr-COO-. We performed *in vivo* experiments to determine the permeability of this inhibitor in U2OS cells. The ability of the inhibitor to disrupt BRCA1 interaction with the protein Abraxas was visualized. The peptide was expressed in U2OS cells, and its kinetics visualized by Fluorescence recovery after photobleaching (FRAP). Overall, we prove the specificity of our inhibitor to BRCA1 BRCT and confirm its permeability in U2OS cells.

ACKNOWLEDGMENTS

First, I would like to thank my supervisor Dr. Mark Glover for the tremendous guidance, and mentorship over the past three years. Dr. Michael Hendzel for his co-supervision over the past year, the unwavering support and encouragement. I really appreciate the opportunity and will be forever thankful for the countless ways you have helped develop me as a scientist.

I am grateful to members of the Glover lab for creating a wonderful working environment. Special thank you to Dr. Rashmi Panigrahi for being an incredible mentor the whole course of my graduate program. Rashmi's enthusiasm for science really encouraged and challenged me to become a better scientist. Dr. Ross Edwards for his advice and insightful scientific contributions as well as ensuring all the machines in the lab run smoothly. Dr. Jun Lu for his scientific advice in lab meetings and sharing expertise. I would also like to thank the wonderful graduate students: Jin Kim, Rabih Abou Farraj, Cameron Murray and Mazzen Black. I would like to extend thanks to all the graduate students in the department who have provided support and friendship over the years. Also, thank you to the undergraduate students in the lab who I have been able to work closely with and share my knowledge.

I also want to thank past and present members of the Hendzel lab especially for their support. Special thank you to Kristal Missiaen for tissue culture training and Dr. Ajit Sharma for immunofluorescence training and guidance. Thank you to Dr. Hilmar Strickfaden for all his help with microscopy and insightful scientific advice. Dr. Zhigang Jin, Stanley Poon and Dan for creating a great lab environment. I would like to thank Natneal Abate for all his support and friendship over the past year.

Thank you to my committee members Dr. Michael Hendzel and Dr Michael Schultz. I genuinely appreciate your input and guidance for the progression of my project. Throughout the program, your comments recommendations were extremely helpful and encouraging. I would also like to thank Dr. Michael Weinfeld for participating as an external examiner. I want to say thank you to Dean Schieve for all the technical help over the years and Lisa Dublin for all the administrative support.

Finally, I would like to thank my family and friends for their support over the years. My parents for their amazing assistance and encouragement from the first day I came to Canada. I truly appreciate the opportunity they have granted me. Special thanks to all my friends who have been my support system and my family away from home.

TABLE OF CONTENTS

LIST OF FIGURES

LIST OF ABBREVIATIONS

ATM	ataxia telangiectasia-mutated kinase
ATR	ATM and Rad3 related
BACH1	BRCA1 associated C-terminal helicase
BARD1	BRCA1-associated RING domain protein 1
BRCA1	Breast cancer type 1 susceptibility protein
BRCT	BRCA1 C-terminal
CK2	casein kinase II
CPP	cell penetrable peptide
DAPI	6-diamidino-2-phenylindole
DDR	DNA damage response
DOX	doxycycline
DSBs	double strand breaks
EGFP	enhanced green fluorescent protein
FRAP	fluorescence recovery after photobleaching
GST	glutathione S-transferases

IR	ionizing radiation
LacI	lac repressor
LacO	lac operator
MDC1	mediator of DNA damage checkpoint protein 1
NCP	nucleosome core particle
PARP	Poly (ADP) ribose polymerase
PPI	protein-protein interaction
ROS	reactive oxygen species
SDS-PAGE	sodium dodecyl sulfate polyacrylamide gel electrophoresis
SEC	size exclusion chromatography
SSBs	single strand breaks
TCEP	Tris (2-carboxyethyl) phosphine

CHAPTER 1: Introduction

1.1 DNA damage, response, and repair.

1.11 DNA damage

DNA is a robust molecule and chemical alteration of the structure can be detrimental to its integrity. DNA damage occurs due to various exogenous sources as well as endogenous cellular processes. Endogenous sources such as hydrolytic reactions and reactive oxygen species (ROS) from oxidative respiration generate thousands of lesions per cell every day (Jackson & Bartek, 2009). Hydrolysis of DNA occurs in various forms due to the instability of the DNA glycosyl bonds. DNA mismatches occasionally occur during replication because of nucleotide misincorporation during synthesis (Jackson & Bartek, 2009; Valko et al., 2006). Depurination results from the cleaving of the β-N-glycosyl bond and the introduction of Apurinic sites (AP) in the DNA (Lindahl & Andersson, 1972). Another form of hydrolysis is deamination of cytosine which results in a base transition to uracil in DNA (Lindahl & Nyberg, 1974). Oxidation by ROS typically results in the adducts that impair base pairing, block DNA replication and transcription or lead to single-stand breaks (SSBs). The most studied mutagenic base lesion from oxidation is the formation of 8-oxoguanine (8-oxoG) from guanine. 8-oxoG preferentially base-pairs with adenine instead of cytosine and results in mutations after replication (Kasai & Nishimura, 1984; Shibutani et al., 1991). DNA base alkylation also results in cytotoxic lesions that pose a major threat to the cell. S-adenosylmethionine (SAM) is a methyl donor compound involved in the methylation of purine residues that form 7-methylguanine and 3-methyladenine

lesions. SAM is present in the nucleus and readily acts as a co-factor for enzymatic DNA methylation (Barrows & Magee, 1982; Rydberg & Lindahl, 1982). The 3-methyladenine is a DNA lesion that blocks replication while the 7-methylguanine has no major effect on the coding specificity of the base (Lindahl, 1993).

Exogenous sources of DNA damage arise from physical and chemical agents that induce lesions. X-rays, ultraviolet light (UV) from the sun, ionizing radiation (IR) from decay of radioactive compounds such as uranium, threaten the genome stability. IR generates SSBs and double stand breaks (DSBs) which is the most toxic type of damage (Ward, 1988). DNA damaging chemicals are produced from tobacco products, which by metabolic activation lead to DNA adducts. Other chemicals are found in food contaminants or by-products from warfare and industrial processes (Wogan et al., 2004).

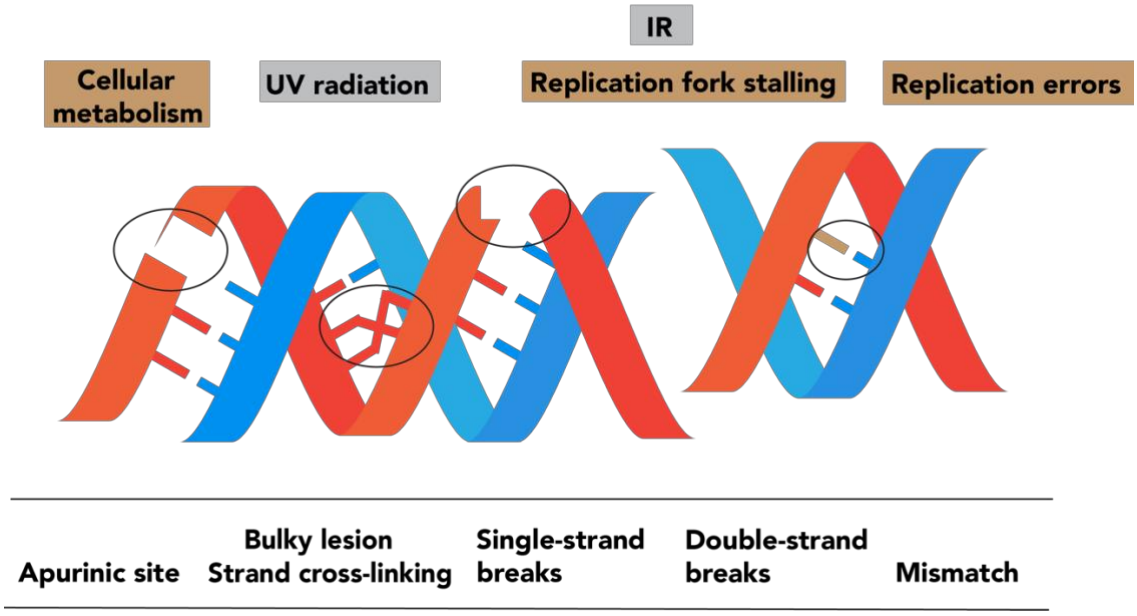

Figure 1.1 Different types of DNA damage. Major types of DNA lesions experienced by genomic DNA and their sources. Endogenous sources colour coded in brown and exogenous sources in grey. Types of lesions indicated below represented by the DNA schematic.

1.12 DNA damage response and repair

In response to DNA damage, cells have evolved a complex DNA damage response (DDR) machinery that detects the lesions, signals their presence, and activates cell cycle checkpoints. This halts cell cycle progression to enable repair of the damage, mediates the activation of transcriptional factors and in some cases induces apoptosis. The cell cycle checkpoints pause the cells at G1/S, G2/M transitions or at intra-S phase. Although the checkpoints are different, the proteins involved in the DNA lesion signalling and cycle arrest are similar (Carusillo & Mussolino, 2020; Houtgraaf et al., 2006; Zhou & Elledge, 2000). Normal cell cycle progression is mostly controlled by one family of proteins, the cyclin dependent kinases (CDKs). CDK1 and CDK2 control the G2-M transition while CDK2 and CDK4 regulate the G1-S transition (Ding et al., 2020). During DNA damage, the PI3K kinases and checkpoint kinase 2 (CHK2) are activated to trigger transcriptional activity of the tumor suppressor protein p53. It is the central mediator of DNA damage checkpoint which is phosphorylated on serine-15 by ataxia-telangiectasia mutated (ATM) or serine-20 by CHK2 to promote its DNA binding activity (Ou & Schumacher, 2018). Transcriptional activity of p53 drives the expression of the cyclin-dependent kinase inhibitor p21 which leads to G1 arrest. If the damage occurs in the G2 phase, p21 blocks retinoblastoma (Rb) phosphorylation and sequesters CDK1 in the nucleus (Carusillo & Mussolino, 2020; Ding et al., 2020). This prevents the transition to the M-phase and provides adequate time for

DNA lesion repair. DNA damage in the S-phase typically results in the slowing down of the replication to repair the lesion.

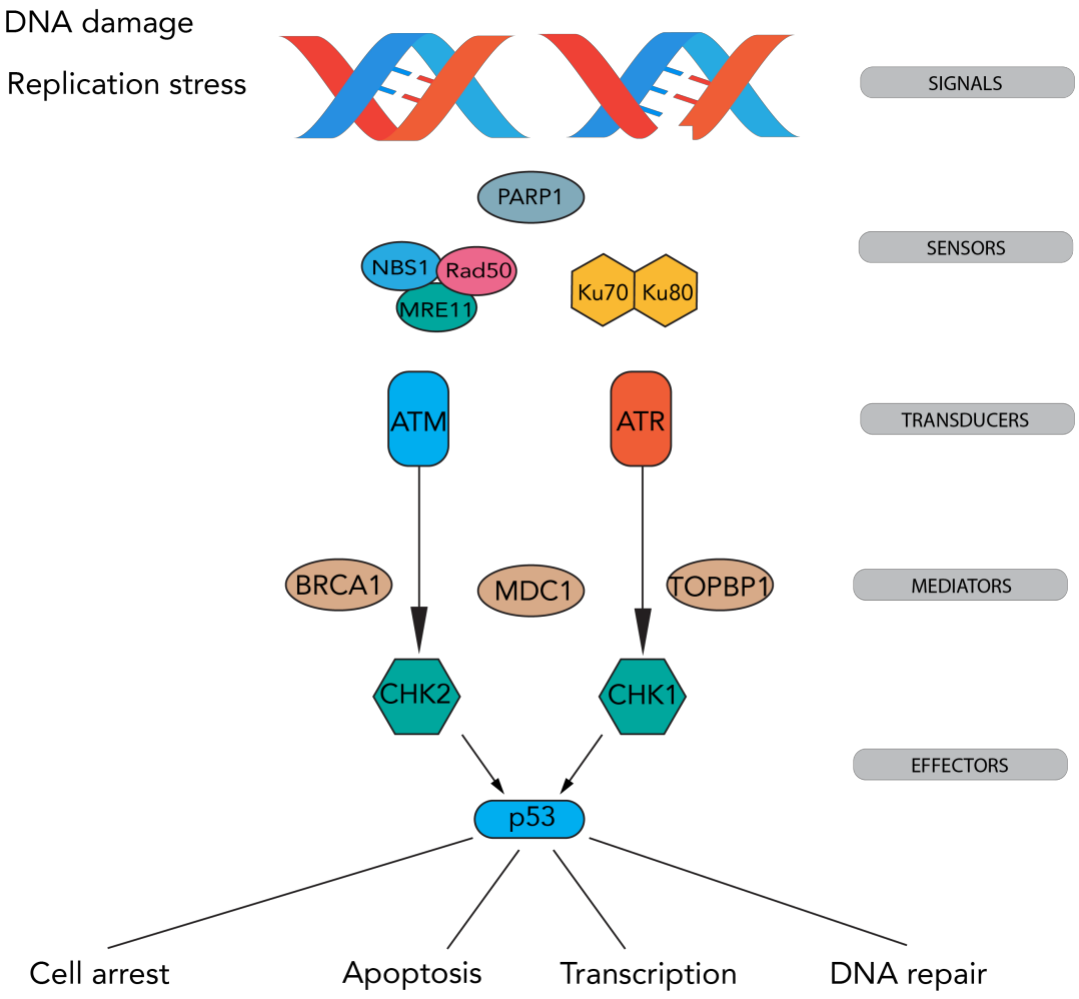

Figure 1.2 DNA damage response. Schematic representation of the general DNA damage response signal-transduction pathway. Arrows denote activation. Classification of proteins in their respective function to signal transduction. Adapted from (Zhou & Elledge 2000)

There are two major pathways for activation of the cell cycle checkpoints, ATM-Chk2 and ATR-Chk1 as shown in figure 1.2. The early response to a DSB is mainly mediated by the ATM-Chk2 checkpoint signaling. In this pathway, the damage is sensed by the Meiotic recombination 11 homolog 1(MRE11)-RAD50-Nijmegen breakage syndrome protein 1 (NBS1) complex (MRN) which localizes to the DSB site. The Nbs1 protein in the complex recruits ATM to the damage site and activates ATM kinase to phosphorylate Chk2 at threonine 68. This mediates its further autophosphorylation and activation of p53 to mediate cell cycle arrest. ATM can also directly phosphorylate p53 to trigger downstream checkpoint activation. Chk2 also phosphorylates Cdc25A which leads to the nuclear localization of CDK2 to trigger G1 arrest (Carusillo & Mussolino, 2020; Houtgraaf et al., 2006; Zhou & Elledge, 2000).

The ATM and Rad3 related (ATR) – Checkpoint 1 (Chk1) activation is dependent on DNA resection. Recruitment of ATR is mediated by ATR interacting protein (ATRIP) binding to the replication protein A (RPA) in the topoisomerase binding protein 1(TOPB1) scaffold. Single-strand DNA overhangs after resection are bound and protected by RPA. ATR mediates the phosphorylation of Chk1 at serine 317 and serine 345. Autophosphorylation of Chk1 at serine 296 causes its release from chromatin to promote checkpoint signaling (Bartek & Lukas, 2007; Houtgraaf et al., 2006). There is a requirement for various distinct lesion-specific repair mechanisms due to the variety of DNA alterations mentioned above. A brief

explanation of the process for some of the repair mechanisms known today is shown in figure 1.3.

Nucleotide Excision Repair (NER)

NER recognizes bulky helix distorting DNA base lesions that result from UV irradiation or chemical agents. This repair mechanism can be divided into two pathways that differ by the lesion recognition process (Scharer, 2013). Global genome NER recognizes bulky DNA lesions by the Xeroderma Pigmentosum group C protein. The transcription coupled NER specifically targets lesions that block transcription and is recognized due to RNA polymerase II stalling. Once the lesion is recognized, the DNA is unwound, and 20-30 base pairs are excised by endonucleases on either side to the damage to produce a single-stranded DNA (ssDNA) (Spivak, 2015). DNA polymerases then fill the gap using the other strand as a template and the DNA ligase seals off the ends.

Base Excision Repair (BER) / Single strand break repair (SSBR)

DNA hydrolysis and endogenous cellular processes can lead to base modification and single strand breaks. The lesions are recognized by DNA glycosylases which mediate the base removal by cleavage of the N-glycosylic bond. The AP site is recognized and bound by the Poly (ADP-ribose) polymerase (PARP 1 and or PARP 2). The PARP complex recruits the human AP-endonuclease 1 (APE1) for nucleotide excision. DNA polymerase and ligase insert the missing nucleotide(s)

and seal the gap respectively (Freudenthal, 2017; Krokan & Bjoras, 2013). SSBs are detected by PARP-1 which recruits the APE2 endonuclease to the damage site. In this mechanism, a more extended single-stranded portion is cleaved by APE2 before the recruitment of DNA polymerases and ligases to seal the gap with free nucleotides (Eustermann et al., 2015; Hossain et al., 2018).

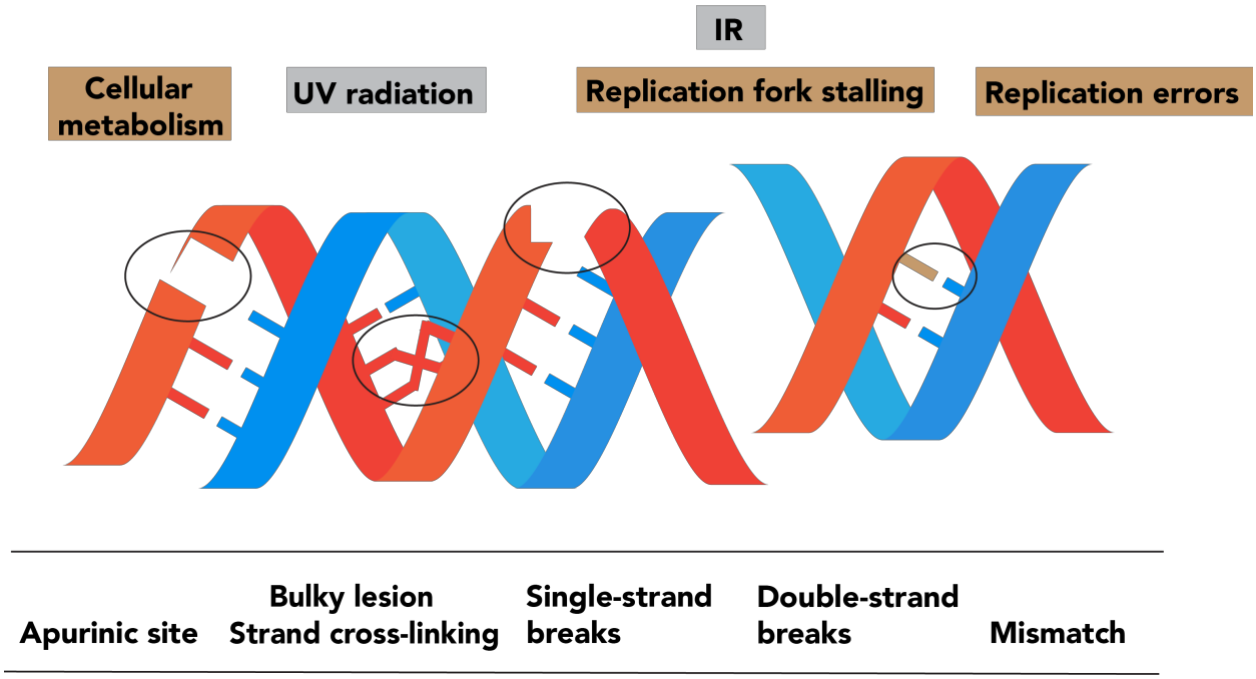

Figure 1.3 DNA damage repair mechanisms. Schematic of DNA repair pathway engaged for resolution of the DNA lesion. Table indicates type of lesion depicted in the figure above and the repair pathway activated by the lesions. Adapted from (Carusillo & Mussolino 2020)

Mismatch repair (MMR)

DNA mismatches typically occur during replication or other cellular processes. Single base pair mismatches and small/large insertion or deletions are recognized by the MutS homolog (MSH) heterodimer complexes. The mismatch recognition causes conformational changes in the complex to mediate recruitment of an exonuclease for a single-strand incision. The gap is then filled with missing nucleotides by the DNA polymerase delta and DNA ligase I to complete the repair (Erie & Weninger, 2014; Li et al., 2016).

Double-strand break repair (DSBR)

When a DSB occurs, there are two major mechanisms for repair used by the cell depending on the cell cycle phase. Non-homologous end-joining (NHEJ) which can operate in any phase of the cell cycle is the error prone repair pathway (Lieber, 2008). The DSBs are recognized by the Ku protein dimer that binds the DNA break ends and promotes the recruitment of the protein kinase DNA-PKcs. This leads to the recruitment of proteins like the X-Ray repair cross-complementing protein 4 (XRCC4), XRCC-4like factor (XLF) and the DNA ligase IV to seal the break ends (Ahnesorg et al., 2006; Chang et al., 2017). The second DSB repair mechanism is the homologous recombination (HR) pathway which is restricted to the S/G2 phase of cell cycle. This is due to the requirement of a sister chromatid as a template, which enables an error free method of repair (San Filippo et al., 2008). The DSB is sensed by the MRN complex that localizes to both ends of the break, mediates DNA

end resection and the generation of ssDNA that invades the sister chromatid template. Eventually, repair is mediated by polymerases, nucleases, helicases, and DNA ligation (Jasin & Rothstein, 2013; Myler et al., 2017).

There are two alternative DSBR pathways, Microhomology-mediated end-joining (MMEJ) and single-strand annealing (SSA) which are shared with HR but error prone. They both involve the loss of nucleotides and require different lengths of homologous sequences on the same chromosome (Carusillo & Mussolino, 2020). MMEJ requires short homology stretches less than 20 nucleotides exposure after DNA end resection followed by alignment of the complementary strands. The SSA requires longer homology stretches of greater than 25 nucleotides which is protected by RPA, then base pairing of homologous sequences is mediated by RAD52. The activity of endonucleases, DNA polymerases and DNA ligases complete the repair (Ceccaldi et al., 2016).

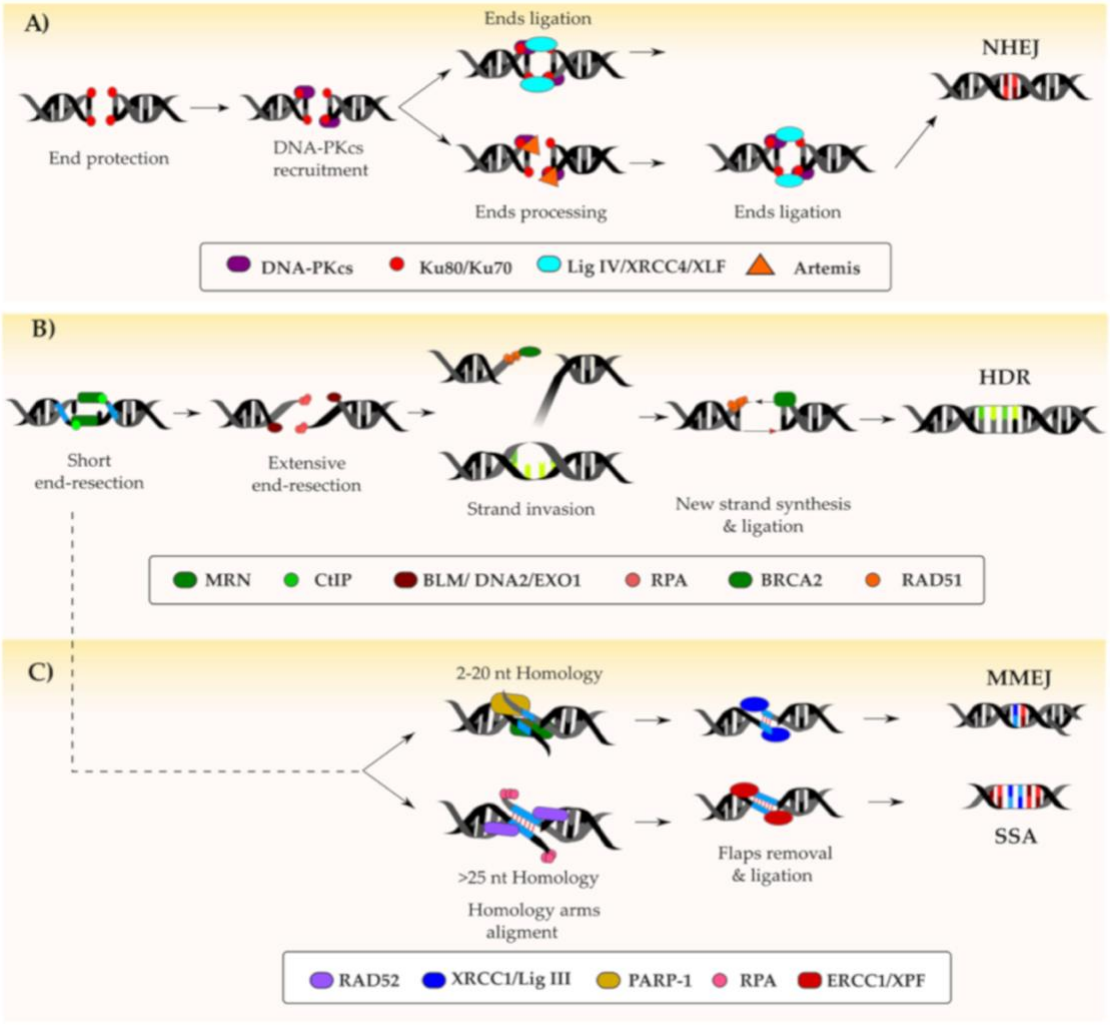

Figure 1.4 Overview of double strand break repair pathways. Reprinted with permission from "DNA Damage: From Threat to Treatment" by Carusillo, A. & Mussolino, C., 2020 *Cells* 9, 1665 (A)Non-homologous end-joining (NHEJ) pathway of repair which involves damaged ends protection by the Ku80/Ku70 dimer that mediate recruitment of DNA-PKcs. Next, the recruitment of Lig IV/XRCC4/XLF complex or Artemis for ligation of DNA ends and repair. (B)Homology-directed repair (HDR) with DNA end resection followed by strand invasion and new strand synthesis before ligation. (C) Microhomology-mediated end joining (MMEJ) and single strand annealing (SSA) post short end resection in HDR.

1.2 Genome organization: DNA to chromosome

The human genome over two metres long with three billion base pairs is precisely packed into the ~ 10 μm nucleus of a cell (Kinner et al., 2008). Such compaction is achieved by the assembly of a DNA-protein complex called chromatin which also maintains coordinated accessibility for cellular processes that require DNA unwinding. Genomic DNA exists as a nucleotide-protein complex which is folded into layers that form higher order structures. The nucleosome is the basic subunit of the chromatin and is composed of four core histone proteins H2A, H2B, H3, H4, linker histone (H1 or H5) and the genomic DNA. Two copies of each core histone assemble to form an octamer onto which 147 bp segment of DNA is wrapped in a left-handed superhelix ~1.7 times around the octameric core to form a nucleosome core particle (Luger, 1997). The nucleosome core associates with the linker histone to bind ~165 bp of DNA and together are called the chromatosome. A complete nucleosome consists of the chromatosome and the linker DNA which connects adjacent nucleosomes for compaction.

Core Histones

Histones are small 11-15 kDa proteins which share a similar structural motif. The highly conserved histone-fold motif is comprised of three α-helices connected by two loops usually denoted by α1-L1- α2-L2- α3 shown in figure 1.5. The C-terminal portions of the α2 and α3 helices mediate the histone dimerization pairing

of H2A-H2B and H3-H4. Highlighted in figure 1.5, the octameric core is assembled from two H3-H4 and two H2A-H2B heterodimers by a four-helix bundle structural motif. H3-H4 dimer forms a tetramer by an H3:H3 interface formed by the $\alpha 2$ and $\alpha 3$ helices. The $(H3\text{-}H4)_2$ tetramer associates with the H2A-H2B dimer by the H4 and H2B helix-bundle interface. Apart from the histone fold region, histones have N- and C-terminal extensions that contribute to the structure, DNA binding and stabilization. The H3 αN helix extension interacts with the H4 histone fold and is responsible for binding ~13bp of the nucleosomal DNA at the entry-exit site. The H2B αC helix packs against the H2A-H2B fold helices and extends from the nucleosome to the DNA edge opposite the dyad. The octamer core of histones carries a strong positive charge and is formed in high salt solutions or when bound by DNA (Arents et al., 1991; Arents & Moudrianakis, 1995, 1995; Luger, 1997) .

The histone octamer associates with DNA at three distinct binding sites composed of structural elements from each dimer. The H2A-H2B heterodimers interact with the DNA in two different parallel planes perpendicular to the DNA axis while the H3-H4 tetramer forms a diagonal tilt connecting the two planes. The histone core accounts for binding ~121 bp of the DNA with contacts at projected arginine side chains, lysine chains as well as the main chain amide nitrogen. Highly conserved arginine residues project into the minor groove of the DNA to help position, facilitate orientation and bending of the superhelix. One of the tightest binding DNA sequences to the histone octamer is known as the Widom 601 (W601) sequence. This was determined from in vitro experiments by isolation of random

synthetic DNA sequences with high affinity for the histone octamer. This is due to the abundant TA base steps in W601 which favours interaction with the octamer where the minor groove faces the histones (Cutter & Hayes, 2015a; Lowary & Widom, 1998; Richmond & Davey, 2003).

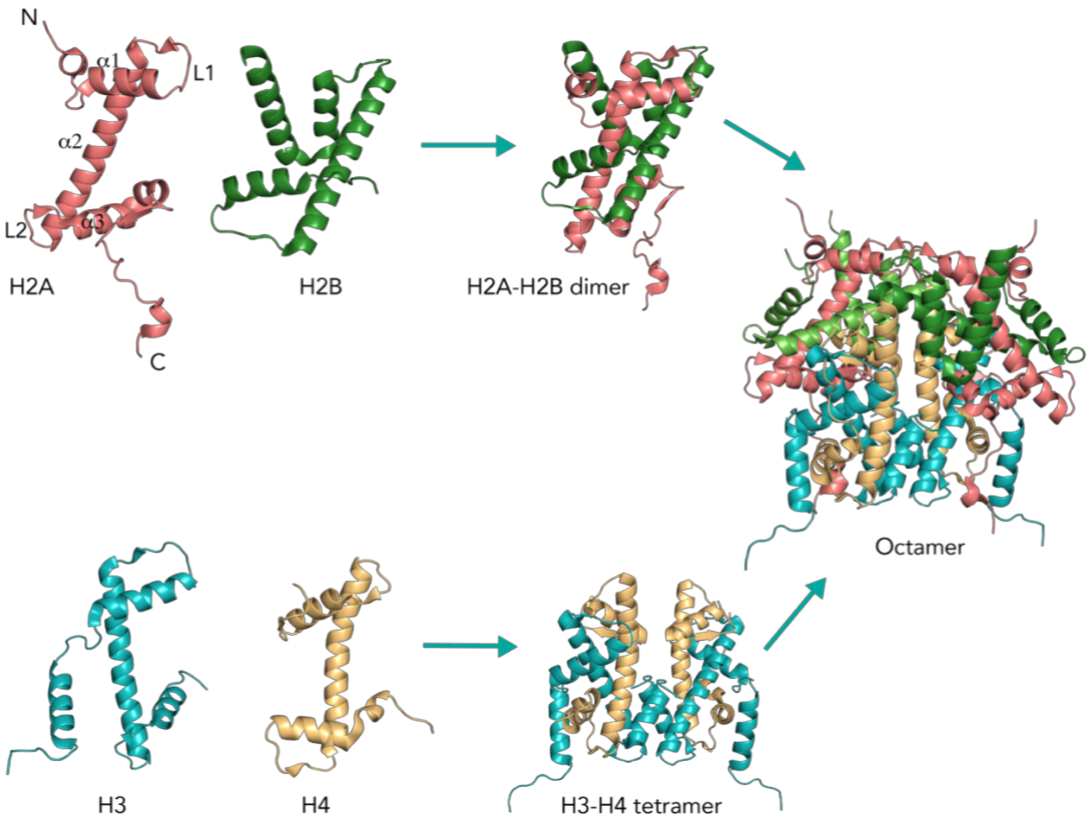

Figure 1.5 Organization of Octamer. Schematic of the histone subunits for octamer formation. Canonical histone fold motif α1-L1- α2-L2- α3 shown in H2A. H2A-H2B dimer and H3-H4 tetramer assemble to form octamer. H2A-H2B dimer and H3-H4 tetramer stable hetero-complex.

The core and linker histones exist as variants with similar structure for incorporation into the nucleosome but non-identical protein sequences. This provides diversification of the nucleosome structure and function while some variants with post-translational modifications impact chromatin environment. The H3 histone variants H3.3 and Centromere protein A (CENPA) are important in maintenance of genome integrity and cell fate transitions (Ferrand et al., 2020). The H2A.X and H1 family of histones are heavily involved in DNA damage response which has been described in section 1.3.

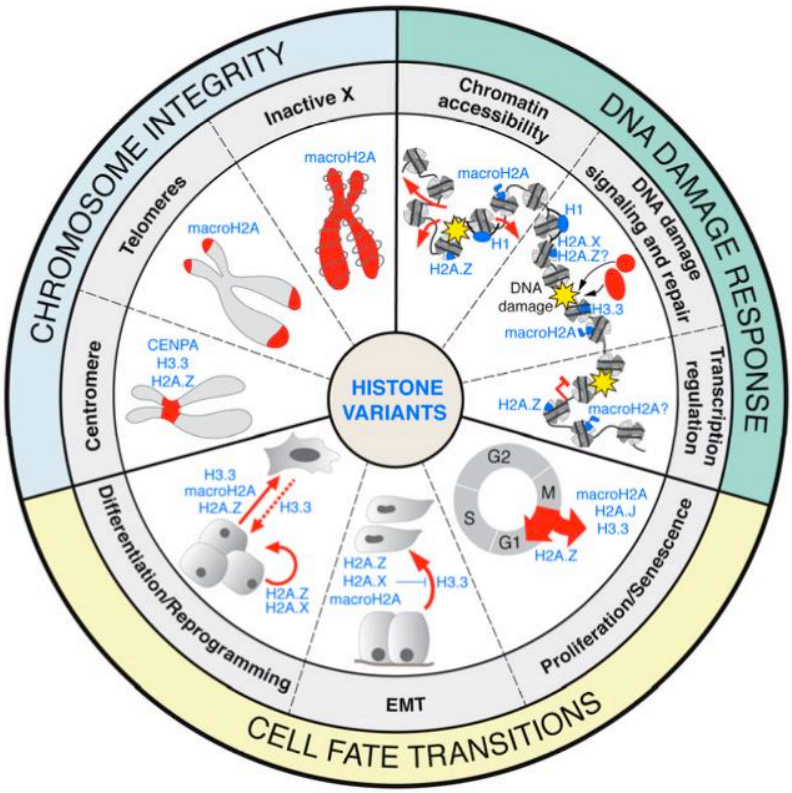

Figure 1.6 Overview of histone variants contribution to genome maintenance. Reprinted with permission from "Histone Variants: Guardians of Genome Integrity" by Ferrand et al., 2020 *Cells*, 9(11), 2424. The roles are divided into DNA damage response, cell fate transitions and chromosome integrity. Key features highlighted in red.

1.3 DNA Double strand break repair signaling

1.31 Histone variant H2AX

The variant H2AX constitutes 2-25% of the mammalian histone H2A varying by organism and cell type. It differs from the other H2A variants by the presence of a unique C-terminal tail which is evolutionarily conserved (Bonner et al., 2008). In humans, the last four residues have an S-Q-E-Y motif. The N- and C-terminal tails of H2AX are sites for post-translational modifications of the H2AX histone such as acetylation, biotinylation, phosphorylation and ubiquitination. H2AX is constitutively phosphorylated at Tyrosine 142 (Y142) under normal growth conditions in cells (Xiao et al., 2009). This phosphorylation is mediated by a tyrosine kinase, Williams-Beuren syndrome transcription factor (WSTF) which is a component of the WICH chromatin remodelling complex (Jones et al., 2000; Xiao et al., 2009). Upon DSB, phosphorylation of H2AX occurs at the serine 139 located in the C-terminus. This phosphorylated H2AX is called the γH2AX and marks the initiation of DSB signaling.

1.32 Formation of Ionizing radiation induced foci

Upon DSB, γH2AX formation is mediated mainly by the ATM kinase. This signaling is very specific to DSB as damaging agents that cause other forms of DNA lesions do not result in γH2AX formation (Georgoulis et al., 2017). ATM kinase recruitment to the damage site is mediated by the MRN complex. The γH2AX

extends rapidly on both sides of the damage along the chromatin acting as a beacon signal for DSB. High levels of γH2AX which persist for several hours, were found to be dependent on the basal phosphorylation of Y142 at the c-terminal of H2AX (Singh et al., 2012; Xiao et al., 2009) . The intermediate di-phosphorylated H2AX (pSer 139, pTyr 142) is specifically recognized by microcephalin 1 (MCPH1) (Singh et al., 2012). It is a protein referred to as the "guardian of the genome" due to its functions in early DDR and tumor suppression (Chaplet et al., 2006). MCPH1 or BRIT 1 has one N-terminal BRCT domain, a condensin II binding motif and two c-terminal BRCT domains. It specifically binds to di-phosphorylated H2AX or γH2AX by the c-terminal BRCTs. However, the EYA2 and EYA 3 phosphatases are responsible for the de-phosphorylation of Y142 following DSB leading to increased levels of the γH2AX. It has been shown that inhibition of the EYA phosphatases could direct DNA damaged cells to the apoptotic pathway. The inhibition leads to increased levels of di-phosphorylated H2AX which mediate activation of cell-stress and pro-apoptotic factors (Cook et al., 2009).

After the γH2AX formation and Y142 dephosphorylation, mediator of DNA damage checkpoint 1 (MDC1) binds in proximity to the damage site. Activated ATM kinase, phosphoserine-1981 (pATM) binds specifically to the FHA domain of MDC1, which mediates its further recruitment to the DSB site. In the absence of MDC1, the further recruitment of pATM to the damage site was impaired (Lou et al., 2006, p. 1; So et al., 2009). This constitutes a feedback loop, as more H2AX histones are phosphorylated and MDC1 is further recruited to amplify the signal.

The threonine phosphorylation in the TQXF repeats of MDC1 by ATM mediates the recruitment of an E3 ubiquitin ligase RNF8. This protein is made up of an N-terminal FHA domain for interaction with the phosphorylated threonine and a C-terminal Really Interesting New Gene (RING) finger domain (Kolas et al., 2007; Mailand et al., 2007, p. 8). RNF8, together with the E2 ubiquitin activating enzyme UBC13 promote the lysine 63 (K63) linked ubiquitination of histone H1 at DSBs. This leads to the recruitment of another E3 ubiquitin ligase RNF 168 which ubiquitinates the H2A/H2AX on lysine 13 (K13) or lysine 15 (K15) with the help of the E2 enzyme UbcH5c (Thorslund et al., 2015). RNF168 specifically binds to the K63 ubiquitinated H1 by its N-terminal ubiquitin-binding domain to mediate the ubiquitination at K13-15 (Horn et al., 2019; Thorslund et al., 2015).

Ubiquitination in proximity to the DNA damage is crucial for the recruitment of the DDR factors such as BRCA1 and the p53 binding protein (53BP1). BRCA1 interaction with the RAP80 protein is required for its localization at DSBs. The ubiquitin binding protein RAP80 interacts specifically with the K63- linked polyubiquitin chains at sites of DNA damage (Sobhian et al., 2007; B. Wang et al., 2007a). 53BP1 interacts specifically with the mono-ubiquitinated K15 of H2A by its ubiquitylation-dependent recruitment (UDR) motif (Panier & Boulton, 2014).

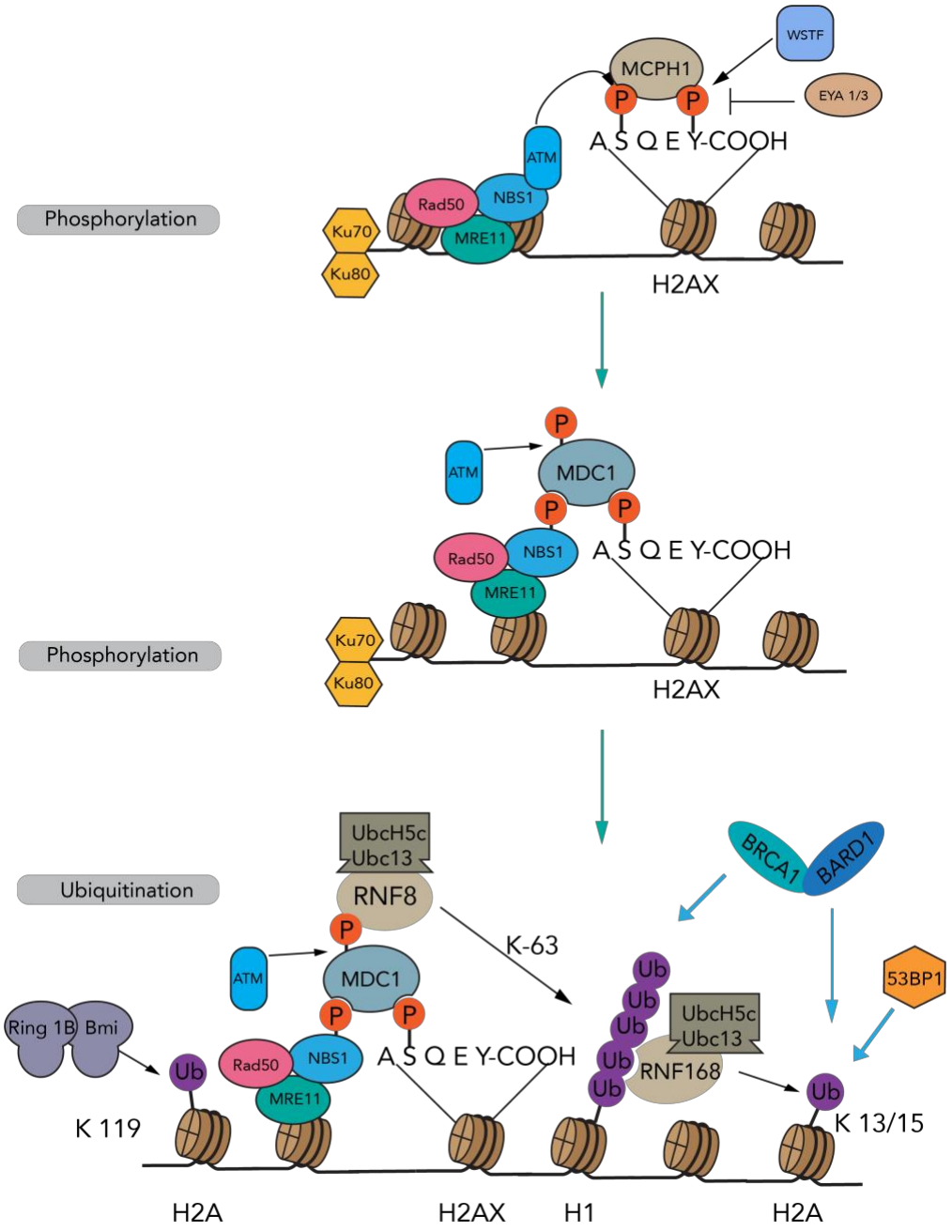

Figure 1.7 Overview of DSB signaling. Outline of phosphorylation and protein binding events that initiate the recruitment of DDR proteins.

1.33 Homologous recombination focus

HR serves to repair the most critical and dangerous types of DNA lesions such as DSB and interstrand crosslinks that arise from stalled replication forks. The process requires the presence of a sister chromatid template which promotes error free lesion repair. Thus, HR is limited to only the S/G2 phase of the cell cycle where a sister chromatid is present. When a DSB occurs, the lesion is sensed by the MRN complex which localize at both ends of the break. The MRE11 mediates resection of oligonucleotides away from the damage site. This antagonizes the NHEJ pathway and mediates the activation of the protein kinase ATM (Garcia et al., 2011; Langerak et al., 2011; Syed & Tainer, 2018). ATM belongs to the phosphatidylinositol 3 (PI3) family of lipid kinases (PI3Ks) which includes DNA dependent protein kinase (DNA-PK) and ATR involved in DNA damage signaling and repair (Shiloh, 2003). NBS1 recruits ATM to the DSB and the kinase mediate the phosphorylation of histone variant H2AX on the nucleosomes, in vicinity of the damage. DNA-PK also phosphorylates the histone H2AX in response to DSBs while ATR is mainly involved in response to ultra-violet (UV) damage or replication stress. The phosphorylation promotes the recruitment of downstream proteins for repair of the DSB and activation of the cell cycle arrest regulators (Kinner et al., 2008).

In the early steps of HR, MRE11 endonuclease activity cuts up to 300 nucleotides away from the damage to initiate DNA resection for HR directed repair. This functions to antagonize the ku dimers and prevent NHEJ repair activation

(Langerak et al., 2011). MRE11 by association with the C-terminal binding protein interacting protein (CtIP) extends the nick 3'-5' towards the DSB (H. Wang et al., 2013). CtIP then dissociates to allow for 5'-3' nuclease activity by Exonuclease 1 (EXO1) with the support of DNA2 and the Bloom syndrome helicase (BLM) (Garcia et al., 2011). SsDNA overhangs generated from resection are immediately bound by the RPA complex to protect the DNA (Chen & Wold, 2014). The Breast cancer type 2 susceptibility protein (BRCA2) in complex with partner and localizer of BRCA2 (PALB2) and other RAD51 paralogues are critical mediators in the displacement of RPA. They promote the loading of a DNA-dependent ATPase (Rad51) to form nucleofilaments with the ssDNA (Ma et al., 2017; Zelensky et al., 2014). When Rad51 is in an ATP bound state, there is an increased affinity for DNA. Rad51-ATP promotes nucleation and filament elongation to direct the repair to HR while suppressing SSA. Rad51 is regulated by the binding of co-factors, interacting proteins and the nucleotide hydrolysis cycle. With Rad51 and other interacting proteins, a nucleoprotein scaffold is formed to engage in homology search and strand invasion (Hilario et al., 2009; Robertson et al., 2009).

Homology search is mediated by Rad51 immediate binding to dsDNA and turnover if the sequence is incorrect. It has been proposed that this process could be mediated by the ATPase activity of Rad51 because of its similarity with RecA protein that performs the homology search in *E. coli* (Bell & Kowalczykowski, 2016). However, due to the slow Rad51 ATPase activity compared to RecA, it is most likely that other proteins or co-factors are involved in the search (Wright et al.,

2018). Upon identification of homologous dsDNA, a synaptic complex is formed which proceeds to form the D-loop. This is a key intermediate with the 3' end of the invading strand intertwined with its complement in the donor strand. At the D-loop, a heteroduplex DNA (hDNA) of the invading strand and donor strand is formed which is similar to the primer-template binding suitable for DNA synthesis (Kowalczykowski, 2015; Wright et al., 2018). The DNA Polymerase δ and proliferating cell nuclear antigen (PCNA) are required for the D-loop extension of the invading strand using the dsDNA donor as a template (Sneeden et al., 2013). DNA helicases unwind the hDNA to remove the extended invading strand and return it to ssDNA which is bound by RPA. The newly synthesized strand is then annealed with the other DSB end to mediate another DNA synthesis. Starting from the annealed end and using the homology strand as a template, DNA synthesis and ligation occurs to complete the repair (Wright et al., 2018).

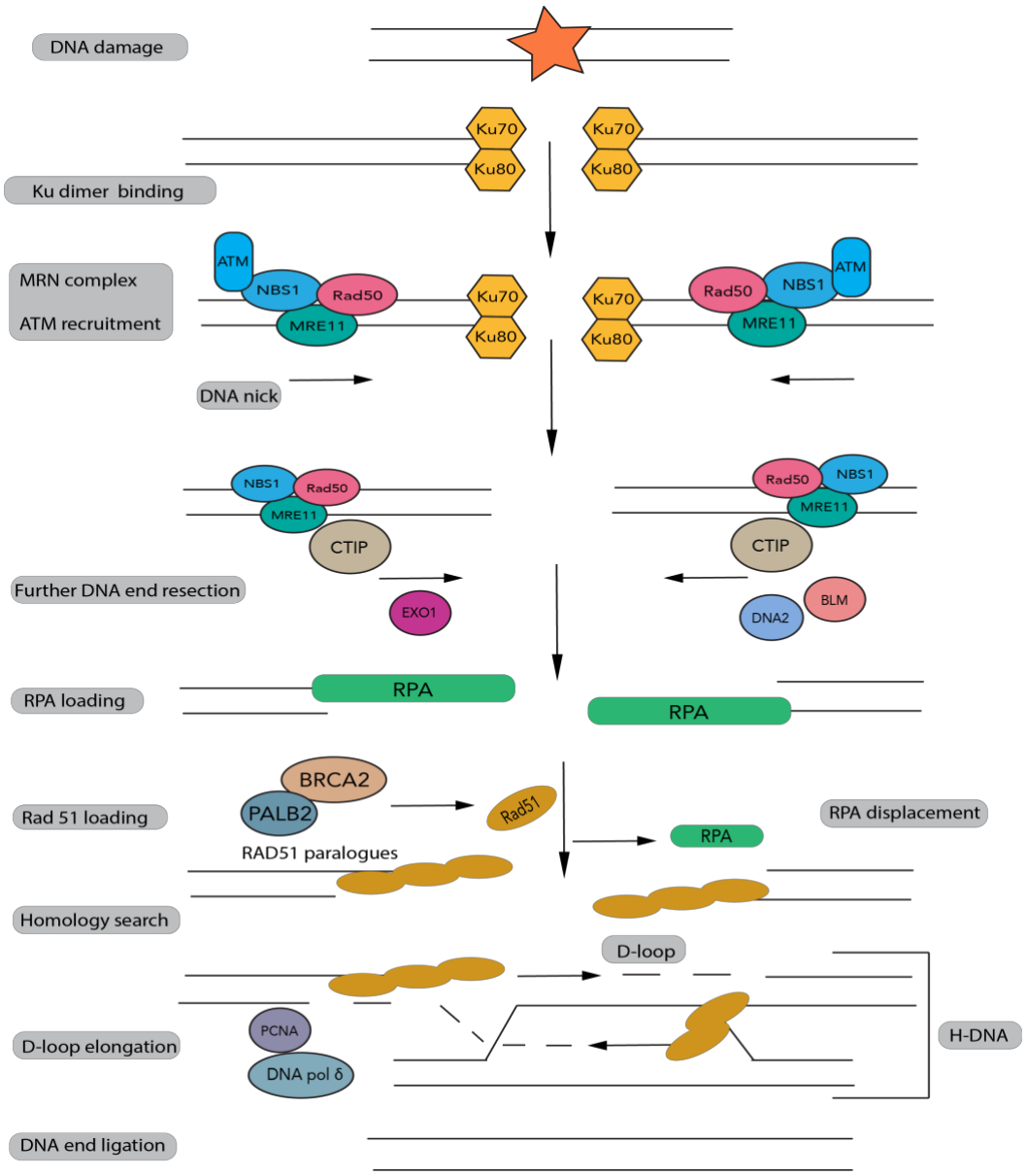

Figure 1.8 Overview of homologous recombination pathway. Schematic representation of steps in HR and the major proteins involved in this pathway are shown. HR begins with the MRN complex recruitment while the Ku dimer binding is a very early DNA protection mechanism. Figure is adapted from (Schwertman et al. 2016)

1.4 BRCT domain proteins

The BRCT domain was first identified in the BRCA1 C terminal where mutations were linked to familial breast cancer (Yu, 2003). The proteins which contain this domain function in DNA damage signaling, checkpoint control and DNA repair. BRCT domain mediates protein-protein interactions, typically with a phosphorylated non-BRCT partner. However, some BRCT domains can bind interacting partners independent of phosphorylation while some bind DNA in a sequence dependent manner (Rodriguez, 2008). The conserved structure of one BRCT fold features four parallel β sheets which are central to a pair of α-helices (1&3) on one face and $\alpha 2$ on opposite face of the sheets. The domain appears typically in tandem with the $\alpha 2$ of one-fold packed against the $\alpha 1\&3$ of the other fold and joined by an α linker (Williams et al., 2001). Single BRCT domain also exists in proteins like PARP1 and DNA ligase III proteins (Rodriguez, 2008). Tandem BRCTs are found in BRCA1 and MDC1 which will be discussed later in this section.

1.41 BRCA1

BRCA1 is a tumor suppressor protein of which mutations have been found in both hereditary and sporadic forms of breast and ovarian cancer (Futreal et al., 1994; Miki et al., 1994). It is a large protein with 1,863 amino acids which form three mainly conserved domains known to date. An N-terminal zinc RING finger domain, a coiled coil (CC) domain and a C-terminal tandem BRCT domain (Huen et al., 2010). The function of BRCA1 RING domain is in the heterodimer formation with

BRCA1-associated RING domain protein 1(BARD1). The BRCA1-BARD1 dimer is involved in the DDR signaling, DNA repair and transcriptional regulation (Huen et al., 2010; Meza et al., 1999). Studies showed the ubiquitin ligase activity of BRCA1 is enhanced by BARD1 in the heterodimer (Xia et al., 2003). The CC domain is important in the complex formation of BRCA1 with PALB2 and BRCA2 (Zhang et al., 2009). The BRCA1 BRCT domain interacts with three major proteins in the cell for different functions. Interaction with the BRCA1-interacting protein C-terminal helicase 1 (BACH1), CtIP and abraxas all happen in a phosphorylation dependent manner (Clapperton et al., 2004; B. Wang et al., 2007b; Yu et al., 1998a). The BRCA1 interaction with abraxas is important for its recruitment to the DNA damage site with the help of RAP80. CtIP interaction with BRCA1 BRCT also assists in its recruitment to the site of DSB for HR. BACH1 interaction with BRCA1 is important for activation of the DSBR pathway. A large central region of BRCA1 contains sequences which could mediate its interaction with DNA, Rad51 and other repair factors (Zhao et al., 2019) .

The BRCT domain of BRCA1 has a distinct structurally conserved interface which allows the specific recognition of the pS-X-X-F motif in the phosphorylated binding partners. An α-helical linker region joins the tandem BRCT repeats which are both important for the peptide binding. The N-terminal BRCT contains the phosphate-binding pocket while the hydrophobic binding pocket is located in the interface between the repeats. The phosphoserine binding pocket is shallow and contains Gly1656 whose main chain NH and the hydroxyl group of Ser1655, form

hydrogen bonding interactions with the phosphate. Thr1700 also hydrogen bonds with the hydroxyl group of the phosphoserine. Salt-bridging interaction of the phosphate with Lys1702 which is supported by the mainchain carbonyls of Val1654 and Asn1678 also improves the binding. The hydrophobic binding pocket comprises of Leu1701, Phe1704, Met1775 and Leu1839 and the sides are lined with Arg1699, Asn1774 and Arg1835. The main chain carbonyl group of Arg1699 hydrogen bonds with the main chain NH of the hydrophobic +3 residue. Also, the main chain carbonyl group of the Phe (+3) interacts with the side chain of Arg1699. This interaction is important for the orientation of the hydrophobic residue in the pocket (Clapperton et al., 2004; Williams et al., 2004).

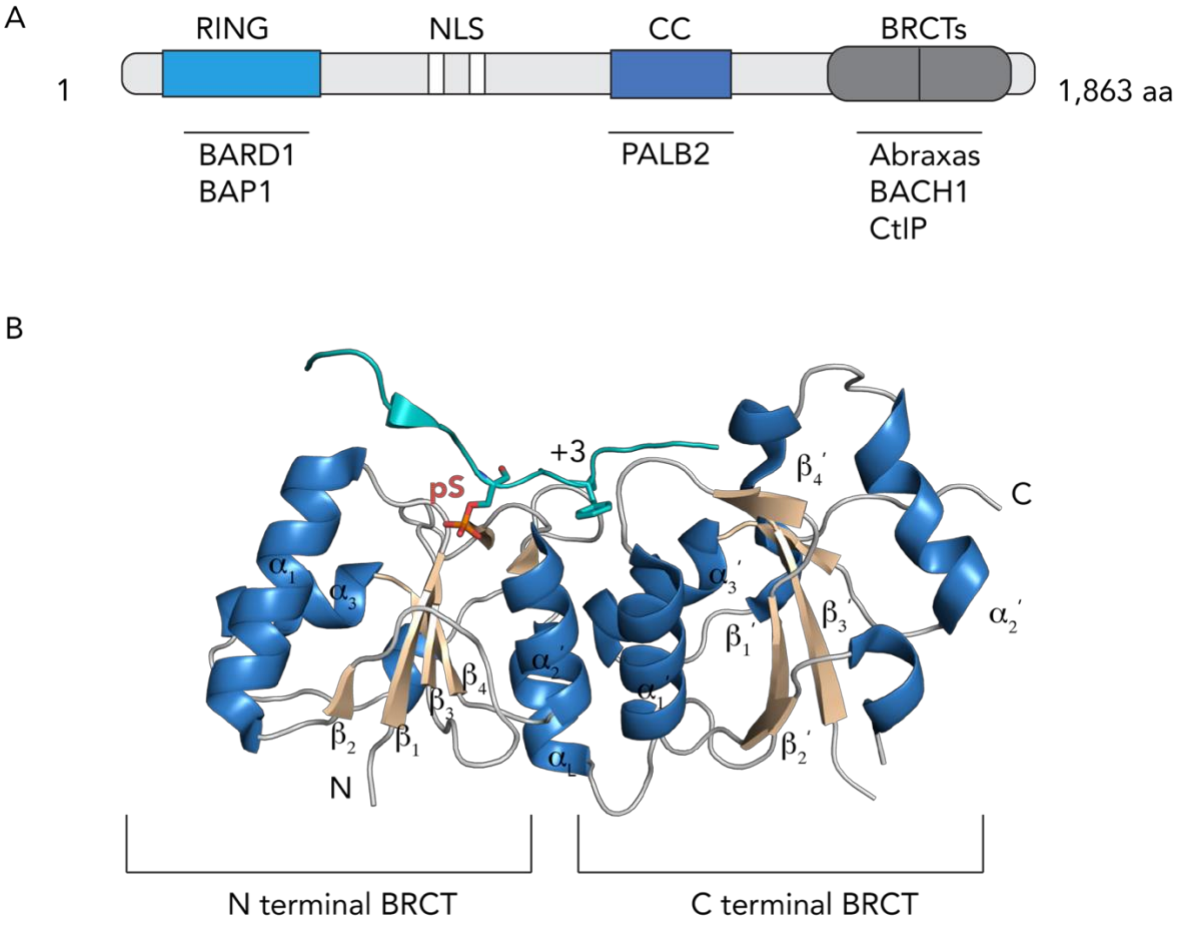

Figure 1.9 BRCA1 domain organization and tandem BRCT structure.

(A) Functional domains of BRCA1 and their protein interactions (B) Structural overview of the BRCA1 BRCT bound to the Bach1 peptide. The figure was made using Pymol (PDB ID: 1T2V). Helices colored blue, sheets coloured brown and BACH1 peptide in teal. Important residues for biniding pSer and +3 Phe shown by stick representation.

1.42 MDC1

MDC1 regulates various aspects of the DDR signaling and cell-cycle checkpoint activation. It also regulates the foci formation of other DDR important proteins which mediate DNA repair or apoptosis of the cells (Lou et al., 2006; Stewart et al., 2003; L. Wu et al., 2008). MDC1 is a large 2,089 residues long protein which consists of three distinct domains. An N-terminal FHA domain, a central Pro/Ser/Thr- rich repeat domain (PST) and a C-terminal tandem BRCT domain. The specific recognition of the pS-Q-E-Y-COO^- motif by the BRCT domain of MDC1 mediates its recruitment to proximity of DSB and other DDR proteins (Coster & Goldberg, 2010) . The overall mode of peptide binding to the MDC1 BRCT is similar to the BRCA1 BRCT. The phosphate binding pocket of MDC1 is made up of Lys1936, Thr1898 and Gly1899 which bind the phosphate in similar fashion to the Lys1702, Ser1655 and Gly1656 of BRCA1. However, in the hydrophobic (+3) binding pocket, Arg1933 has a stronger hydrogen bonding pattern with the Glu2063 and forms strong salt-bridging interaction with the carboxyl terminus. This explains the strong preference and higher affinity of MDC1 binding to a carboxyl-terminus peptide as additional residues will abolish this interaction (Stucki et al., 2005).

Although the structural moiety of the BRCT domain and the important residues for peptide binding are conserved, some subtle changes exist which influence specificity of the protein binding partners. This allows for the design of small inhibitors that can target specific BRCT domain proteins for therapeutics.

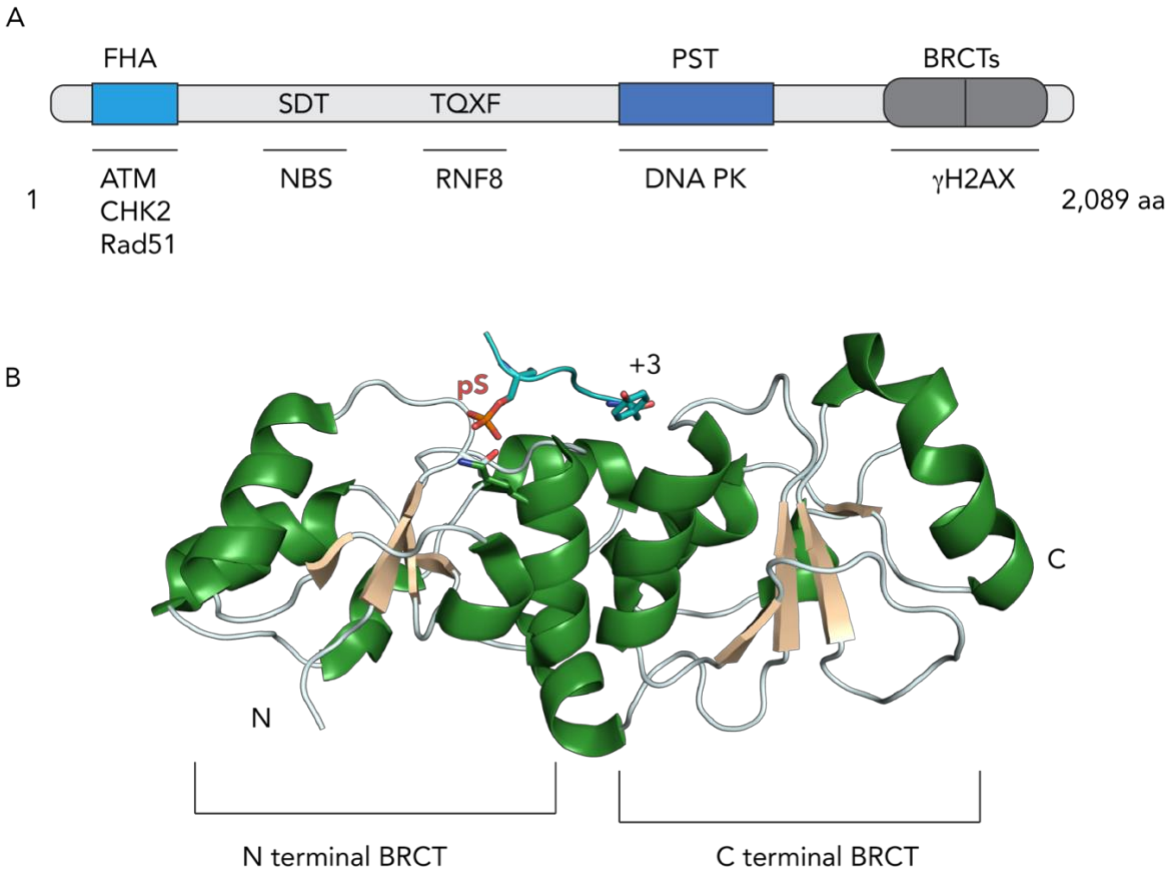

Figure 1.10 MDC1 domain organization and tandem BRCT structure.

(A) Functional domains of MDC1 and their protein interactions (B) Structural overview of the MDC1 BRCT bound to the γH2AX peptide. The figure was made using Pymol (PDB ID: 2AZM). Helices colored green, sheets coloured brown and γH2AX peptide in teal. Important residues for biniding pSer and +3 Tyr shown by stick representation.

1.5 BRCA1 in Homologous Recombination.

BRCA1 is mostly characterized for its important roles in promoting HR in DSB repair. This is because of its interaction with proteins involved at different stages of HR. BRCA-negative cells are HR deficient and sensitive to DNA damaging agents (Turner et al., 2004). BRCA1 recruits to the DSB mainly in the S/G2 phase of cell cycle where HR is favoured. It antagonizes the p53 binding protein 1 (53BP1) to direct the DSB repair choice towards HR. DNA resection and generation of ssDNA to facilitate the Rad51 filaments formation for stand invasion is promoted by BRCA1 (Liu & Lu, 2021). The heterodimer of BRCA1/BARD1 was recently found to promote Rad51 mediated homologous pairing. BARD1 promotes the localization of BRCA1 to chromatin through its interacting domains. It has an N-terminal RING domain, three Ankyrin repeats (ANK) and two C-terminal BRCT domains (Cimmino et al., 2017).

The recruitment of BRCA1 to the DSB is dependent on two major pathways, its complex A formation with Abraxas/RAP 80 and by BARD1. A visual representation of the pathways has been highlighted in figure 1.11. Poly-ubiquitination of the histone H1 by RNF8 leads to the mono-ubiquitination of H2A at K13/15. The ubiquitin interacting motif (UIM) of RAP 80 recognizes the K63 ubiquitin chains on H1, this mediates the recruitment of BRCA1 bound to phospho-abraxas by the BRCT domain. BARD1 with its ankyrin repeats binds to the unmethylated lysine 20 of the H4 histone (H4K20me0). This explains the recruitment of BRCA1 to the DSB in the S/G2 phase. The H4K20me0 is present in

newly synthesized histone H4 which is incorporated into the chromatin during replication. The BRCT domain of BARD1 recognizes the mono-ubiquitination on K15 of H2A (H2AK15Ub) which is catalysed by RNF168 and recognizes poly(ADP) ribosylation (PAR) generated at DSBs (Becker et al., 2020; Cimmino et al., 2017; Nakamura et al., 2019)

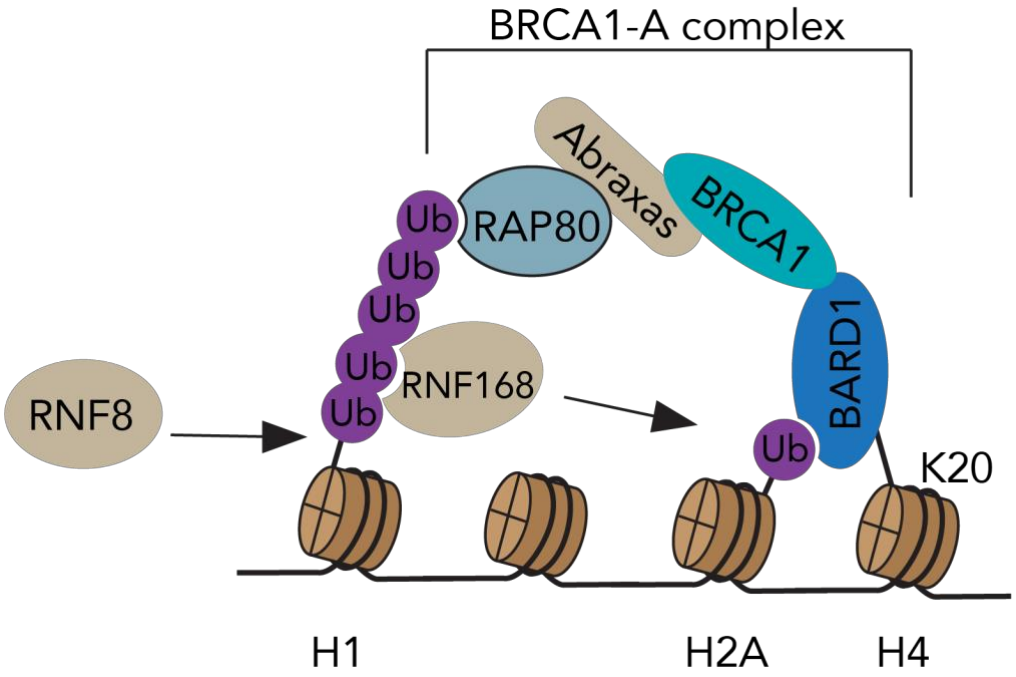

Figure 1.11 BRCA1 recruitment to DSB. RNF8 polyubiquitination of histone H1which is recognized by RNF168. Mono-ubiquitination of H2A on lysine 13/15 and the H4K20me0 which is only present in S/G2 phase mediates the interaction of BARD 1. RAP80 also recognizes the K-63 linked chains on H1 and recruits proteins in the BRCA1 A complex to DSB site.

BRCA1 promotes DNA end resection which inhibits NHEJ and prevents 53BP1 assembly at the site of damage. It is not entirely clear the mode in which BRCA1 performs this function but there are currently some hypotheses. BRCA1 interacts with the end resection promoter protein, phosphorylated CtIP through its BRCT domain which also regulates BRCA1 recruitment to the DSB (Varma et al., 2005; Yu et al., 1998b). CtIP promotes the MRN short and long-range resection in HR which counteracts the 53BP1-end blocking. Recently, a study showed that the H2AK15Ub can be phosphorylated at Thr12 of ubiquitin. The H2AK15pUb significantly reduced 53BP1 foci which suggests the modification might be to exclude it from the damage site. However, the pUb is permissive to recognition by the BRCA1/BARD1 heterodimer complex (Walser et al., 2020). The E3 ubiquitin ligase activity of BRCA/BARD1 has been shown to ubiquitinate the histone H2A on lysine 125,127 and 129 which can also promote end resection. The SMARCAD1 chromatin remodeling complex binds to the H2A K127Ub and mobilizes the 53BP1 complex for long-range resection to proceed (Densham et al., 2016; Kalb et al., 2014).

Rad51 loading to promote filament formation and RPA exclusion from the DSB is essential for HR progression. Like we discussed earlier, BRCA2-PALB2 promotes the Rad51 loading and mediates RPA displacement. BRCA1-PALB2 interaction mediated by the CC domains on both proteins is observed only in the S/G2 phase. Disruption of this interaction, compromises BRCA2 and RAD51 foci at DSB (Orthwein et al., 2015; Sy et al., 2009, p. 2). These findings show BRCA1-

PALB2 interaction facilitates Rad51 filament formation by loading BRCA2/Rad51 to the DSB. BRCA1-BARD1 binds to the D-loop, replication fork, dsDNA and ssDNA and directly to Rad 51 in a heterodimer-dependent manner (Zhao et al., 2017). They also discovered that BRCA1-BARD1 promotes and strongly enhanced DNA strand invasion. This is due to the high affinity of the complex for the D-loop.

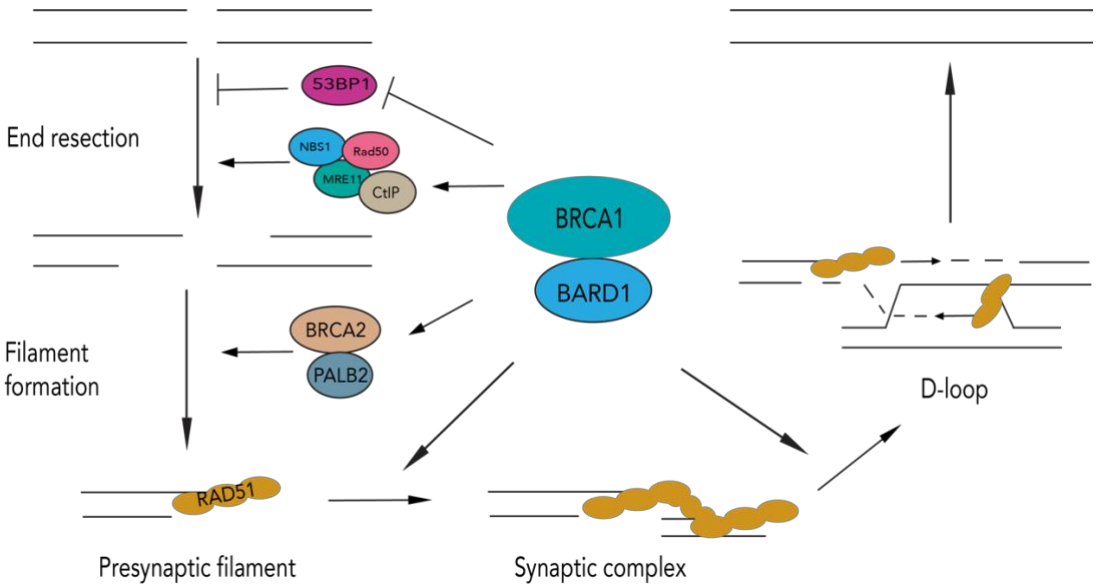

Figure 1.12 Functions of BRCA1-BARD1 in HR. Summary of BRCA1-BARD1 heterodimer functions in HR. Cooperative roles with MRN complex and CtIP, antagonist of the 53BP1 protein which prevents resection. Interaction with PALB2-BRCA2 in promoting Rad51 presynaptic filament assembly. Assisting Rad51 protein in strand invasion and promoting D-loop formation.

1.6 Thesis overview

This thesis aims to investigate the proteins involved in DDR signaling and repair. Also, to explore the therapeutic potential of a BRCA1 protein inhibitor in treating genomic instability diseases.

Phosphorylation of H2AX Octamer (Chapter 3).

The γH2AX is a hallmark for DSB signaling and is important for the localization of DDR proteins to the site of damage. MDC1 is an early player in the DDR pathway that interacts with the γH2AX. The details of this interaction in the context of chromatin are yet to be explored. Here, we present the preparation of phosphorylated H2AX containing nucleosome by two distinct methods. We test our phosphorylation methods by binding MDC1 to the γH2AX containing dimer.

BRCA1 Peptide Inhibitor Studies (Chapter 4). BRCA1 BRCT has been considered as a potential target of synthetic lethality inhibitor drug development for cancer therapy. The development of a viable inhibitor has been very challenging due to the requirement of a phosphorylated binding partner. A non-phosphorylated peptide inhibitor that was developed through an mRNA display library screen is tested through biochemical assays to show inhibition of the BRCA1 BRCT.

Lac Array system for peptide inhibitor studies (Chapter 5). The potency of a non-phosphorylated BRCA1 BRCT inhibitor is tested in vivo. Cellular internalization of the non-phosphorylated inhibitor is achieved by the addition of a hydrophobic group. Using a LacI/LacO system, we present cellular studies on a cell penetrable inhibitor.

Conclusion (Chapter 6). The final chapter will summarize the results described in this thesis, as well as the future directions to these findings.

CHAPTER 2: Material & Methods

2.1 H2AX Octamer phosphorylation

2.11 Octamer Overexpression and purification

pETDuet-1-$(His)_6$-TEV-H2AX-H2B and pCDFDuet-1-$(His)_6$-TEV-H3.1-H4 were co-transformed in Rosetta 2(DE3) and grown in Terrific Broth (TB) medium at 37°C for 16 hours. Culture was induced at OD_{600} of 0.8 with 1 mM IPTG for 8 hours at 30°C. Cells were lysed using emulsiflex cell disruptor and lysis buffer [50 mM Tris pH 7.5, 2 M NaCl, 5% glycerol, 1 mM TCEP, 1 mM PMSF, protease inhibitor]. The octamer was purified using nickel affinity chromatography with Ni-NTA column. The beads were washed two times with octamer buffer [50 mM Tris pH 7.5, 2 M NaCl, 5% glycerol, 1 mM TCEP] containing 30 mM imidazole. Protein was eluted with octamer buffer containing increasing concentrations of imidazole [100 mM, 250 mM, 500 mM, 1 M and 2 M]. The purest fractions were combined and concentrated using Amicon Ultra-15 centrifugal filter unit and loaded on to the size exclusion columns. Octamer was further purified using Superdex 200 16/60 equilibrated with the size exclusion buffer [25 mM HEPES pH 7.5, 2 M NaCl, 5% glycerol, 1 mM TCEP]. Octamer fractions were pooled, concentrated, and stored at 4°C.

2.12 In-vivo phosphorylated Octamer Overexpression and purification

Casein kinase 2 [pRSF DUET-mCK2a-mCK2b] along with histones [pETDuet-1-$(His)_6$-TEV-H2AX-H2B, pCDFDuet-1-$(His)_6$-TEV-H3.1-H4] were co-expressed in TB media. Overexpression and purification were performed using the same protocol mentioned above for octamer. Purified phosphorylated octamer and the alanine mutant were stored at 4°C.

2.13 Radioactive kinase assay

Radioactive kinase assay was performed in kinase buffer [20 mM Tris pH 7.5, 150 mM KCl, 10 mM $MgCl_2$]. Nucleosome was assembled by Dr. Rashmi Panigrahi. 1:1 molar ratio of octamer/nucleosome to Casein kinase 2 (CK2), 1 mM cold ATP, and 1 μL of [^{32}P] ATP (approximately 0.0021μCi/μmole) were incubated at room temperature. 10 µL sample was taken after 2 and 4 hours and 1 molar equivalent of CK2 was added and incubated for additional 2 hours (4+). Reaction was terminated with 8 µL 2X SDS sample buffer and all the samples were analyzed by SDS PAGE followed by autoradiography. The gel was vacuum dried for 2 hours and then exposed to a phosphoscreen cassette. The ^{32}P radioactive signal was developed using a typhoon scanner.

2.14 MDC1 overexpression and purification

Human MDC1-BRCT (1890-2089) cloned in pET47b vector with a C-terminal Tobacco Etch Virus (TEV) protease cleavage site was transformed in Rosetta 2 (DE3) E. coli cells. The E. coli culture was induced at OD_{600} between 0.6 and 0.8 with 1 mM IPTG and the BRCT protein was expressed at 30°C for 6 hours. Cells were lysed using emulsiflex cell disruptor and lysis buffer [50 mM Tris pH 7.5, 400 mM NaCl, 1 mM TCEP, 1 mM PMSF, protease inhibitor]. The BRCT domain was purified using nickel affinity chromatography with Ni-NTA column. Protein was eluted with elution buffer [50 mM Tris-HCl pH 7.5, 400 mM NaCl, 1 mM TCEP] containing increasing concentrations of imidazole [100 mM, 250 mM, 500 mM, 1M]. His-tagged MDC1 BRCT was purified by Superdex 200 16/60 column in storage buffer [50 mM Tris-HCl pH 7.5, 150 mM NaCl, 1 mM TCEP]. Protein was stored at 4°C

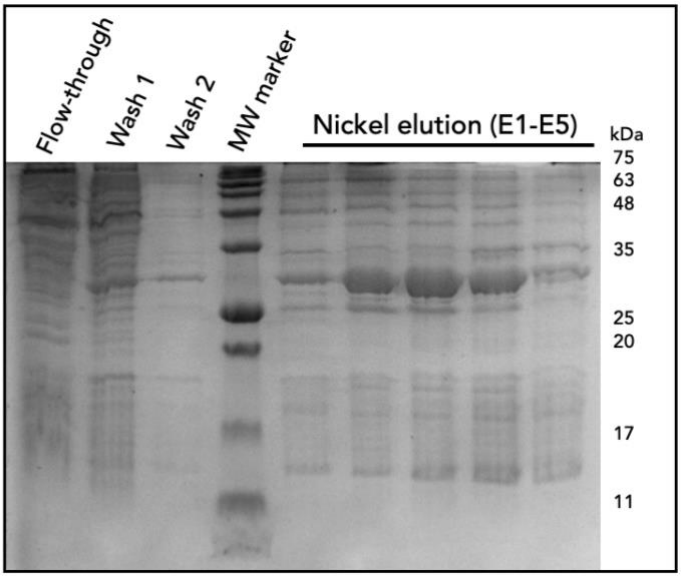

Figure 2.1: SDS-PAGE gel of MDC1 BRCT Ni^{2+} affinity purification. Fractions from nickel affinity purification were run on 14% SDS-PAGE gel at 170V for 45 min. Gel was stained with Coomassie blue and de-stained in 15% acetic acid. Purified MDC1 BRCT is found in the elution fractions E1-E4 along with impurities. E1-E4 were concentrated for further purification.

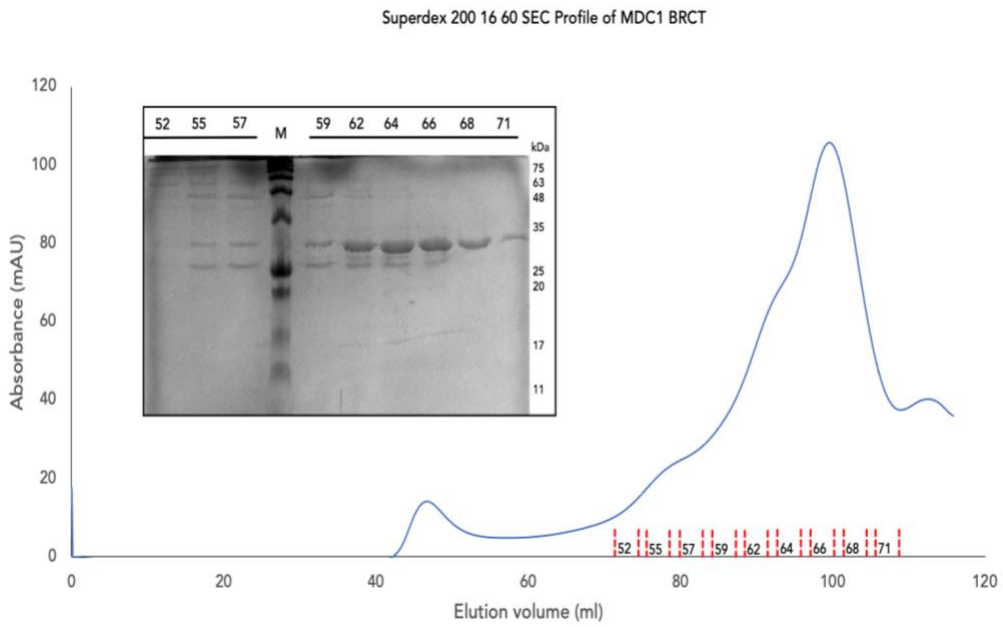

Figure 2.2 Size exclusion chromatography of MDC1 BRCT purification.
Elution fractions E1-E4 were pooled, concentrated, and loaded on to the Superdex 200 16 60. The higher molecular weight contaminants and aggregate eluted out in the void volume (~40 mL). The MDC1 BRCT peak eluted at about 90 mL elution volume. Peak fractions were run on 14% SDS-PAGE gels at 170 V for 45 min. Gel was stained with Coomassie blue and de-stained in 15% acetic acid. Fractions 62-68 were pooled and concentrated for Fluorescence polarization experiments.

2.15 Preparation of MDC1/ H2AX-H2B dimer complex

Direct binding assay was performed in buffer [20 mM HEPES pH 7.5, 150 mM NaCl]. Equimolar ratio of H2AX-H2B dimer or in vivo phosphorylated H2AX-H2B was mixed with purified MDC1 BRCT and incubated at 4°C overnight. The sample loaded on a Superdex 200 10/300 analytical column, and the respective peaks were collected and analyzed by SDS-PAGE. MDC1 with respective molar ratios as indicated were incubated with in vivo phosphorylated dimer.

2.2 BRCA1 peptide inhibitor studies

2.21 BRCA1 overexpression and purification

Human BRCA1-BRCT (1528-1863) cloned in pGEX6P-1 vector as a GST fusion protein was transformed in Escherichia coli BL21-DE3 cells. Protein expression was induced at OD_{600} between 0.6 and 0.8 with 1 mM IPTG at 18°C overnight. Cells were lysed using emulsiflex cell disruptor and lysis buffer [50 mM Tris pH 7.5, 400 mM NaCl, 1 mM DTT, 1 mM PMSF, protease inhibitor]. The protein was purified using glutathione affinity chromatography with glutathione Sepharose beads (GE Healthcare) and eluted with elution buffer [50 mM Tris-HCl pH 7.5, 150 mM NaCl, 1 mM DTT] containing increasing concentrations of reduced glutathione [20 mM, 50 mM, 70 mM, 100 mM]. Glutathione was removed by buffer exchange with

storage buffer (50 mM Tris-HCl pH 7.5, 150 mM NaCl, 1 mM DTT) and GST was cleaved with 3C protease overnight at 4°C. Residual GST and 3C were removed by incubation with glutathione beads (GE Healthcare). BRCA1 BRCT was purified by Superdex 200 16/60 column in storage buffer [50 mM Tris-HCl pH 7.5, 150 mM NaCl, 1 mM DTT]. Protein was stored at 4 °C. BRCA1-GST predicted to ~ 72 kDa.

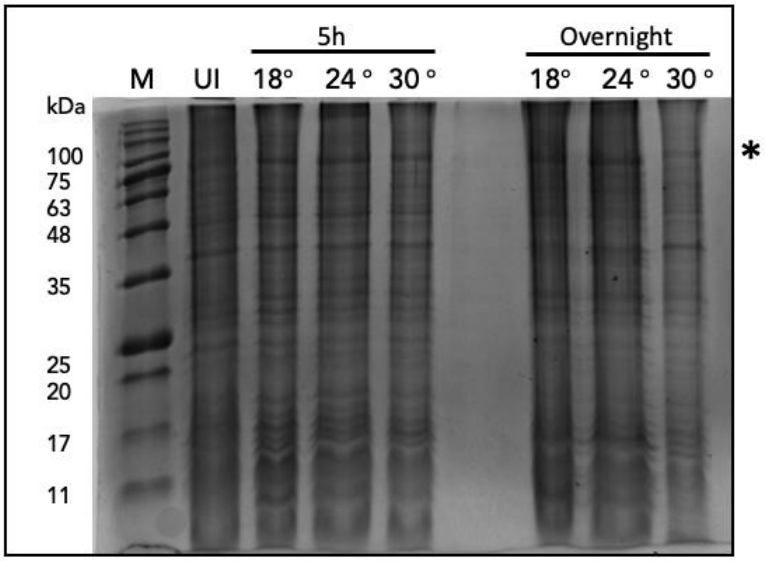

Figure 2.3 SDS-PAGE gel of BRCA1 BRCT expression check. Cell lysates from samples taken at un-induced (UI), different temperatures at 5-hour time point and overnight after addition of 1mM IPTG. Lysate and 4X SDS loading dye were heated at 98 °C for 20 min before loading onto 14% SDS-PAGE gel at 170 V for 45 min. Gel was stained in Coomassie blue and de-stained in 15% acetic acid. *= BRCA1 BRCT expression.

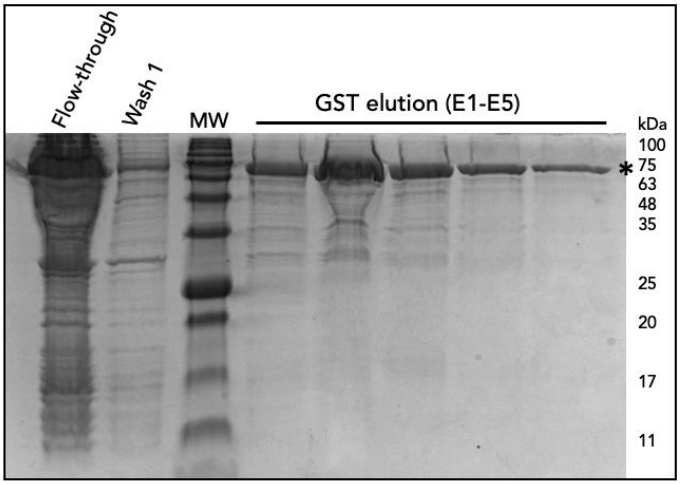

Figure 2.4: SDS-PAGE gel of BRCA1 GST-tag affinity purification. Fractions from GST-tag affinity purification were run on 14% SDS-PAGE gel at 170 V for 45 min. Increasing concentration of reduced glutathione (20 mM-100 mM) were used for elution of the protein (E1-E5). Gel was stained with Coomassie blue and de-stained in 15% acetic acid. Purified BRCA1 BRCT-GST fusion is found in the elution fractions E1-E5. *=BRCA1 BRCT

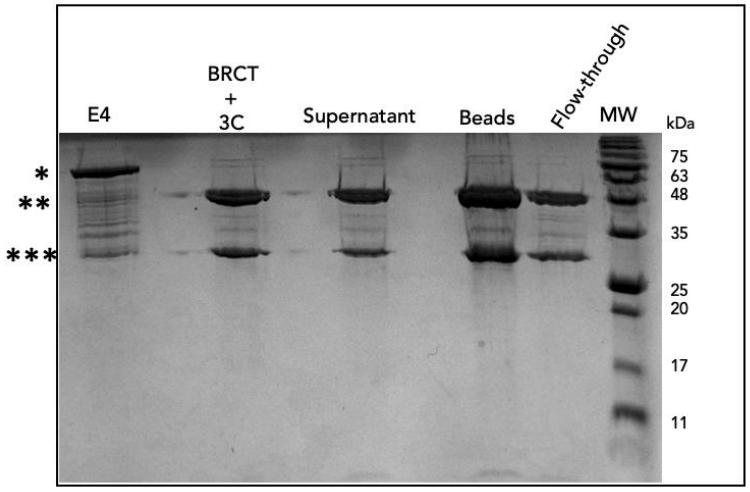

Figure 2.5: SDS-PAGE gel of BRCA1 BRCT 3C protease cut. Fractions from GST-tag affinity purification were run on 14% SDS-PAGE gel at 170 V for 45 min. The E4 fraction is a sample from the affinity purification eluent. BRCT+3C is a sample from the overnight incubation of BRCA1 with 3C protease, supernatant is a sample of the proteins suspended in buffer. A sample from the GST beads was also loaded and the flow-through which was concentrated for size exclusion. *= BRCA1-BRCT-GST. **= BRCA1-BRCT or 3C protease. ***= Free GST.

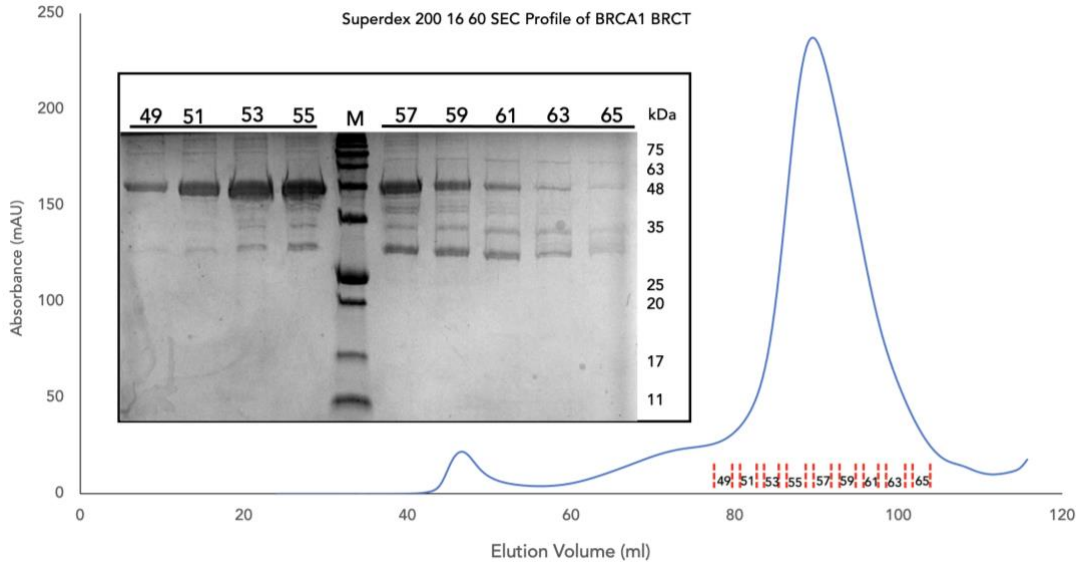

Figure 2.6 Size exclusion chromatography of BRCA1 BRCT purification. Flow-through from 3C cut was concentrated and loaded on to the Superdex 200 16 60. The higher molecular weight contaminant and aggregated eluted out in the void volume (~40 mL). The BRCA1 BRCT peak eluted at about 90 mL elution volume. Peak fractions were run on 14% SDS-PAGE gels at 170 V for 45 min. Gel was stained with Coomassie blue and de-stained in 15% acetic acid. Fractions 49-53 were pooled and concentrated for Fluorescence polarization experiments.

2.22 Fluorescence Polarization assay (BRCA1)

The affinity of the BRCA1-BRCT protein for the pSer-x-x-Phe peptide derived from BACH1 (FITC-SRSTpSPTFNK-NH_2) was determined by direct FP binding assay. Labeled peptide was mixed with increasing concentrations of WT BRCA1. Fluorescein was excited at a wavelength of 485 nm and the emission was measured at 538 nm. The change in polarization was graphed as a function of the log of the protein concentration and dissociation constant (K_d) was obtained from the resulting sigmoidal curve. For all assays, a concentration of 100 nM of labelled peptide was used in a reaction volume of 21 μL. FP measurements were carried out using an Envision multi-label plate reader (Perkin Elmer) using 384-well Opti Plates (Perkin Elmer).

2.23 Fluorescence polarization assay (MDC1)

FP measurements were carried out using an Envision multi-label plate reader (Perkin Elmer) using 384-well Opti Plates (Perkin Elmer). Fluorescein-labelled peptide was obtained from the Alberta Peptide Institute (API) and sequence is as follows: γH2AX peptide - Fluorescein-KKATQApSQEY-COO^-. Fluorescein peptide binding to MDC1 BRCT was verified by titrating an increasing concentration of protein into a constant concentration of labelled peptide. Fluorescein was excited at a wavelength of 485 nm and the emission was measured at 538 nm. The change in polarization was graphed as a function of the log of the

protein concentration and dissociation constant (K_d) was obtained from the resulting sigmoidal curve. For all assays, a concentration of 100 nM of labelled peptide was used in a reaction volume of 21 µL.

2.24 Competitive Fluorescence Polarization Assay (BRCA1)

The competition assay was performed between CPP 4i 8.6 and fluorescein labelled BACH1 where the ability of CPP 4i 8.6 to compete off the labelled peptide was measured. CPP 4i 8.6 (MCTIDFDEYRFRKT-NH_2) was incubated at serial-dilution concentrations with a mixture of BRCA1 BRCTs (4.5 µM) and 100nM Fluorescein-BACH1 peptide. The concentration of protein used in the competition assay was determined based on the K_d of the labelled peptide to BRCA1 BRCT. The change in polarization was graphed as a function of the log of the protein concentration and an Inhibition concentration (IC_{50}) was obtained from the resulting sigmoidal curve. The IC_{50} obtained from the competition assay is used to calculate the Inhibitor constant (K_i) using the Coleska-Wang equation. For all assays, a concentration of 100 nM of labelled peptide was used in a reaction volume of 27 µL. FP measurements were carried out using an Envision multi-label plate reader (Perkin Elmer) using 384-well Opti Plates (Perkin Elmer).

2.25 Competitive Fluorescence Polarization Assay (MDC1)

The competition assay was performed between CPP 4i 8.6 and fluorescein-labelled γH2AX where the ability of the peptide to compete off the labelled peptide was measured. CPP 4i 8.6 (MCTIDFDEYRFRKT-NH_2) was incubated at serial-dilution concentrations with a mixture of MDC1 BRCTs (5 μM) and 100nM Fluorescein-γH2AX peptide. The concentration of protein used in the competition assay was determined based on the K_d of the labelled peptide to MDC1 BRCT. The same protocol as described above was adopted.

2.3 BRCA1 cellular peptide inhibitor studies

2.31 U2OS 263 cell culture and plasmid transfection

The U2OS 2-6-3 cells were provided by the Janicki lab (The Wistar institute, Philadelphia). The culture media was supplemented with 10% fetal bovine serum (FBS), 1% Pen Strep and 100 μg/ml of Hygromycin B. Cells were cultured at 37 °C and 5% CO_2. pDEST-mCherry-LacR-BRCA1 was a gift from Daniel Durocher (Addgene plasmid #71115) and TRIPZ-EGFP-8.6 was provided by Kristoffer Valerie (Virginia Commonwealth University). Both plasmids were transfected using Effectene (Qiagen), following the manufacturer's instructions. Doxycycline ($1 \mu g mL^{-1}$) was added to TRIPZ-EGFP-8.6 transfected cells. The cell-penetrable peptide 8.6 when added to the cells, was added in serum-free medium. All cells were

deemed mycoplasma contamination negative at the time of experiments based upon the absence of DAPI positive spots in the cytoplasm. Cells were irradiated with gamma-cell irradiator at a dose rate of 0.599 Gy/min.

2.32 Immunofluorescence Microscopy

Cells were seeded onto sterilized glass coverslips prior to transfection, and fixed when 50-80% confluent. Transfection was done following Qiagen Effectene protocol and cells were irradiated with 3 Gy. Prior to fixation, coverslips were washed with Hepes-buffered saline (HBS; 135 mM NaCl, 10 mM KCl, 0.4 mM $MgCl_2$, 1 mM $CaCl_2$, 10 mM Na-Hepes, pH 7.4). Fixation was performed as described in (Brock et al., 1999). The cells were fixed with 4% (w/v) paraformaldehyde in HBS at 4°C for 5 min followed by room temperature for 10 min. Coverslips were washed 3 X 5 min with HBS and another fixation and permeabilization with methanol for 6 min at -20°C, followed by an HBS wash. Cells were incubated with HBS containing 0.5% Triton X-100 for 5 min and washed twice with HBS. The cells were incubated with 40µL aliquots of blocking solution, 3% BSA in HBS for 30 min at room temperature. Coverslips were rinsed with HBS containing 0.1% Triton X-100 and washed 3 X 5 min with HBS before 1-hour incubation with appropriate primary antibody. Cells were rinsed with HBS containing 0.1% Triton X-100 and washed 3 X 5 min with HBS followed by 1 hour incubation with secondary antibody conjugated to a fluorophore. Cells were rinsed

with 0.1% Triton X-100 HBS and washed twice with HBS and incubated with 20µl of 1 in 1000 DAPI in 2ml 1X HBS. Coverslips were mounted onto slides containing Mowiol. Commercially available primary antibody rabbit anti-Abraxas (ab139191 Abcam) was used to detect Abraxas colocalization at BRCA1 lac-array. Proteins were visualized with anti-rabbit Cy5-conjugated secondary antibody, mCherry tagging of BRCA1 and EGFP tagging of the peptide. Cells were observed using a microscope (Leica TCS SP8 MP), and composite figures of collected images were assembled in ImageJ (NIH).

2.33 Live cell imaging

Cells were plated on 35-mm glass bottom culture dishes (MatTek corporation) 24 hours before experiment. Cells were transfected following the Qiagen Effectene manufacturer's protocol and doxycycline (1 μgmL^{-1}) was added to TRIPZ-EGFP-8.6 transfected cells. Irradiation was performed with gamma-cell irradiator at a dose rate of 0.599 Gy/min and cells were placed on a heated stage (37 ℃). Live-cell observation was carried out using the PerkinElmer Ultra view spinning-disk confocal microscope (Zeiss Axiovert 200M inverted). The 100X 1.4NA, oil immersion lens was used for imaging. GFP fluorescence imaging was recorded after excitation with a 488-nm argon laser using a 515-540 nm band pass filter. CY3 fluorescence were recorded after excitation with a 561-nm solid state laser using a 565-590 nm band pass filter.

2.34 Fluorescence recovery after photobleaching (FRAP)

Cells were cultured on 35-mm glass bottom culture dishes (MatTek) 24 hours before experiments. Transfection was done following the Qiagen Effectene manufacturer's protocol and doxycycline ($1 \mu g mL^{-1}$) was added to TRIPZ-EGFP-8.6 transfected cells. 2 hours post- irradiation, cells were placed on a heated stage (37 ℃) of PerkinElmer Ultra view spinning-disk confocal microscope (Zeiss Axiovert 200M inverted). GFP fluorescence was irreversibly photobleached at the lacO using a 488 nm argon laser set to 100% output. Fluorescence images were collected at 1 second intervals for two minutes total duration.

CHAPTER 3: Phosphorylation of H2AX Octamer

CONTRIBUTIONS

I would like to acknowledge the contributions of Dr. Rashmi Panigrahi and Md Touhidul Islam (Apu) in this chapter. H2AX-S139A was previously cloned by Apu. Octamer preparation, DNA preparation, nucleosome assembly, CK2 preparation and phosphorylation reactions were designed and performed by Dr. Rashmi Panigrahi. I performed the H2AX-H2B dimer purification and radioactive analysis. The clone for CK2 containing the subunits α and β was a gift from Professor Jun-ichi Nakayama, National Institute of Basic Biology, Okazaki, Japan.

3.1 Introduction

DNA damage is a threat to the integrity of genetic information and its transmission across generations. Various environmental and chemical agents such as ionizing radiation (IR), ultraviolet (UV) light, reactive oxygen species (ROS) as well as metabolic processes in the cell induce DNA damage (Jackson & Bartek, 2009). To deal with the damage, a series of critical cellular defense machineries have evolved crucial for DNA damage repair. They help preserve the genomic integrity and prevent genotoxic consequences that lead to tumorigenesis (Ciccia & Elledge, 2010). DNA damage response (DDR) involves a plethora of signalling events that chemically modify the DNA to facilitate repair. Mutations in DDR genes such as ATM, Breast cancer (BRCA1), RAD51 and tumor protein p53 are linked to many hereditary and sporadic forms of human cancer.(Dietlein et al., 2014) Recent advancements in targeted therapy have exploited these genes, as shown by the success in treatment of BRCA-deficient cancers by poly (ADP-ribose) polymerase (PARP) inhibitors and the antitumor activity by ATM inhibitors (Cremona & Behrens, 2014; Rouleau et al., 2010). Despite these advancements, detailed molecular insights into DDR signaling remains to be explored which can lead to novel cancer therapies.

DNA packaging in the nucleus of a human cell is facilitated through its interaction with proteins and their organization into chromatin. The genomic DNA which consists of 147 base pairs is wrapped around an octamer of four core histone proteins: H2A, H2B, H3 and H4 (Kinner et al., 2008). Each of the core histones

contain the hydrophobic fold that mediates H2A-H2B and H3-H4 heterodimerization. The histone octamer is assembled by the interaction of two H3/H4 dimers that form a tetramer with two H2A/H2B dimers using a structural motif known as the helix bundle (McGinty & Tan, 2015). The exposed surface of the histone heterodimers is positively charged which helps stabilize the octamer-DNA interaction (McGinty & Tan, 2015). The nucleosome has a compact histone core with flexible N and C terminal tails that provide binding sites for various histone binding proteins. Accessibility of the tails are important for posttranslational modifications which induce epigenetic signalling (Cutter & Hayes, 2015b).

Although the histone fold is conserved, there are non-canonical histone variants that are expressed throughout the cell cycle and have specialized function in regulating chromatin dynamics. The variants have the histone fold to ensure their incorporation into the nucleosomes but differ by the presence of extra tails for post-translational modification. In humans, H2AX, an H2A variant exists and is crucial for response to double strand breaks (Kamakaka, 2005). The histone variant has a C-terminal tail which is mainly phosphorylated by ATM kinase on serine 139 to form γH2AX. DNA-PKcs also responds to DSB and can regulate the γH2AX levels independent of ATM. DNA-PKcs and ATM belong to a family of PI3K-like protein kinases (PIKKs) which possess the serine/threonine kinase activity (Panigrahi & Glover, 2021). The γH2AX leads to the recruitment of chromatin modifying proteins to the DSB site for repair of the damage.

Mediator of DNA damage checkpoint protein 1 (MDC1) is an early player in the DDR pathway and its knockout phenotypes present significant genomic instability. MDC1 functions as adaptor because of its protein-protein interaction domains such as its FHA and BRCT domains (Stewart et al., 2003, p. 1). Through these interactions, they are able to control the formation of damage induced 53BP1, BRCA1 foci and promote H2AX phosphorylation spread, 1-2 mega bases around the DSB (Stewart et al., 2003, p. 1). The BRCT domain of MDC1 specifically interacts with the phosphorylated C-terminal tail of γH2AX in the nucleosome. This interaction is highly specific to the pSxxY-COOH sequence which has been evidenced by crystallographic analysis and biochemical assays (Stucki et al., 2005). The intrinsic details of this interaction in the context of the chromatin are yet to be explored.

Our lab is interested in probing the specific interactions of the BRCT domain with the nucleosome. To study this, the production of γH2AX nucleosomes for binding to the BRCT domain is required. The purification of the 350 kDa ATM protein, which is the ideal kinase for H2AX nucleosome phosphorylation would be a major problem. Another serine/threonine protein kinase which can be readily purified is the casein kinase II (CK2), for the octamer phosphorylation. The optimal peptide substrate for CK2 is RRRA-DDSDDDDD, where the serine is flanked by negative charged aspartic acid residues. Studies have shown that the most important substitutions which are detrimental to CK2 activity are in the +1 and +3 positions from the serine. Also, the addition of acidic residues at other locations in proximity

to the serine can help increase the activity of CK2 (Sarno et al., 1997). Due to the requirements of CK2 recognition motif, the histone tail of H2AX was mutated from KATQASQEY to KAEQDSEEY. The mutations were selected specifically because, the substitutions can help enhance CK2 activity but not affect the MDC1 BRCT binding to the c-terminal tail. We test the efficiency of CK2 *in vitro* and *in vivo* phosphorylation of the nucleosome core particles.

3.2 Objective

The dynamics of DDR proteins binding to the nucleosome is very important for understanding DNA repair mechanism. This chapter aims to validate methods of octamer phosphorylation for producing γH2AX nucleosomes. The modified nucleosomes will be used for MDC1 BRCT binding and structural studies. Previously, the mutation of H2AX tail to make it a better substrate of CK2 was performed. Also, octamer purification and the phosphorylation of H2AX-H2B dimer *in vitro* by CK2 was attempted (Islam, 2018). Enzymatic phosphorylation studies performed, showed that 1:1 molar ratio of substrate to CK2 enzyme produced phosphorylation signal that could be monitored. Increasing the concentration of enzyme led aggregation of the substrate. A high concentration of CK2 was used to stimulate complete phosphorylation of the H2AX tail.

First, radioactive kinase assays were performed to test the effect of glycerol on CK2 phosphorylation activity. The effect of widom 601 DNA in nucleosome on the CK2 phosphorylation of H2AX was also tested compared to the octamer. A cellular method of octamer phosphorylation was developed, and the extent of phosphorylation was compared with the *in vitro* phosphorylation method. A co-expression method of phosphorylation has been used in a study on the phosphorylation of heterochromatin protein 1 in *E. coli* cells (Hiragami-Hamada et al., 2011). The tandem BRCT domain of MDC1 was overexpressed and purified for binding studies with the octamer. A direct binding assay by fluorescence polarization was used to determine the binding affinity of MDC1 BRCT with the

γH2AX peptide. Finally, *E. coli* phosphorylated dimer was complexed with MDC1 BRCT to assess the phosphorylation efficiency.

3.3 Results

3.3.1 Effect of glycerol on CK2 in vitro phosphorylation of Octamer

We proposed that the presence of glycerol in the CK2 protein purification buffer reduced its ability to phosphorylate octamer. A radioactive kinase assay to visualize the effect of glycerol on the phosphorylation of octamer by CK2 was performed. The octamer was incubated with CK2 (with or without glycerol), ATP and γATP in kinase buffer. A time course phosphorylation of the octamer was performed to see if the intensity of H2AX will increase over time. An SDS PAGE gel of the samples was used to visualize the kinase reaction in Figure 3.1. Coomassie stained gel of octamer shows 4 histone bands but ^{32}P signal allows only visualization of phosphorylated proteins. The first three gel lanes are samples from octamer phosphorylation in the absence of glycerol. A CK2 protein band is seen at ~70 kDa which is due to the autophosphorylation of CK2 while the phosphorylation of H2AX histone is indicated by the ~17 kDa protein band. ^{32}P signal observed after 2 hours indicates phosphorylation of H2AX in octamer by CK2. After 4 hours, there is no increase in ^{32}P intensity and the addition of 1 molar equivalent of CK2 (4+), does not increase phosphorylation intensity. Compared to this, in the presence of glycerol H2AX phosphorylation intensity decreases as seen in the last three gel lanes. There is also a significant reduction of CK2 autophosphorylation intensity at ~70 kDa.

Glycerol negatively affects CK2 phosphorylation of the octamer *in vitro* as evidenced by the radioactive assay.

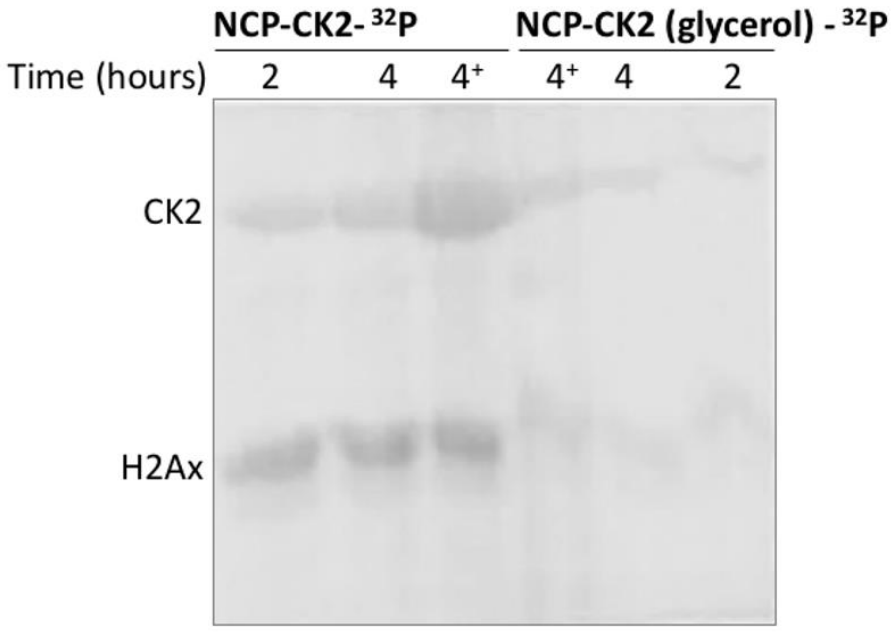

Figure 3.1: Effect of glycerol on CK2 phosphorylation of Octamer.
Time course comparison of CK2 mediated phosphorylation of octamer +/- glycerol. CK2 represents autophosphorylation signal and H2AX represents phosphorylation signal of the histone H2AX. (Image courtesy- Dr Rashmi Panigrahi).

3.3.2 Comparison of octamer and nucleosome *in vitro* phosphorylation

Now that we understand the effect of glycerol on CK2 activity, the next step to producing γH2AX nucleosomes was to perform a kinase reaction with nucleosomes. First, we were interested in comparing the CK2 phosphorylation extent in nucleosomes to the octamer. Due to the negative effect of glycerol, we wanted to test the effect of widom 601 DNA on the CK2 phosphorylation. The same radioactive kinase assay as above was performed to visualize H2AX phosphorylation in octamer and nucleosomes. The CK2 auto phosphorylation ^{32}P signal in both reactions indicates the activity of the enzyme (Figure 3.2). The histone H2AX is phosphorylated by CK2 in the octamer and the intensity does not increase over time. In contrast, there is no ^{32}P signal intensity of H2AX phosphorylation in nucleosome. Also, we noticed ^{32}P signal in a lower band which corresponds to the H2B histone protein. There are three serine residues in the H2B histone which are involved in other cellular signaling pathways (Rossetto et al., 2012). Over time, there is phosphorylation of the serine residues by CK2 which leads to the ^{32}P signal observed. The presence of widom 601 DNA negatively affects the phosphorylation of H2AX by CK2.

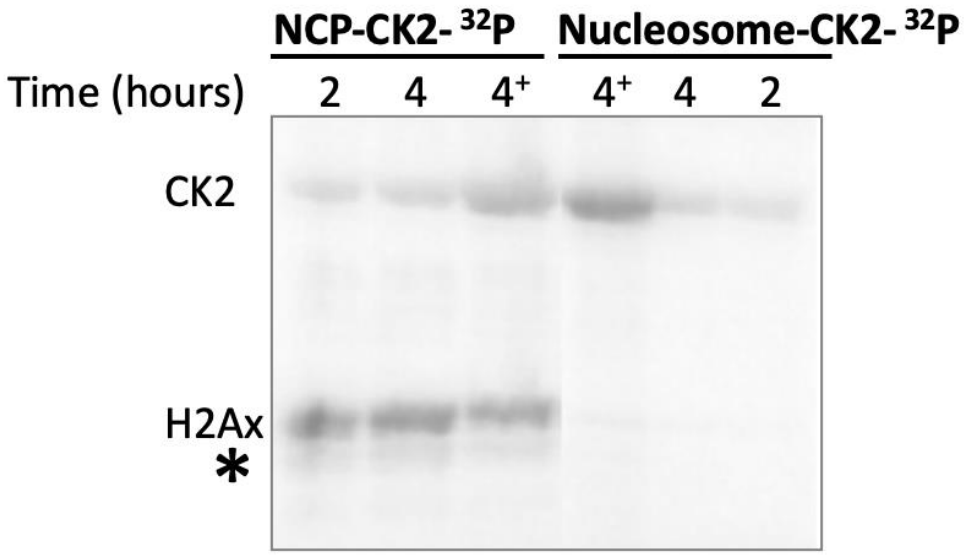

Figure 3.2: CK2 phosphorylation of octamer compared to Nucleosome.

Time course comparison of CK2 mediated phosphorylation of octamer and nucleosome.

CK2 represents autophosphorylation signal and H2AX represents phosphorylation signal of the histone H2AX.

* Indicates histone H2B phosphorylation.

(Image courtesy- Dr Rashmi Panigrahi).

3.3.3 Cellular phosphorylation of octamer

To enhance the phosphorylation of the octamer by CK2, a co-expression method was adopted to facilitate in vivo phosphorylation of the H2AX c-terminal tail. A small-scale expression check of this method was done to confirm phosphorylation. IPTG was used to induce the expression of CK2 and the histones. Cell lysate fractions of uninduced and IPTG induced samples were run on an SDS PAGE gel. Western blot probing for the phosphorylated S139 in the cell lysate fractions was performed. The alanine 139 (A139) mutant of H2AX was also co-expressed as a control for the *E. coli* phosphorylation. For the wild-type histone, S139 is phosphorylated by CK2 as indicated by the western blot in the induced lane (Figure 3.3). The blot also shows no phosphorylation of the A139 mutant in the cell lysate fractions. This confirms our co-expression method of H2AX phosphorylation is functional and large-scale amount of γH2AX containing octamer can be purified.

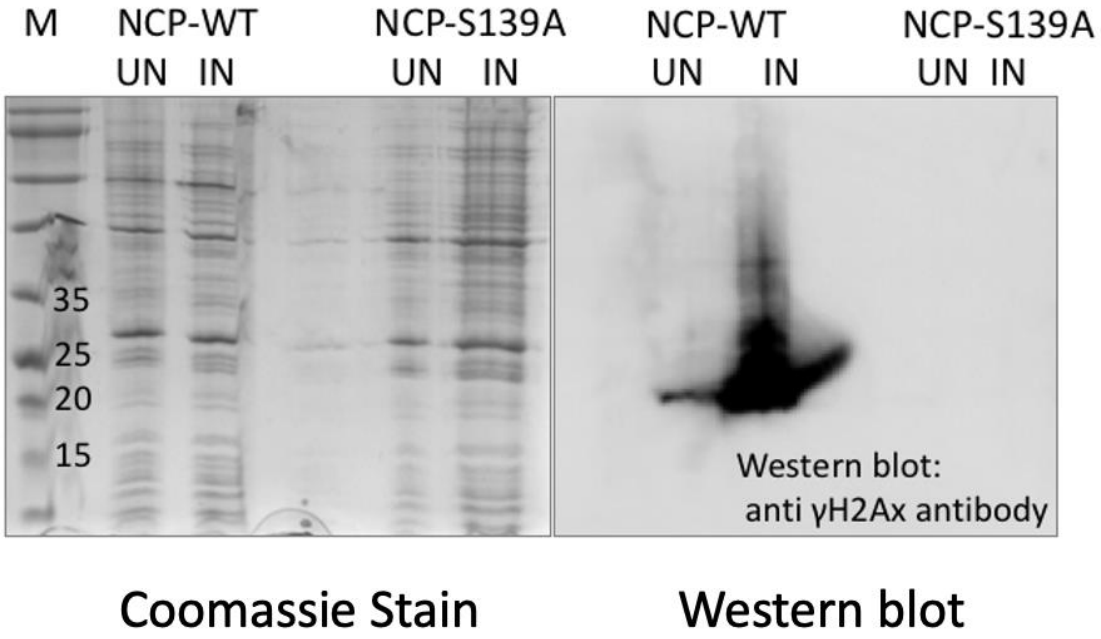

Figure 3.3 SDS-PAGE gel and western blot of octamer expression check.

In the left-hand panel: SDS-PAGE of samples from expression check, Un-induced (UI) and Induced (IN) cell lysate fractions of WT octamer and S139A octamer mutant.

In the Right-hand panel: Western blot of cell lysate samples probing for phospho-serine 139. (Image courtesy- Dr Rashmi Panigrahi).

3.3.4 Efficiency of cellular octamer phosphorylation

H2AX phosphorylation *in vivo* was performed, and the efficiency was compared to the *in vitro* method by western blot and radioactive kinase assay. The octamer was purified and incubated with CK2 and ATP *in vitro* to mediate phosphorylation. The *in vivo* phosphorylated octamer was also incubated *in vitro* with CK2, and ATP for 4 hours followed by a western blot probing specifically for phosphoserine 139. Using the octamer as a control, we observed further phosphorylation of the *in vivo* phosphorylated octamer upon incubation with CK2 (Figure 3.4A). Although, we are unable to quantify the percentage of phosphorylation, we decided to compare the phosphorylation levels to the octamer with the radioactive kinase assay (Figure 3.4B). We observed further phosphorylation of the *in vivo* phosphorylated octamer after 2,4 hours which confirms our western blot findings. Although, both methods do not yield complete phosphorylation of the H2AX histone, the *in vivo* phosphorylation method was used for binding studies with MDC1.

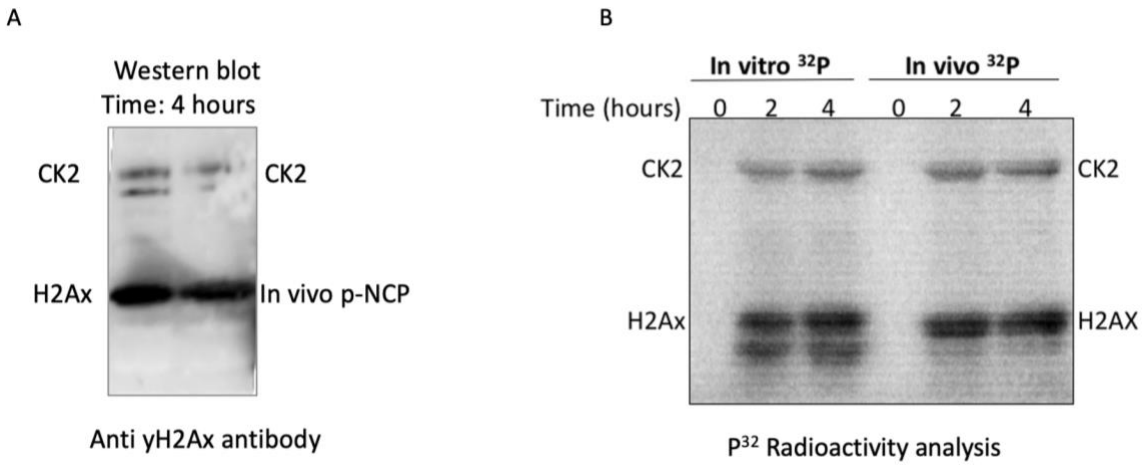

Figure 3.4 Octamer in-cell compared to *in vitro* phosphorylation. (A) Western blot of sample from kinase reaction after 4 hours. (B) Time course comparison of octamer phosphorylation by radioactive assay *in vitro*. CK2 mediated phosphorylation of octamer in vitro compared to further phosphorylation of purified *in vivo* phosphorylated octamer.
(Image courtesy- Dr Rashmi Panigrahi).

3.3.5 MDC1 BRCT binding to cell phosphorylated H2AX-H2B dimer.

The H2A and H2B dimer is stable in solution and the binding of MDC1 BRCT (fragment of MDC1 containing BRCTs) was tested as a preliminary step before the *in vivo* phosphorylated octamer. The γH2AX-H2B dimer was purified and incubated with the MDC1 BRCT. The complex was then loaded on an SEC column to confirm the interaction and the fractions were analysed by SDS PAGE. The results from the size exclusion chromatography are shown in figure 3.5. MDC1 BRCT purification elution peak on the same SEC column yields protein present in the C8-C13 fractions. The presence of MDC1 in the C5-C7 fractions when incubated with the *in vivo* phosphorylated H2AX-H2B dimer demonstrates the interaction. The un-phosphorylated dimer does not interact with the MDC1 BRCT as the protein is absent in the C5-C7 fractions. The intensity of MDC1 in the complex fractions is not equal to the dimer and an increase in the molar ratio of MDC1 to γH2AX-H2B dimer has no effect. The results show our *in vivo* phosphorylated dimer specifically interacts with the MDC1 BRCT, but the incomplete phosphorylation of H2AX limits the complex formation.

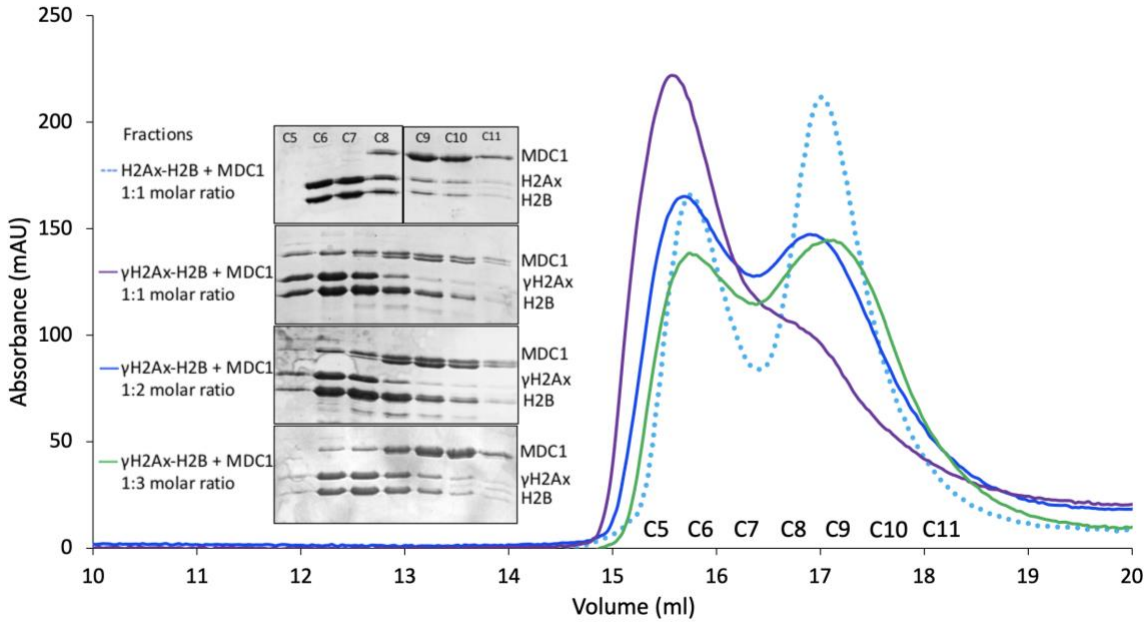

Figure 3.5: MDC1 BRCT binding γH2AX-H2B dimer. Size exclusion profile of MDC1 and H2AX-H2B dimer incubation. Dotted blue line indicates profile of unphosphorylated dimer and MDC1. Solid lines are profiles with varying molar ratio of MDC1 BRCTs with γH2AX-H2B dimer. SDS-PAGE analysis of fractions corresponding to each elution peak is included.

(Image courtesy- Dr Rashmi Panigrahi).

3.4 Discussion

This chapter aimed to produce γH2AX nucleosomes for binding to the MDC1 BRCTs which can eventually be used for structural studies. The H2AX C-terminal tail had been mutated to include acidic residues and make it a better substrate for CK2 phosphorylation. First, we performed radioactive kinase assays to examine the effect of glycerol on CK2 phosphorylation of the octamer. We found that glycerol negatively affects the ability of CK2 to phosphorylate the octamer. Glycerol has been used over the years to stabilize proteins after purification and prevent aggregation. In some cases, glycerol has been found to increase the enzymatic activity of proteins and improve activity (Leandro et al., 2001; Vagenende et al., 2009). In this case, the negative effect of glycerol can be explained with Kramer's theory. The increase in solvent viscosity due to the glycerol, resulted in a decrease in the CK2 enzyme motion thereby preventing the conformational changes required for enzyme kinase activity. In fact, a direct correlation was found between viscosity (η) and the inhibition of the maximum rate of catalysis (V_{max}) (Uribe & Sampedro, 2003). Next, the in vitro phosphorylation preference of octamer or nucleosome by CK2 was probed. We concluded that CK2 phosphorylates the H2AX in octamer and not the nucleosome which was confirmed by the radioactivity analysis. This finding could be because of electrostatic repulsion with the DNA present in nucleosome that prevent interaction of CK2 with the H2AX c-terminus tail. The ATM kinase which phosphorylates the H2AX tail in vivo contains a "leucine zipper" domain which are commonly found in transcription factors(Savitsky et al., 1995; Zeng et al., 1997).

This domain has a DNA binding property as well as facilitating protein-protein dimerization (Landschulz et al., 1988). In the ATM kinase, it could function in promoting interaction with the H2AX histone in the nucleosome. CK2 lacks this domain which explains the loss of interaction with the nucleosome.

We observed the phosphorylation of histone H2B by CK2 in vitro which could be any of the serine/threonine sites present in the protein. We moved on to a co-expression method of octamer phosphorylation *in vivo* which was validated by western blot of the protein expression. Probing specifically for phosphoserine 139, we confirmed the *in vivo* phosphorylation of H2AX and purified the phosphorylated octamer. We compared the extent of this phosphorylation by radioactivity assay to the non-phosphorylated octamer. Although, mutations were performed to the H2AX c-terminal tail to increase the CK2 recognition, both phosphorylation methods were incomplete. Also, we still visualized the incorporation of ^{32}P in the kinase assay performed with *in vivo* phosphorylated octamer. A high concentration of CK2 (1:1 molar ratio) was used to prevent the incomplete phosphorylation, as well as the long hours of incubation. This only led to a lack of specificity observed by the phosphorylation of the H2B histone. The γH2AX/H2B dimer was then purified to test the interaction with MDC1 BRCTs by SEC. Our results showed the MDC1 interacts with γH2AX/H2B dimer and not the H2AX/H2B dimer as expected. However, the intensities of MDC1 and dimer were not equal and increasing the molar ratio of MDC1 did not change the outcome. This result reiterates the incomplete phosphorylation of the octamer by CK2 in the *in vivo* method.

CHAPTER 4: BRCA1 PEPTIDE INHIBITOR STUDIES

4.1 Introduction

DNA damage persistence leads to the accumulation of mutations and instability of the genome. Mutations in DNA repair genes are associated with organ-specific cancers and are responsible for tumorigenesis, progression, and resistance (Dietlein et al., 2014). Ironically, the conventional treatments for cancer progression involve the use of DNA damaging agents to incapacitate the DNA damage repair mechanism and force death of the cancer cells (Samadder et al., 2016; Tubbs & Nussenzweig, 2017). This exploits the weakness and dependency of tumor cells on a specific pathway of DNA repair which are mostly absent in normal cells. Targeting DDR proteins by an approach known as synthetic lethality can help improve the specificity and efficiency of cancer therapy (O'Connor, 2015). The concept of synthetic lethality involves the situation where a cell is viable with defect in one gene, but the loss of function of another gene combined with this defect leads to cell death (Lord et al., 2015). The development of novel inhibitors which disrupt the DDR pathway in cancer cells can take adequate use of the synthetic lethality concept. This is evidenced by the recently developed PARP inhibitors (Rouleau et al., 2010).

BRCA1 is a widely known tumor suppressor protein and belongs to the BRCT family of proteins which are significantly involved in DNA damage responses. The BRCT domain which typically exist as tandem repeats, mediate phosphorylation-dependent protein-protein interactions (Rodriguez et al., 2003).

Majority of cancer-related mutations in BRCA1 are located in the BRCT and RING domains (Lee et al., 2010). The location of these mutations prevents the protein-protein interaction (PPI) required for BRCA1 function in HR. This has led to the successful results of cancer treatment with PARP inhibitors and opens an avenue for the development of new therapies. Although, the sporadic form of breast and ovarian cancers are not driven by BRCA1 mutations (Johnson et al., 2013). The development of inhibitors which block the BRCT domain can result in a mimic of the HR deficient BRCA1 mutant. This coupled with PARP inhibitors or other cancer therapies can help suppress DDR in cancer cells and sensitize them, thereby improving treatment efficiency.

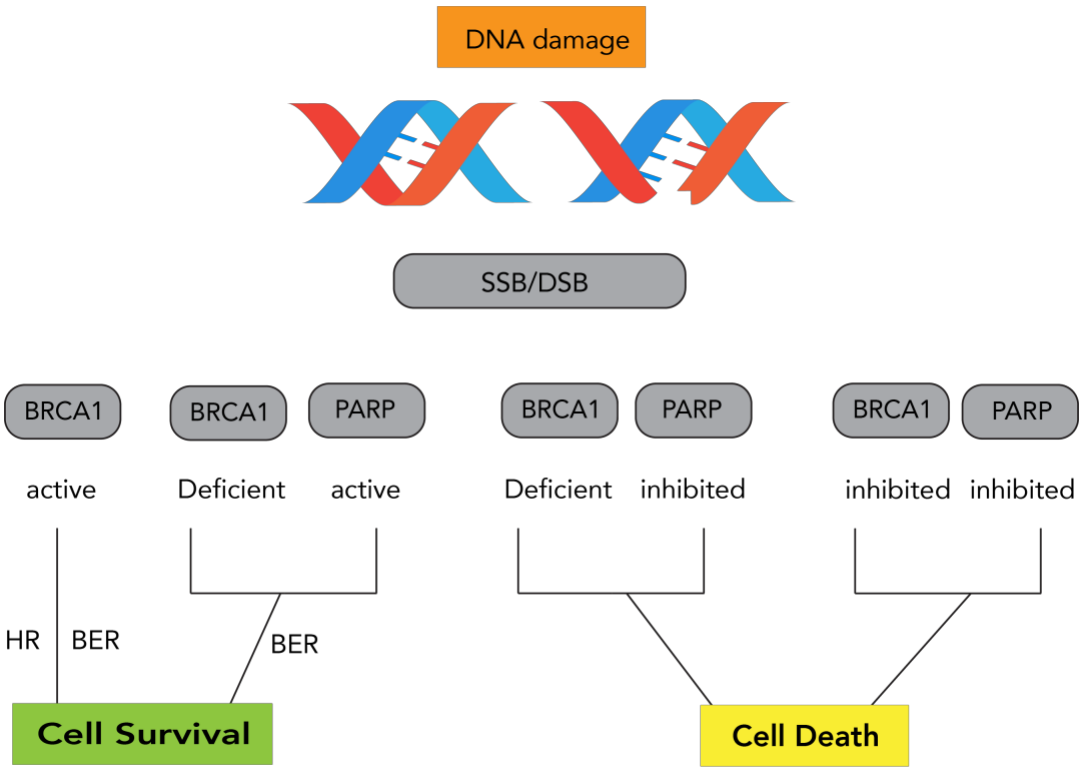

Figure 4.1 Synthetic Lethality PARP & BRCA1 inhibitors.

Single strand breaks and double strand breaks are repaired by base excision repair and homologous recombination respectively in normal cells. BRCA1 deficient cells rely on BER to repair damage for cell survival. Inhibition of PARP in BRCA1 deficient tumor cells results in genomic instability and cell death after DNA damage. BRCA1 inhibitor leads to HR deficiency in tumor cells, coupled with PARPi/ DNA damaging agents result in cell death.

The development of inhibitors for the BRCT domain has been challenging due to the phosphorylation requirement of their binding partner. Recently, a potent non-phosphopeptide which binds to the BRCT domain of BRCA1 with similar affinity to its native phosphoserine-containing peptide, was developed and tested. The peptide known as peptide 8.6 nat (MCTIDFDEYRFRKT-NH_2) was able to block BRCA1 BRCT interaction with other proteins. It was developed by mRNA screening and a ribosomal translation system known as "PURE" (Figure 4.2). Fluorescence polarization was used to validate the ability of peptide 8.6 nat to compete off BACH1/FANCJ peptide and abolish the interaction with the BRCA1 BRCT. The crystal structure (Figure 4.3A) of the peptide 8.6 nat bound in the same phospho-binding pocket as BACH1 peptide in the BRCA1 BRCT domain was also solved to 3.05 Å (White et al., 2015). Our collaborator Dr. Matt Hartman (Department of Chemistry, Virginia Commonwealth University) has developed a cell penetrable peptide 8.6 (CPP 4i 8.6) version of the peptide 8.6 nat which can be readily imported into cells (Abrigo et al., 2020). This creates the possibility of in-vivo studies of the peptide on BRCA1 BRCT interactions to assess the drug potential of this inhibitor.

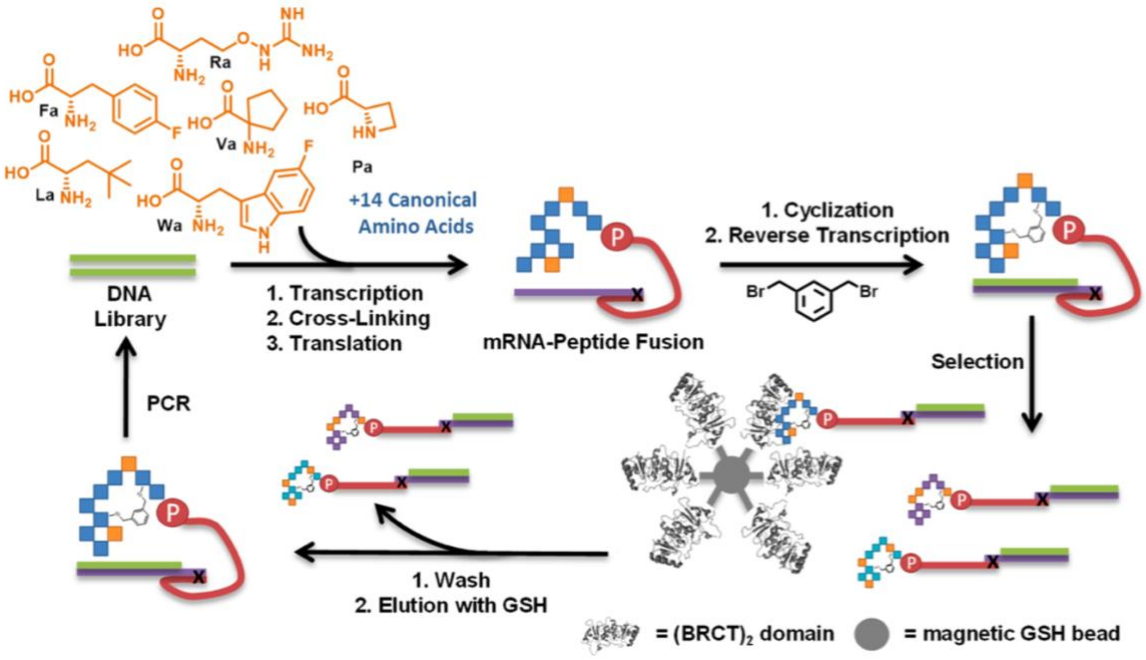

Figure 4.2 Model for peptide selection strategy of BRCA1 BRCT inhibitor. Reprinted from "Peptide Library Approach to Uncover Phosphomimetic Inhibitors of the BRCA1 C-Terminal Domain" by White, E.R., Sun, L., Ma, Z., Beckta, J.M., Danzig, B.A., Hacker, D.E., Huie, M., Williams, D.C., Edwards, R.A., Valerie, K. and Glover, J.M., 2015. ACS chemical biology, 10(5), Copyright 2021 by Elsevier Inc. Reprinted with permission.

The DNA library encodes 12 amino acid random region with an N-terminal cysteine. Translation is done in vitro, the unnatural amino acids (Pa, La, Fa, Ra, Wa, Va) shown are incorporated into the peptide library along with 14 canonical amino acids. The single letter abbreviation denotes which amino acid is replaced by the analog (e.g., Fa replaces F). After mRNA-peptide fusion formation, peptides with a second cysteine are cyclized with dibromo xylene. Purified mRNA-peptide fusions undergo reverse transcription before being selected for binding to GST-$(BRCT)_2$ fusion immobilized on magnetic resin. Unbound peptides are washed away, bound peptides are eluted, PCR amplified, and carried through another round of selection.

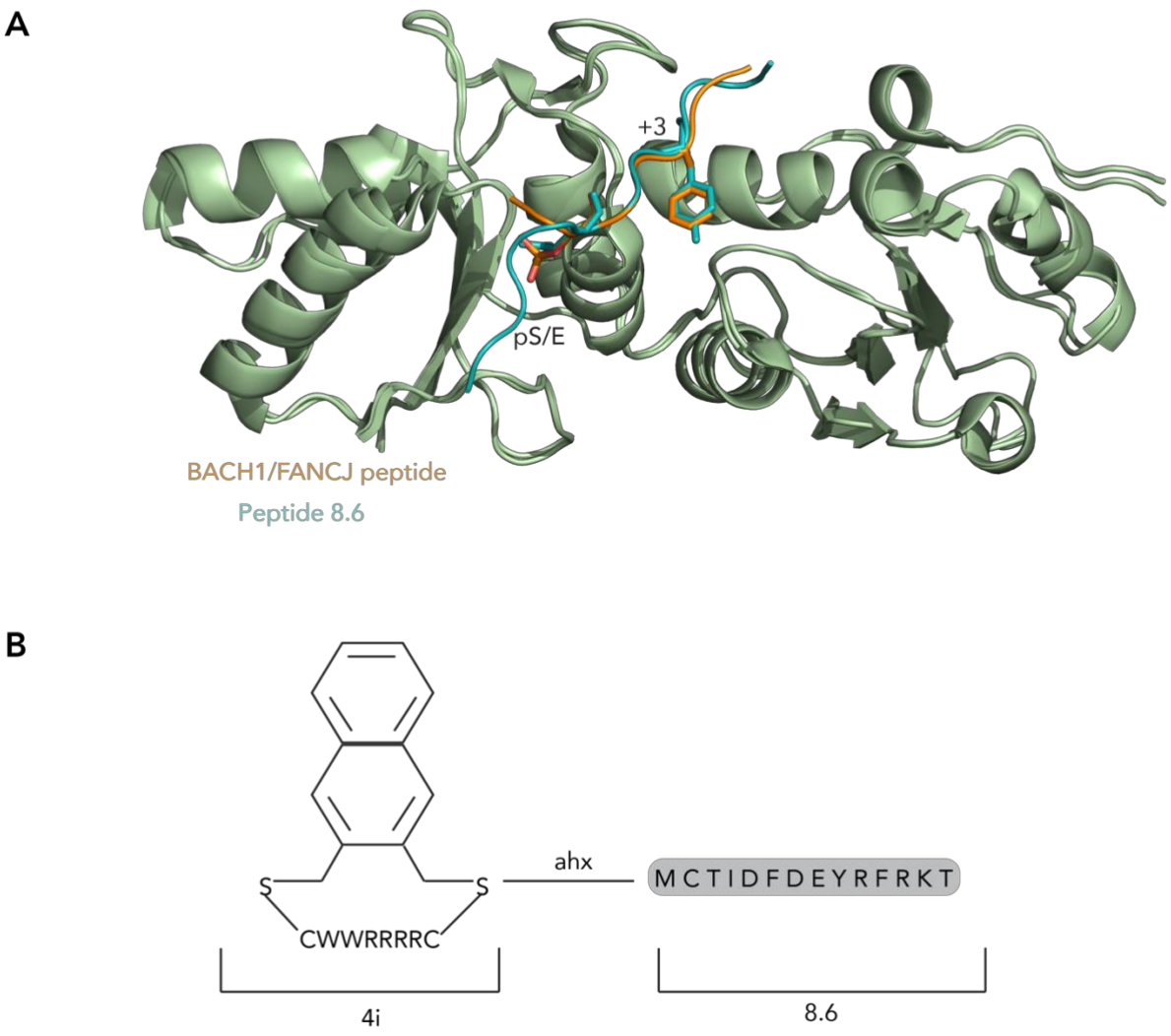

Figure 4.3 BRCA1 BRCT and CPP 4i 8.6.

(A) Crystal structure of BRCA1 BRCT bound to peptide 8.6 (PDB ID: 4OFB) superimposed on the structure of BRCA1 BRCT bound to BACH1 peptide. (PDB ID: 1T15). BACH1 peptide in orange and peptide 8.6 nat in teal. (B) Visual representation of CPP 4i 8.6. Hydrophobic group (4i) spaced from peptide by 6-aminohexanoic acid (ahx).

4.2 Objective

The addition of a hydrophobic group to the peptide 8.6 nat could affect the binding affinity to BRCA1 BRCT. We needed to test the ability of CPP 4i 8.6 to prevent BRCA1 interaction with its binding peptide and compare to recent finding before *in vivo* experiments are performed. This chapter aims to address the binding ability and specificity of CPP 4i 8.6 by fluorescence polarization assays.

First, the tandem BRCT domains of BRCA1 and MDC1 were overexpressed and purified. Direct fluorescence polarization assay was used to determine the binding affinity of the purified BRCTs domain to their native binding peptides. We also, show that the BRCT domain of BRCA1 can bind to the γH2AX peptide and that of MDC1 can bind the BACH1/FANCJ (SRSTpSPTFNK-NH_2) peptide. Using a competitive fluorescence polarization assay, we test the ability of CPP 4i 8.6 to compete with the BACH1/FANCJ peptide on the BRCA1 tandem BRCT domains in vitro. We also test the ability of this peptide to block interactions between the MDC1 BRCT and γH2AX peptide to show its specificity.

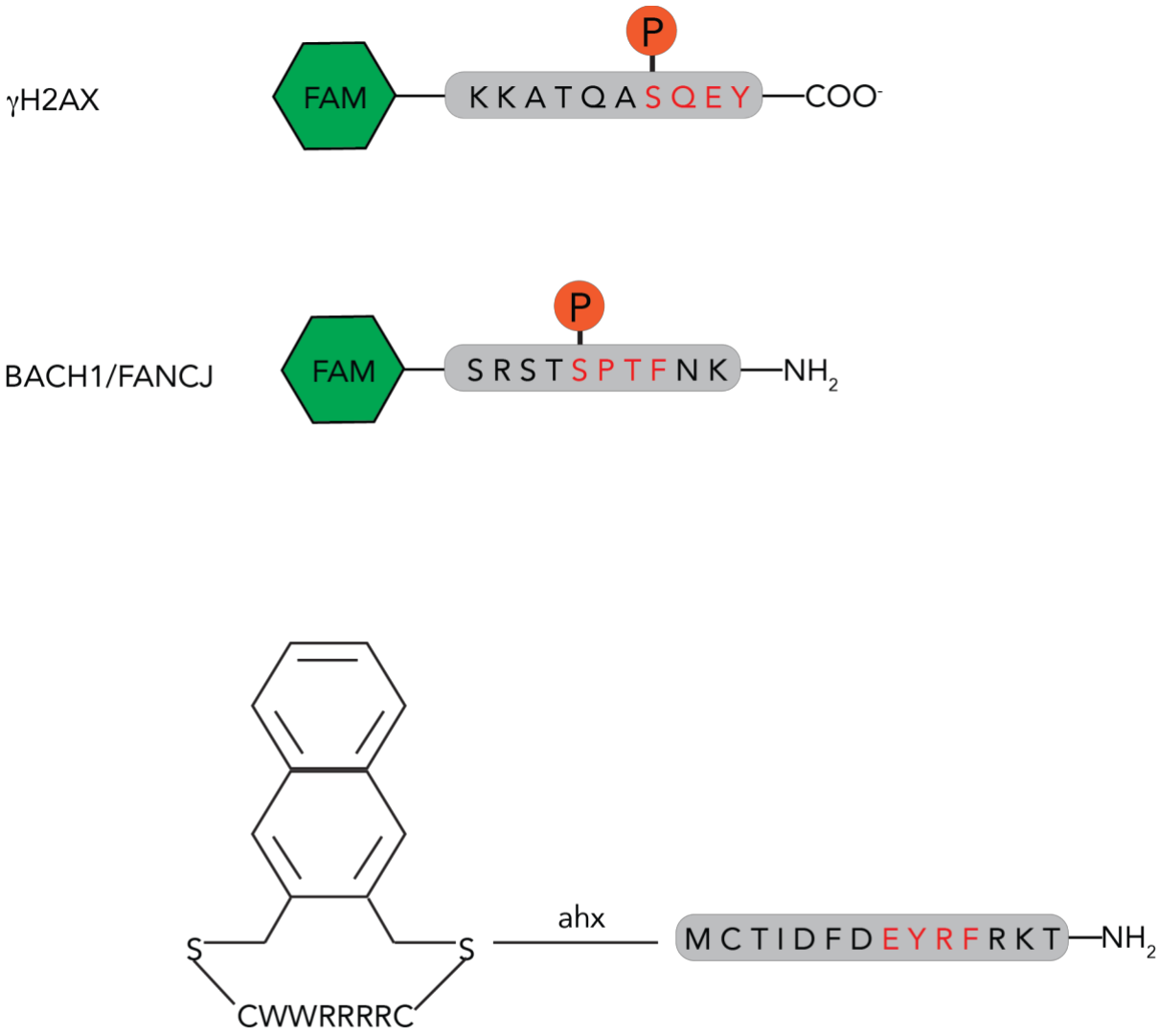

Figure 4.4 Fluorescence Polarization Peptides. Respective sequences of γH2AX, BACH1/FANCJ and CPP 4i 8.6 peptides. Important residues for binding to BRCT domain highlighted in red.

4.3 Results

4.3.1 BRCA1 BRCT binding to BACH1 and γH2AX peptide

To test the specificity and ability of the inhibitor (CPP 4i 8.6) to bind BRCA1, we purified BRCA1 BRCT and fluorescence polarization was used to measure its interaction with the BACH1/FANCJ peptide. A binding affinity of ~0.46 μM (Figure 4.5A) was obtained. We also tested the possibility of BRCA1 BRCT binding to the γH2AX peptide which is the native binding partner of MDC1 BRCT. We found that BRCA1 BRCT also binds to the γH2AX peptide with a binding affinity of ~28.13 μM (Figure 4.5B). In conclusion, our purified BRCA1 BRCT binds to the BACH1/FANCJ peptide with similar affinity that was previously reported in (Sun, 2017). The γH2AX peptide is also recognized by the BRCT but with ~ 60-fold lower affinity.

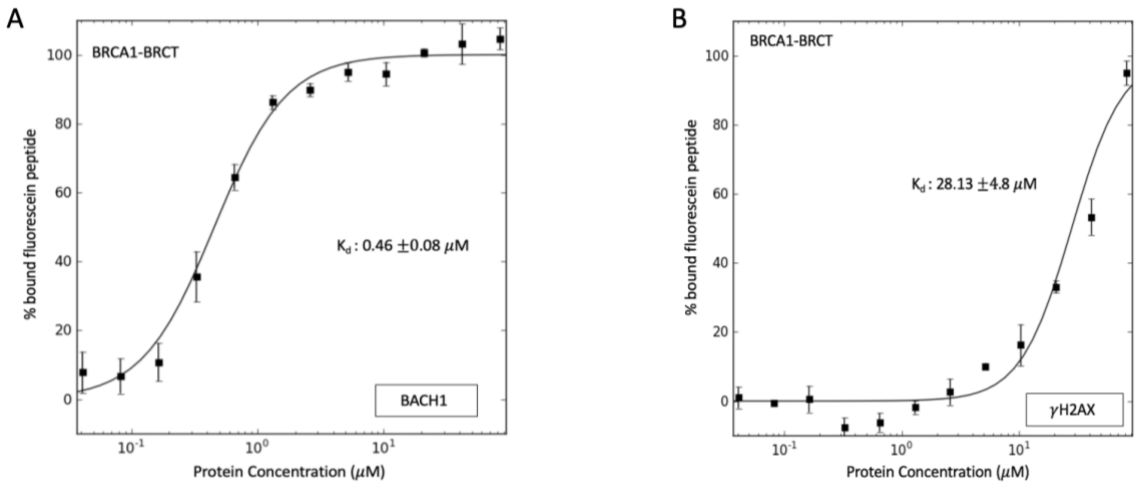

Figure 4.5: Fluorescence polarization studies with BRCA1 BRCT. (A) FP direct binding assay of BRCA1 BRCT with Bach1/FancJ peptide. (B) FP direct binding assay of BRCA1 BRCT with γH2AX peptide.

4.3.2 MDC1 BRCT binding to BACH1 and γH2AX peptide

We were interested to see if the MDC1 BRCT domain can bind to the BACH1/FANCJ peptide. Fluorescence polarization was used to measure the interaction of MDC1 BRCT with the BACH1/FANCJ peptide and we obtained a binding affinity of ~5.15 μM (Figure 4.6B). This binding was expected with lower affinity as the BACH1/FANCJ peptide does not contain the carboxyl-terminus at +3 position. We performed the binding of MDC1 BRCT to the γH2AX peptide and obtained an affinity of ~1.1 μM (Figure 4.6A). This is similar to the previously reported finding in (Campbell et al., 2010). The results demonstrate our purified MDC1 BRCT can bind both BACH1 and γH2AX peptides.

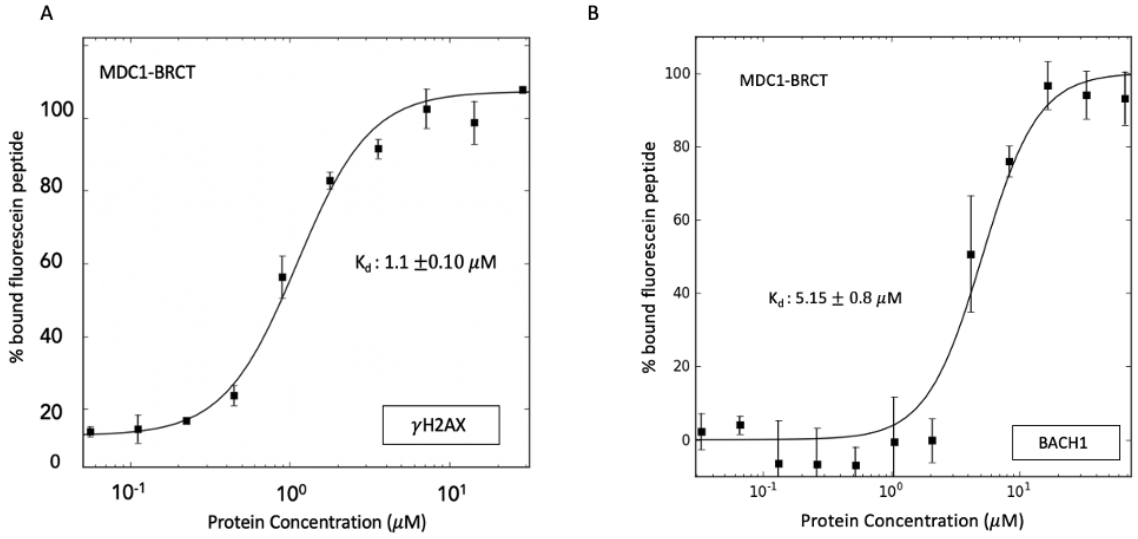

Figure 4.6: Fluorescence polarization studies with MDC1 BRCT. FP direct binding assay of MDC1 BRCT with BACH1/FANCJ and γH2AX peptide.

4.3.3 CPP 4i 8.6 is specific to BRCA1 and inhibits its interaction with other binding partners

Previously, our collaborators have developed the peptide 8.6 nat inhibitor and shown its ability to prevent the binding of phosphorylated binding partners (White et al., 2015). A cell-penetrable version of this peptide has now been developed which will allow for *in-vivo* studies of the inhibitor (Abrigo et al., 2020). We were interested to validate if the new version of the inhibitor will behave similarly to the previous studies. This is because of the hydrophobic group addition to the N-terminus which might mediate other interactions with the BRCT domain. Using fluorescence polarization, competition assay was performed by introducing increasing concentrations of the cell-penetrable peptide 8.6 (CPP 4i 8.6) to BRCA1 BRCT phosphopeptide complexes. A decrease in polarization was observed which indicates the CPP 4i 8.6 inhibits the interaction of BRCA1 BRCT with BACH1 peptide. The inhibition curve has an $IC_{50} \sim 151.4$ μM which is equivalent to $K_i \sim$ 12.5 μM calculated using the Coleska-Wang equation (Figure 4.7A).

We also examined the specificity of the CPP 4i 8.6 on the BRCT domain by performing the same competition assay against the MDC1 BRCT phosphopeptide complex. There was no decrease in polarization observed which indicates the peptide cannot disrupt the binding of MDC1 BRCT to the γH2AX peptide. This suggests the CPP 4i 8.6 is specific to the BRCA1 BRCT and does not bind to MDC1

BRCT. A control experiment was also performed in the absence of the MDC1 BRCT as shown in blue (Figure 4.7 B).

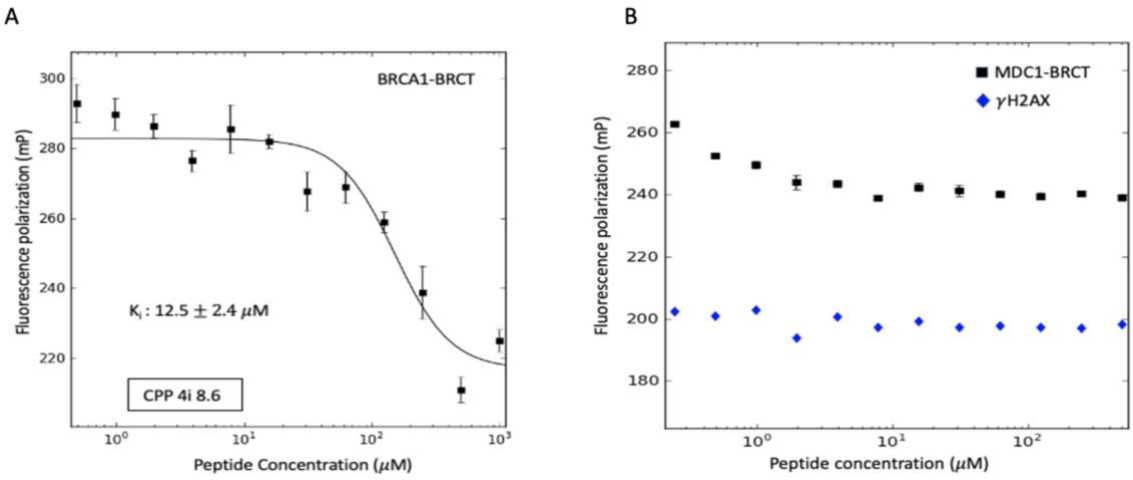

Figure 4.7: CPP 4i 8.6 is a specific inhibitor for BRCA1 BRCT. (A) FP competition assay of CPP 4i 8.6 against BACH1/FANCJ peptide. (B) FP competition assay of CPP 4i 8.6 against γH2AX peptide.

4.4 Discussion

In summary, this chapter aims to characterize the ability of CPP 4i 8.6 to disrupt BRCA1 BRCT PPI and test the specificity of this peptide. Using fluorescence polarization, we determined the binding affinity of purified BRCA1 BRCT to BACH1/FANCJ peptide to be ~ 0.46 μM. In 2015, our collaborator developed the peptide 8.6 nat and showed that the peptide binds to BRCA1 BRCT with a K_D of 3.7 μM by isothermal titration calorimetry (ITC) (White et al., 2015). The CPP 4i 8.6 contains a cell penetrating peptide sequence as well as an aromatic group upstream of the BRCT-binding peptide (Abrigo et al., 2020). Although, these additions are important for the cellular uptake of the peptide, they could affect the solubility and binding ability of the peptide to the BRCA1 BRCT in vitro. The aromatic group and peptide sequence added might also enhance non-specific protein binding due to the hydrophobic nature.

Using competitive fluorescence polarization, it was reported that a decrease in polarization was observed with increase in peptide 8.6 nat concentration (Sun, 2017). An inhibition curve with IC_{50} ~ 98.3 μM, corresponding to K_i ~ 11 μM was generated from the assay. We decided to perform the same in vitro experiments with the CPP 4i 8.6 and compare its inhibition constants. A clear decrease in polarization was observed and the inhibition curve generated an IC_{50} ~ 151.4 μM, corresponding to K_i ~ 12.5 μM. This suggests that the CPP 4i 8.6 binds to BRCA1 BRCT with comparable affinity to the free peptide 8.6 nat. Testing the specificity of CPP 4i 8.6, we introduced the peptide with increasing concentrations until solubility to the

MDC1 BRCT γH2AX peptide complex. There was no decrease in polarization which indicates the peptide is unable to bind the MDC1 BRCT domain.

Finally, we solidify our claim of CPP 4i 8.6 specificity by showing the ability of the BRCT domains to bind other phospho-peptides. The BRCA1 BRCT binds to the γH2AX peptide with about a 20-fold lower affinity compared to MDC1 binding the peptide. BRCA1 BRCT bound to the γH2AX (pSQEY-COO^-) with a K_d ~ 28.13 μM. BRCA1 has been shown to bind a tetrapeptide with a free C-terminal carboxylate (pSPTF-COO^-) in a study done to determine the specificity of the BRCT domains. MDC1 dramatically preferred the free carboxylate (pSQEY-COO^-) and a 50-fold increase in affinity was observed for the amidated peptide (pSQEY-$CONH_2$) (Campbell et al., 2010). We observed MDC1 BRCT binding to the BACH1/FANCJ peptide with a K_d ~ 5.15 μM. The fact that BRCT domains of MDC1 and BRCA1 can bind contrasting phosphopeptide is understandable due to the conserved structure of the BRCT domain. The BRCA1 BRCT peptide sequence pS-P-X-F is relatively similar to the γH2AX peptide sequence pS-Q-E-Y-COOH. Difference in the hydrophobic binding pocket environment of both BRCTs results in the peptide specificity. A conserved arginine residue, Arg1933 in MDC1 and Arg1699 in BRCA1 forms a double salt bridge interaction with the C-terminal carboxylate in γH2AX or backbone oxygen of C-terminal amide in BACH1/FANCJ peptide. In BRCA1, the Arg1699 guanidium group is stabilized by internal interactions with Asp1840 and Glu1836 which keeps it more buried in the pocket. The side chain nitrogen (Nε) of Arg1699 forms hydrogen bond interaction with the peptide

backbone. However, the BRCA1 Asp1840 has been replaced in MDC1 BRCT with a Thr2067. The Arg1933 forms internal interaction with only the Glu2063 which makes it slightly less buried. The arrangement of the residues in the hydrophobic binding pocket of MDC1 allows the Arg1933 guanidium group to form stronger interactions with peptide containing a free carboxylate group. Although, we have shown some cross-interaction between MDC1 and BRCA1 BRCTs, CPP 4i 8.6 is highly specific to the BRCA1 BRCT.

The peptide 8.6 nat binding to BRCA1 was improved by the addition of residues which interact with the BRCA1 BRCTs outside of the phosphoserine and hydrophobic binding pockets (White et al., 2015). The peptide residues N- and C-terminal to the glutamate interact with the BRCT in ways predicted to improve the binding. The high degree of peptide 8.6 nat specificity to BRCA1 BRCT has been depicted in figure 4.8. The peptide +1 tyrosine stacks against the N1774 in BRCA1 which is equivalent to P2009 in MDC1. The E1698 in BRCA1 interacts with arginine residues in +2 and +4 positions of the peptide. E1698 is equivalent to R1932 in MDC1 which points away from the arginine residues. Lysine at +5 position of peptide interacts with D1840 and E1836 of BRCA1 BRCT. The Ile at -4 position and 4FPhe at -2 of the peptide interact with an hydrophobic groove formed by F1662, P1659, L1657 and V1654 in BRCA1. However, these residues are not conserved in MDC1 BRCT which prevents the critical interactions outside of the peptide binding pockets important for recognition. Based on the structural alignment

in figure 4.8, the additional surfaces for interaction of BRCA1 BRCT with peptide 8.6 nat are not well conserved in MDC1 BRCT.

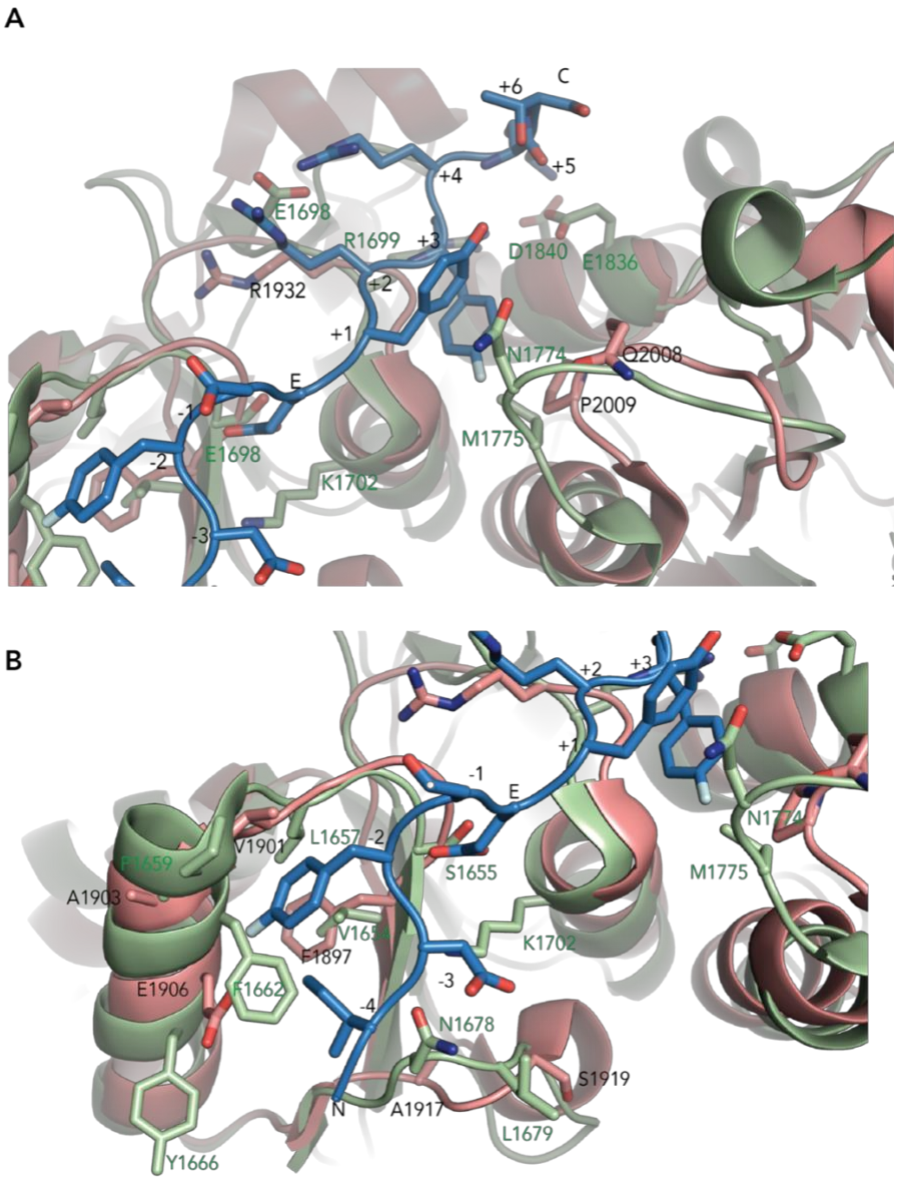

Figure 4.8 Peptide 8.6 nat specifically binds BRCA1 BRCT compared to MDC1 BRCT. Alignment of BRCA1 BRCT (green) -peptide 8.6 (blue) complex (PDB id: 4OFB) with the MDC1 BRCT domain (pink, PDB id: 2AZM). Key residues at the peptide-BRCT interface shown as sticks and labelled (BRCA1: green & MDC1: black).

CHAPTER 5: LAC ARRAY SYSTEM FOR BRCA1 PEPTIDE INHIBITOR STUDIES

5.1 Introduction

The development of inhibitors that target the key DDR proteins has been a promising approach in cancer therapy improvement. The dysfunctional DDR pathways in cancer cells allow for the development of specific targets by synthetic lethality. PARP inhibitors have improved the treatment of BRCA-deficient cancers and there is a growing interest in other effective inhibitors that target DDR (Rouleau et al., 2010). BRCA1 is a widely studied protein that is heavily involved in DDR pathways, cell cycle checkpoint, transcriptional regulation, and protein ubiquitination (Sato et al., 2012; Raimundo et al., 2021). The recruitment of BRCA1 to the site of DNA damage is dependent on the BRCA1 A complex which comprises Abraxas, BRCC36, Rap80, and other proteins (B. Wang et al., 2007a). Abraxas (also known as CCDC98) contains the pSPxF BRCA1 binding motif at the C-terminus, a coiled-coil domain for dimerization with the BRCC36 protein, and, an N-terminal MPN domain for interactions with the receptor-associated protein (RAP80) (Kim et al., 2007). In the BRCA1 A complex, Abraxas connects BRCA1 with Rap80 which contains the ubiquitin interacting motif (UIM) necessary for the complex retention at the damage site (B. Wang et al., 2007a) .

Following DNA damage, the phosphorylation of H2AX (γH2AX) happens in immediate vicinity of DSBs and leads to the recruitment of MDC1. The ubiquitination of the histones H1 is then mediated by MDC1 direct interaction with the E3 ubiquitin ligase -RING finger protein 8 (RNF8) with help from the E2 ubiquitin-conjugating enzyme 13 (UBC 13) (Schwertman et al., 2016). Rap80

specifically interacts with the Lys 63 ubiquitin chains at the foci (Sobhian et al., 2007). BRCA1 is also involved in DNA end resection and ATM signaling through the BRCA1C complex. This is composed of CtBP interacting protein (CtIP) and the meiotic recombination 11 (MRE11)-RAD50-NBS1 complex (MRN complex) (Huen et al., 2010). BRCA1 interacts directly with CtIP with its BRCT domain in a phosphorylation-dependent manner (Varma et al., 2005). This enables the recruitment of BRCA1 to the site of DNA damage for the homologous recombination pathway of DNA damage repair.

Studies over the years have revealed BRCA1 to be a central component in the multiple pathways of DDR. Small molecules which target the BRCT domain of BRCA1 can prevent its interaction with the BRCA1 A and C complexes for DDR function. A small non-phosphorylated peptide (peptide 8.6 nat) developed by mRNA selection was shown to prevent the binding of BRCA1 *in vitro* to its binding partners (White et al., 2015). Cellular internalization of this peptide is required for further studies on its ability to inhibit BRCA1 function *in vivo*. The issue of cell permeability was solved by the recent development of short cell-penetrating peptide (CPP) technology. The linear peptide is fused to a CPP cyclized with an aromatic group (CPP 4i 8.6) to improve the uptake and endosomal escape. The uptake of the fluorescein labelled CPP 4i 8.6 peptide was confirmed in mammalian cells by flow cytometry (Abrigo et al., 2020). To directly probe the inhibitory ability of the peptide, we used a previously characterized Lac-repressor/operator tethering system (Orthwein et al.,

2015). This system was used to visualize the ability of CPP 4i 8.6 to disrupt the BRCA1-abraxas interaction.

In the previous chapter, we have shown by fluorescence polarization how the CPP 4i 8.6 is able to specifically inhibit BRCA1 BRCT binding to the BACH1 peptide. Here we test the cell-permeability of the CPP 4i 8.6 and develop a system to visualize the inhibitory effect of the peptide.

5.2 Objective

This chapter aims to test the permeability of the newly designed CPP 4i 8.6 and its ability to inhibit BRCA1 interaction with Abraxas. Using the Lac repressor (lacI)/ Lac operator (lacO) system which has been used to visualize specific protein-protein interactions in DDR (Orthwein et al., 2015; Robinett et al., 1996; Soutoglou et al., 2007) . U2OS cells stably expressing an array of 256 copies of the lacO gene were used for the experiments. In this case, mCherry-BRCA1 fused to the lacI protein can be tethered to the lacO due to the high affinity of DNA binding by lacI. This provides a controllable system that takes advantage of the DDR Abraxas phosphorylation for interaction with BRCA1 away from the damage site. Thus, we can visualize the direct effect of the peptide specifically on the disruption of the BRCA1-Abraxas interaction. This eliminates the complexity of potential interactions with other DNA damage proteins found at DNA double-strand break foci. A schematic of the lac array system has been depicted in figure 5.1.

First, U2OS reporter cells were transfected with the mCherry-tagged LacR-BRCA1 to confirm the localization to the lac array. We then probed the localization of Abraxas to the lac array using a fluorescent antibody. Abraxas co-localization with BRCA1 at the array was visualized before and after irradiation. Next, we visualized the cellular uptake of CPP 4i 8.6 and its effect on abraxas localization to the lac array. Peptide 8.6 nat was overexpressed as a fusion to EGFP using a doxycycline (DOX)-controlled promoter. We observed an interaction between the

fusion peptide and BRCA1 at the lacO. Fluorescence recovery after photobleaching (FRAP) was used to confirm the interaction of BRCA1 with the EGFP-peptide 8.6.

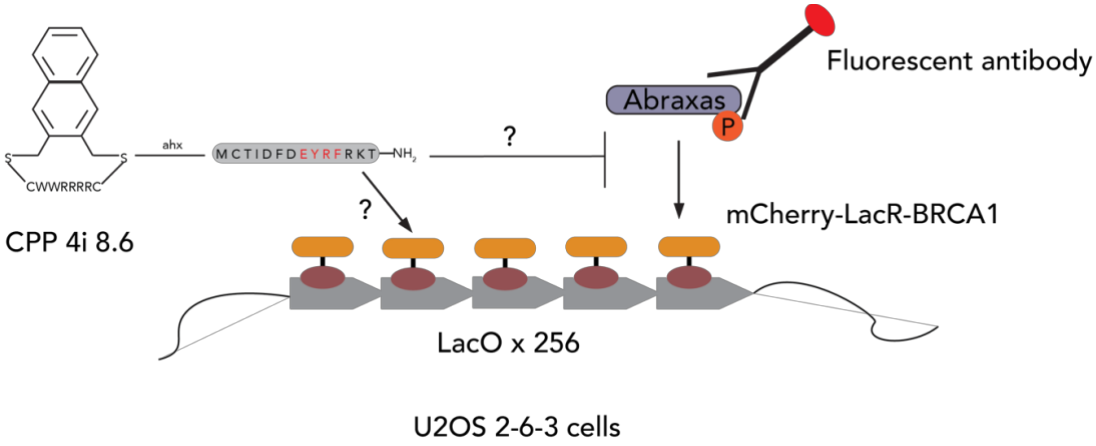

Figure 5.1 Lac array system. Schematic of LacO/LacR system used to test effect of CPP 4i 8.6 on BRCA1-Abraxas interaction.

5.3 Results

5.3.1 BRCA1 localization at the lac operon

We first tested the operation of the lacR/lacO reporter system. To determine whether BRCA1 accumulates at the lac array site. U2OS 2-6-3 cells were transiently transfected with the mCherry-BRCA1-LacR and visualized 18 hours post transfection. Labelled BRCA1 localized at the array which was visualized as the small dot containing high concentration of BRCA1-LacI in the nucleus (Figure 5.2). DAPI fluorescence was used to identify the cell nucleus. Due to the high affinity of lacR binding to LacO, the transfected BRCA1 is not visualized in other parts of the nucleus. BRCA1 binds specifically to the lac array in the nucleus.

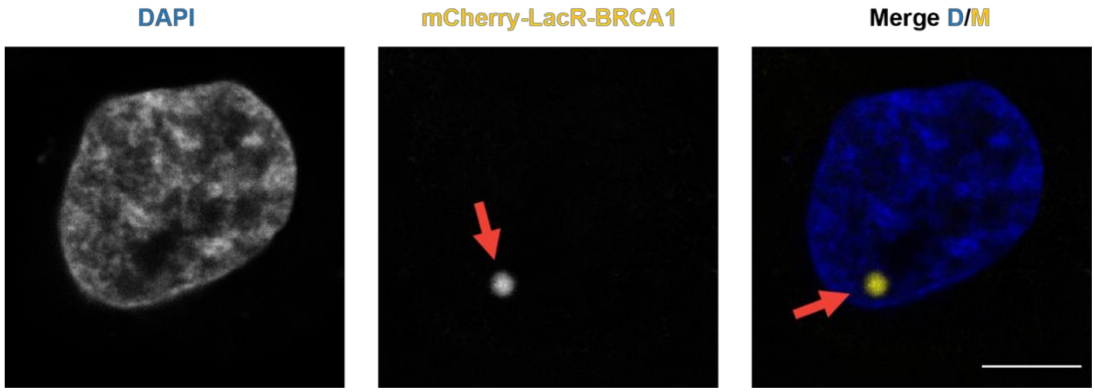

Figure 5.2 BRCA1 localization at array. Recruitment of BRCA1 to Lac array in the nucleus. Arrows indicate condensed array. The scale bar represents 5 μm.

5.3.2 Abraxas and BRCA1 colocalization at the lac operon

Next, we wanted to probe the binding of Abraxas to BRCA1 tethered at the lac array. To test the BRCA1-abraxas interaction, U2OS 2-6-3 cells transfected with mCherry-LacR-BRCA1 were stained for Abraxas 18 hours post transfection. This experiment was performed without irradiation of the cells. We observed the co-localization of Abraxas and BRCA1 at the lac array, indicative of specific binding (Figure 5.3A). This also confirms that the phosphorylation of abraxas *in vivo* required for binding BRCA1 is independent of irradiation. Irradiated cells also showed Abraxas localization to the array (Figure 5.3B). However, we observed the formation of Abraxas foci in other parts of the nucleus, which reflects its function in DNA damage repair. There was no localization of abraxas to the array in un-transfected cells. This shows, the localization of Abraxas to the lacO is dependent on its binding to the BRCA1 tethered at the array. Abraxas binds to BRCA1 independent of irradiation.

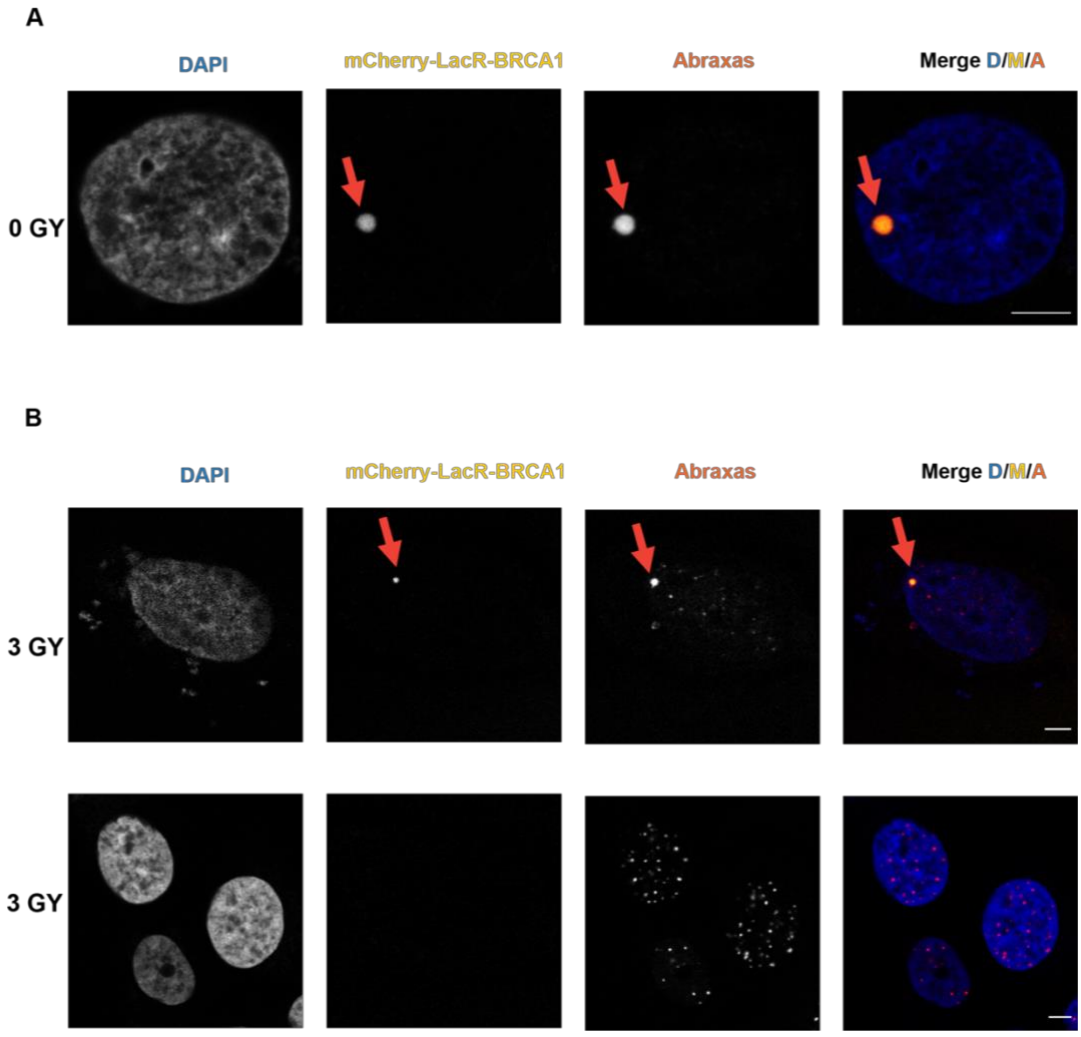

Figure 5.3 Abraxas binds to BRCA1 at the Lac array. (A) Recruitment of BRCA1 and Abraxas to the Lac array in the nucleus. (B) BRCA1-Abraxas Lac array colocalization in U2OS 2-6-3 cells irradiated with 3GY. Control un-transfected cells with Abraxas foci.

Arrows indicate condensed array. The scale bar represents 5 μm.

5.3.3 CPP 4i 8.6 is cell penetrable

After establishing this system, the next step was to introduce the CPP 4i 8.6 to probe its effect on the BRCA1-abraxas interaction. A mixture of fluorescein-labelled CPP 4i 8.6 and CPP 4i 8.6 was prepared to better visualize peptide uptake by fluorescence. Stock solution of 60 μM fluorescein-CPP 4i 8.6 was mixed with 10mM CPP 4i 8.6. First the peptide mixture was diluted (1/1000) into serum-free media of the cells. The BRCA1 transfected cells were incubated with the serum-free media containing the peptide mixture for 3 hours. The cells were left to recover for 2 hours after irradiation. In the untreated cells, we visualized the localization of Abraxas at the Lac array containing BRCA1 (Figure 5.4). We observed the diffusion of CPP 4i 8.6 into the cells treated with the peptide mix visualized by the green fluorescence. Increasing the concentration of peptide led to the localization of BRCA1 to the cytoplasm. However, we still observe the localization of Abraxas to the lac array. The CPP 4i-8.6 is cell permeable but enriched in the cytoplasm compared to the nucleus. It does not disrupt the BRCA1-Abraxas interaction at the array in the nucleus.

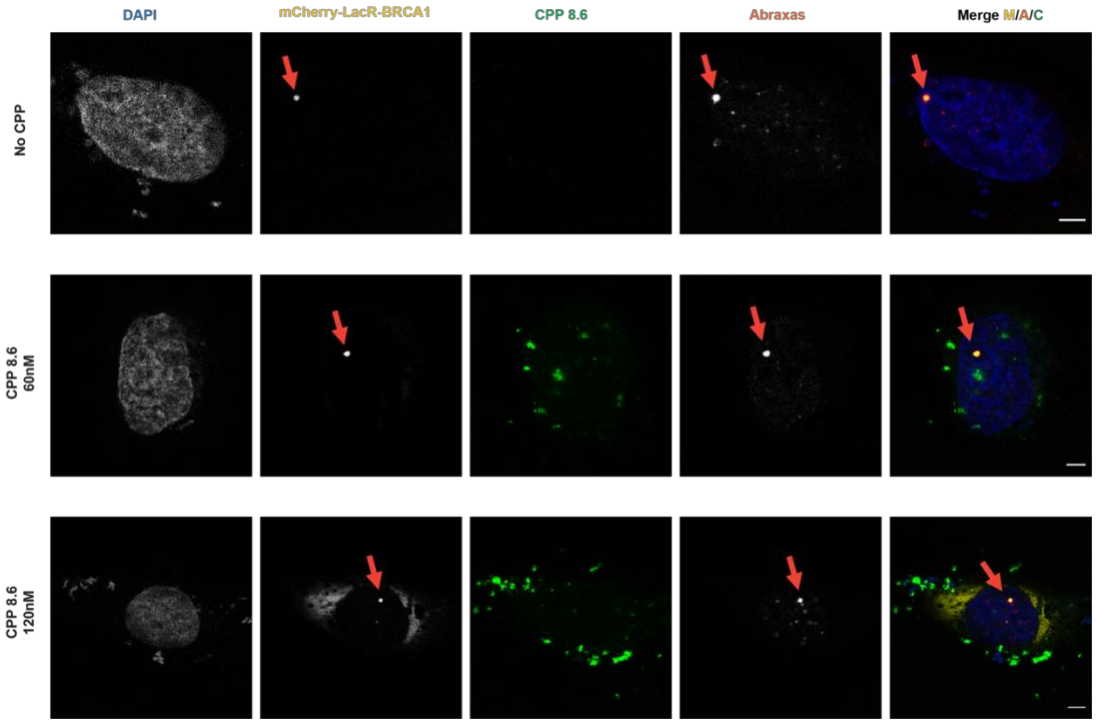

Figure 5.4 CPP 4i-8.6 is cell-permeable. Images from BRCA1 transfected U2OS cells treated with CPP 4i 8.6 peptide mix. CPP 8.6 60 nM indicates cells treated with 10 μM of unlabelled CPP 4i 8.6 and 60 nM fam-CPP 4i 8.6 mix. CPP 8.6 120 nM indicates cells treated with 20 μM of unlabelled CPP 4i 8.6 and 60 nM fam-CPP 4i 8.6 mix. Cells were treated with 3 Gy radiation.
Arrows indicate condensed array. The scale bar represents 5 μm.

5.3.4 EGFP 8.6 peptide interacts with BRCA1

To further probe the effect of peptide 8.6 on BRCA1-Abraxas interaction *in vivo*, we overexpressed the peptide as a fusion with EGFP. The peptide expression can be induced with doxycycline following transfection into the cells. Lentiviral co-transfection of TRIPZ-EGFP-8.6 and mCherry-lacR-BRCA1 was performed, and doxycycline was added to the media. As a control, cells were also co-transfected with BRCA1 and free EGFP. About 18 hours post-transfection, cells were irradiated with 3 Gy. To visualize the effect of EGFP-8.6 on BRCA1, the cells were stained for Abraxas after 2 hours recovery. We observed the peptide interaction with BRCA1 in cells treated with doxycycline while the untreated cells showed no peptide expression (Figure 5.5). Abraxas was still localized at the lac array in both cells co-transfected with the EGFP 8.6 and BRCA1. Also, we observed an interaction between the EGFP control and the lac array which is similar to the EGFP 8.6. We proposed this interaction to be a cell-fixation artifact as this observation has never been reported despite the widespread use of this system. EGFP 8.6 interacts with BRCA1 tethered to the lac array but does not abolish the recruitment of Abraxas to the array.

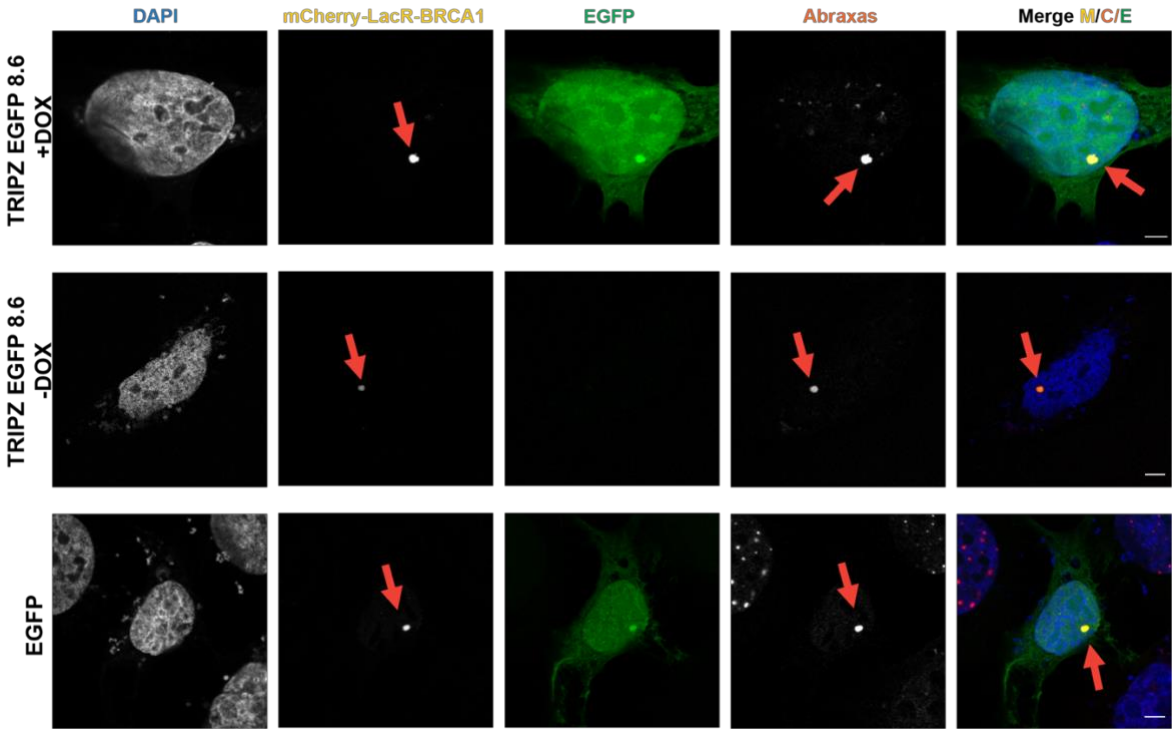

Figure 5.5 EGFP 8.6 interacts with BRCA1. U2OS 2-6-3 cells transfected with TRIPZ-EGFP 8.6 or EGFP C1 plasmids. TRIPZ-EGFP 8.6 cells were treated with or without DOX for 18 hours. DNA damage was induced with 3Gy radiation. Arrows indicate condensed array. The scale bar represents 5 μm.

5.3.5 Live cell imaging to confirm LacO interaction.

To confirm the free EGFP interaction with the lac array, live cell imaging was performed with co-transfected cells. In this experiment, the radiation was performed 6 hours post-co-transfection of the constructs. We observed the EGFP 8.6 interaction with BRCA1 as seen in figure 5.5. However, there was no interaction of the lac array with free EGFP which confirms our hypothesis (Figure 5.6). EGFP 8.6 binds specifically to BRCA1 *in vivo* and EGFP does not interact with the lacO.

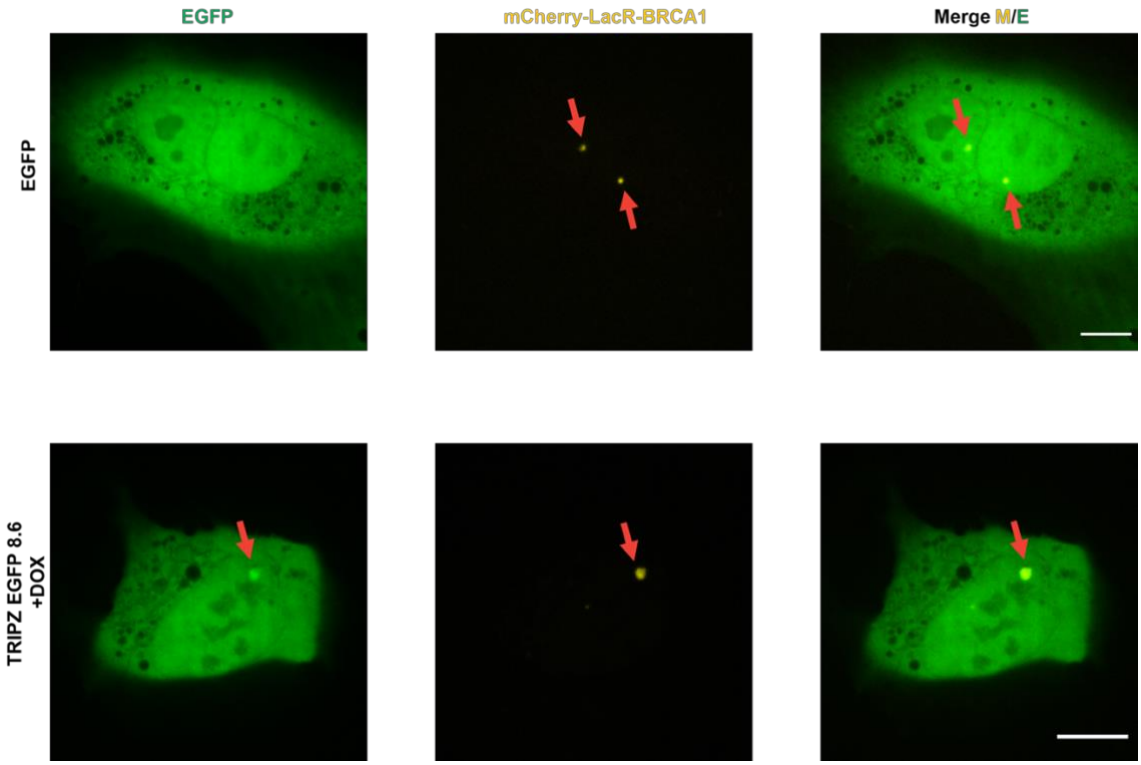

Figure 5.6 EGFP 8.6 specific interaction with BRCA1. U2OS 2-6-3 cells co-transfected with TRIPZ-EGFP 8.6 or EGFP C1 plasmids and BRCA1. Cells were treated with DOX for 6 hours DNA damage was induced with 3Gy radiation.

5.3.6 EGFP 8.6 binding to BRCA1

The kinetics of peptide 8.6 nat binding specifically to BRCA1 and its ability to prevent interaction with other protein binding partners has been shown in vitro (Sun, 2017; White et al., 2015). We wanted to determine the binding kinetics of the CPP 4i 8.6 to BRCA1 in vivo. Six hours after co-transfection with EGFP 8.6 and BRCA1, cells were treated with ionizing radiation. This is to promote the phosphorylation of Abraxas and provide a competition for EGFP 8.6 binding to BRCA1. Fluorescence recovery after photobleaching (FRAP) was used to examine the peptide mobility and interaction. We observed the recovery of EGFP 8.6 to the array after bleaching which indicates its reversible binding to BRCA1. We also found that about 20% of the peptide bound population are immobile, implying an irreversible interaction on this time scale. EGFP 8.6 binds specifically and reversibly to BRCA1.

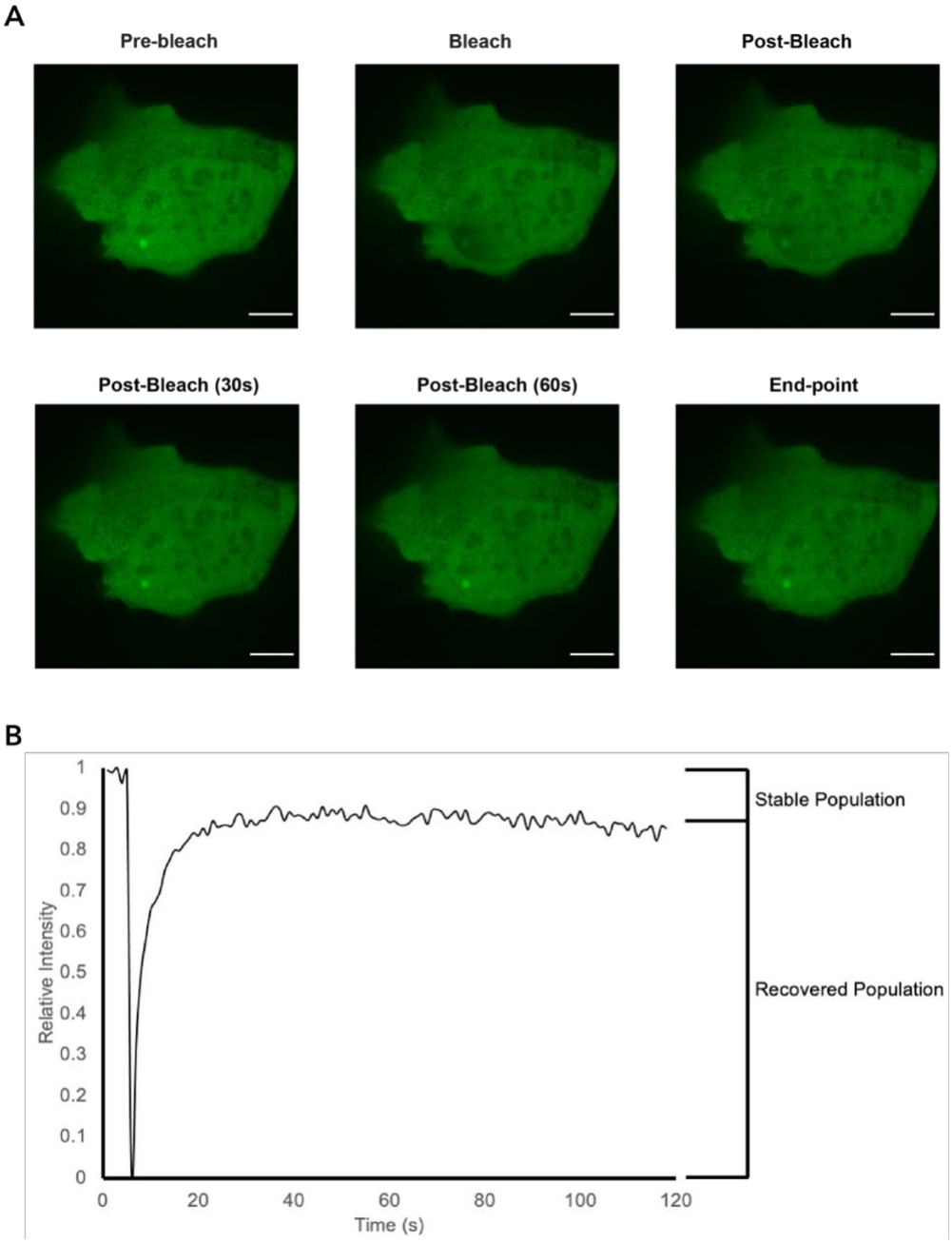

Figure 5.7 FRAP analysis of EGFP 8.6 binding to BRCA1. U2OS 2-6-3 cells expressing EGFP 8.6 were treated with doxycycline. Fluorescent recovery after photobleaching was performed to determine the kinetics of peptide binding to the array. Relative intensities of the bleached region normalized by the total nuclear fluorescence were plotted over time.

5.4 Discussion

In this chapter, we have adopted the lacI/lacO system to visualize the interaction of BRCA1 with Abraxas *in vivo*. We also used this system to probe the ability of CPP 8.6 to disrupt the interaction. First, we showed the localization of BRCA1 to the lac arrays through the high affinity binding of the lacI DNA biniding domain to its binding sequence. Next, we stained BRCA1 transfected cells for Abraxas and confirmed the interaction at the lac array. We observed the binding of Abraxas to BRCA1 independent of IR. Following irradiation, a doubly phosphorylated Abraxas (GFGEYpSRpSPTF) is enriched in cells. It has been reported that single C-terminal phosphorylation of Abraxas at serine 406 (S406) is required for BRCA1 binding (B. Wang et al., 2007a). Also, it was shown that the S406 phosphorylation occurs independently of IR (B. Wang et al., 2007a; Q. Wu et al., 2016). The upstream phosphorylation at S404 is IR-dependent and it is important for BRCA1 dimerization at DNA damage sites (Q. Wu et al., 2016). Therefore, Abraxas binding to BRCA1 is independent of DNA damage but IR improves the binding by the dimer formation.

We have also shown that the CPP 4i 8.6 is cell-permeable but poorly diffuses into the nucleus of U2OS cells. At the concentrations of peptide tested, we did not observe a disruption of the BRCA1-Abraxas complex. However, at the highest concentration tested, we observed localization of BRCA1 to the cytoplasm, which could be an indication of cellular trapping by the peptide. Using the doxycycline inducible TRIPZ EGFP 8.6 construct, we decided to overexpress the EGFP 8.6 in

the cells. An interaction of the peptide with BRCA1 at the lac array was observed but not the loss of Abraxas binding. We also observed the interaction of free EGFP with the array, but this was fixation-dependent. Cell fixation involves the denaturation and coagulation of proteins for staining and imaging. In this case, the fixation led to the coagulation of rapidly diffusing EGFP molecules to the lac array. We avoided this to demonstrate specific binding by using live cell imaging where EGF did not enrich at the array. The live cell imaging confirmed the specific binding of EGFP 8.6 to BRCA1. The binding kinetics of the peptide to BRCA1 was tested by FRAP. We observed the recovery of the peptide to the bleached array.

A peptide bound population of ~10% were slow-exchanging and did not recover over the course of the time-lapse. This finding could be due to the strong competition of our peptide with Abraxas in proximity to the array. However, about 80% of the peptide population were fast-exchanging and after 8 seconds, 50% of the population was recovered. More FRAP experiments will be performed to further understand the binding kinetics of EGFP 8.6 to BRCA1 *in vivo*. FRAP experiments will also be performed with the CPP 4i 8.6 at higher concentrations.

Chapter 6: CONCLUSION

The first part of this thesis sought to develop a method for post-translational modification of the octamer. Phosphorylation of H2AX in proximity to the site of DNA damage is important for the signal transduction and recruitment of downstream factors for cellular response. MDC1 early binding to the γH2AX is an important step for the DSB signaling and the dynamics of binding is yet to be explored in the context of chromatin. In order to get structural information on the dynamics, octamer containing γH2AX with adequate yield and purity needed to be produced.

A high yield method of octamer expression and purification had been developed previously in our lab. The H2AX histone C-terminal tail had been mutated to promote CK2 recognition while maintaining interacting residues for MDC1 BRCT binding. Phosphorylation of the H2A-H2B dimer was performed in vitro by CK2 (Islam, 2018). As outlined in Chapter 3, we performed radioactive kinase assays to visualize the phosphorylation of our H2AX tail in octamer by CK2. Upon successful phosphorylation of the octamer, we tested the effect of widom 601 DNA on phosphorylation by CK2. We also developed a cellular method of octamer phosphorylation by co-expression with CK2. A radioactive kinase assay was used to compare the extent of phosphorylation by the two methods. We showed that γH2AX-H2B dimer phosphorylated in cells can bind purified MDC1 BRCT domain in a phosphorylation-dependent manner. In conclusion of this chapter, incomplete phosphorylation of the octamer was observed using both methods of

phosphorylation. MDC1 binding to the phosphorylated dimer was not stoichiometric. Future studies will entail developing new protocols to efficiently phosphorylate the octamer. This will provide particles for structural studies to understand the role of phosphorylation in DNA damage signaling.

The second aim of this thesis was testing a potential inhibitor for the BRCA1 BRCT. First the purified tandem BRCTs of BRCA1 and MDC1 were tested for interaction with their binding partners. Next, the BRCTs were tested for their ability to bind alternative peptides. The results showed cross reactivity of the BRCTs due to the similarity of peptide binding sequence. In Chapter 4, the CPP 4i 8.6 was tested in vitro on its ability to inhibit BRCA1 binding to Bach1 peptide. Also, the specificity of the peptide was probed by its ability to disrupt the MDC1 BRCT- γH2AX peptide complex. The CPP 4i 8.6 proved to be specific and potent for inhibition of BRCA1 BRCT. We proceeded to *in vivo* studies of the CPP 4i 8.6 using the LacI/LacO system to visualize its effect on BRCA1-Abraxas interaction. The diffusion of CPP 4i 8.6 into the cytoplasm was observed but poor import of the peptide into the nucleus. This could be the reason for the persistent BRCA1-Abraxas interaction that was observed in peptide treated cells. We performed FRAP experiments with the EGFP 8.6 construct and observed its interaction with the BRCA1 protein localized at the lac array. The EGFP 8.6 bound reversibly to the BRCA1 and ~80% of the population exchanged rapidly in under two minutes. However, we observed the presence of a peptide fraction bound irreversibly to the protein. This could be because of competition with Abraxas in close proximity to the

lac array. In the future, the nuclear uptake of the CPP 4i 8.6 will be improved by increasing the concentration of peptide treatment or addition of a nuclear localization sequence to the peptide. FRAP experiments will be performed with the higher concentrations of the CPP 4i 8.6 peptide to visualize its inhibitory effect on BRCA1-Abraxas interaction. A competition experiment between the CPP 4i 8.6 and EGFP 8.6 can also be performed.

REFERENCES

References:

1. Abrigo, N. A., Dods, K., Mitra, K., Newcomb, K., Le, A., & Hartman, M. (2020). *Cyclic, Cell-Penetrating Peptides Tailor-Made for the Creation of Peptide Libraries with Intrinsic Cell Permeability* [Preprint]. https://doi.org/10.26434/chemrxiv.12445226.v1
2. Ahnesorg, P., Smith, P., & Jackson, S. P. (2006). XLF Interacts with the XRCC4-DNA Ligase IV Complex to Promote DNA Nonhomologous End-Joining. *Cell*, *124*(2), 301–313. https://doi.org/10.1016/j.cell.2005.12.031
3. Arents, G., Burlingame, R. W., Wang, B. C., Love, W. E., & Moudrianakis, E. N. (1991). The nucleosomal core histone octamer at 3.1 A resolution: A tripartite protein assembly and a left-handed superhelix. *Proceedings of the National Academy of Sciences*, *88*(22), 10148–10152. https://doi.org/10.1073/pnas.88.22.10148
4. Arents, G., & Moudrianakis, E. N. (1995). The histone fold: A ubiquitous architectural motif utilized in DNA compaction and protein dimerization. *Proceedings of the National Academy of Sciences*, *92*(24), 11170–11174. https://doi.org/10.1073/pnas.92.24.11170

5. Barrows, L. R., & Magee, P. N. (1982). Nonenzymatic methylation of DNA by S-adenosylmethionine *in vitro*. *Carcinogenesis*, *3*(3), 349–351. https://doi.org/10.1093/carcin/3.3.349
6. Bartek, J., & Lukas, J. (2007). DNA damage checkpoints: From initiation to recovery or adaptation. *Current Opinion in Cell Biology*, *19*(2), 238–245. https://doi.org/10.1016/j.ceb.2007.02.009
7. Becker, J. R., Bonnet, C., Clifford, G., Groth, A., Wilson, M. D., & Chapman, J. R. (2020). *BARD1 links histone H2A Lysine-15 ubiquitination to initiation of BRCA1-dependent homologous recombination* [Preprint]. Molecular Biology. https://doi.org/10.1101/2020.06.01.127951
8. Bell, J. C., & Kowalczykowski, S. C. (2016). RecA: Regulation and Mechanism of a Molecular Search Engine. *Trends in Biochemical Sciences*, *41*(6), 491–507. https://doi.org/10.1016/j.tibs.2016.04.002
9. Bonner, W. M., Redon, C. E., Dickey, J. S., Nakamura, A. J., Sedelnikova, O. A., Solier, S., & Pommier, Y. (2008). ΓH2AX and cancer. *Nature Reviews Cancer*, *8*(12), 957–967. https://doi.org/10.1038/nrc2523
10. Brock, R., Hamelers, I. H. L., & Jovin, T. M. (1999). Comparison of fixation protocols for adherent cultured cells applied to a GFP fusion protein of the epidermal growth factor receptor. *Cytometry*, *35*(4), 353–362. https://doi.org/10.1002/(SICI)1097-0320(19990401)35:4<353::AID-CYTO8>3.0.CO;2-M

11. Campbell, S. J., Edwards, R. A., & Glover, J. N. M. (2010). Comparison of the Structures and Peptide Binding Specificities of the BRCT Domains of MDC1 and BRCA1. *Structure*, *18*(2), 167–176. https://doi.org/10.1016/j.str.2009.12.008
12. Carusillo, A., & Mussolino, C. (2020). DNA Damage: From Threat to Treatment. *Cells*, *9*(7), 1665. https://doi.org/10.3390/cells9071665
13. Ceccaldi, R., Rondinelli, B., & D'Andrea, A. D. (2016). Repair Pathway Choices and Consequences at the Double-Strand Break. *Trends in Cell Biology*, *26*(1), 52–64. https://doi.org/10.1016/j.tcb.2015.07.009
14. Chang, H. H. Y., Pannunzio, N. R., Adachi, N., & Lieber, M. R. (2017). Non-homologous DNA end joining and alternative pathways to double-strand break repair. *Nature Reviews Molecular Cell Biology*, *18*(8), 495–506. https://doi.org/10.1038/nrm.2017.48
15. Chaplet, M., Rai, R., Jackson-Bernitsas, D., Li, K., & Lin, S.-Y. (2006). BRIT1/MCPH1: A Guardian of Genome and an Enemy of Tumors. *Cell Cycle*, *5*(22), 2579–2583. https://doi.org/10.4161/cc.5.22.3471
16. Chen, R., & Wold, M. S. (2014). Replication protein A: Single-stranded DNA's first responder: Dynamic DNA-interactions allow replication protein A to direct single-strand DNA intermediates into different pathways for synthesis or repair. *BioEssays*, *36*(12), 1156–1161. https://doi.org/10.1002/bies.201400107

17. Ciccia, A., & Elledge, S. J. (2010). The DNA Damage Response: Making It Safe to Play with Knives. *Molecular Cell*, *40*(2), 179–204. https://doi.org/10.1016/j.molcel.2010.09.019

18. Cimmino, F., Formicola, D., & Capasso, M. (2017). Dualistic Role of BARD1 in Cancer. *Genes*, *8*(12), 375. https://doi.org/10.3390/genes8120375

19. Clapperton, J. A., Manke, I. A., Lowery, D. M., Ho, T., Haire, L. F., Yaffe, M. B., & Smerdon, S. J. (2004). Structure and mechanism of BRCA1 BRCT domain recognition of phosphorylated BACH1 with implications for cancer. *Nature Structural & Molecular Biology*, *11*(6), 512–518. https://doi.org/10.1038/nsmb775

20. Cook, P. J., Ju, B. G., Telese, F., Wang, X., Glass, C. K., & Rosenfeld, M. G. (2009). Tyrosine dephosphorylation of H2AX modulates apoptosis and survival decisions. *Nature*, *458*(7238), 591–596. https://doi.org/10.1038/nature07849

21. Coster, G., & Goldberg, M. (2010). The cellular response to DNA damage: A focus on MDC1 and its interacting proteins. *Nucleus*, *1*(2), 166–178. https://doi.org/10.4161/nucl.11176

22. Cremona, C. A., & Behrens, A. (2014). ATM signalling and cancer. *Oncogene*, *33*(26), 3351–3360. https://doi.org/10.1038/onc.2013.275

23. Cutter, A. R., & Hayes, J. J. (2015a). A brief review of nucleosome structure. *FEBS Letters*, *589*(20PartA), 2914–2922. https://doi.org/10.1016/j.febslet.2015.05.016

24. Cutter, A. R., & Hayes, J. J. (2015b). A brief review of nucleosome structure. *FEBS Letters*, *589*(20PartA), 2914–2922. https://doi.org/10.1016/j.febslet.2015.05.016

25. Densham, R. M., Garvin, A. J., Stone, H. R., Strachan, J., Baldock, R. A., Daza-Martin, M., Fletcher, A., Blair-Reid, S., Beesley, J., Johal, B., Pearl, L. H., Neely, R., Keep, N. H., Watts, F. Z., & Morris, J. R. (2016). Human BRCA1–BARD1 ubiquitin ligase activity counteracts chromatin barriers to DNA resection. *Nature Structural & Molecular Biology*, *23*(7), 647–655. https://doi.org/10.1038/nsmb.3236

26. Dietlein, F., Thelen, L., & Reinhardt, H. C. (2014). Cancer-specific defects in DNA repair pathways as targets for personalized therapeutic approaches. *Trends in Genetics*, *30*(8), 326–339. https://doi.org/10.1016/j.tig.2014.06.003

27. Ding, L., Cao, J., Lin, W., Chen, H., Xiong, X., Ao, H., Yu, M., Lin, J., & Cui, Q. (2020). The Roles of Cyclin-Dependent Kinases in Cell-Cycle Progression and Therapeutic Strategies in Human Breast Cancer. *International Journal of Molecular Sciences*, *21*(6), 1960. https://doi.org/10.3390/ijms21061960

28. Erie, D. A., & Weninger, K. R. (2014). Single molecule studies of DNA mismatch repair. *DNA Repair*, *20*, 71–81. https://doi.org/10.1016/j.dnarep.2014.03.007

29. Eustermann, S., Wu, W.-F., Langelier, M.-F., Yang, J.-C., Easton, L. E., Riccio, A. A., Pascal, J. M., & Neuhaus, D. (2015). Structural Basis of Detection and Signaling of DNA Single-Strand Breaks by Human PARP-1. *Molecular Cell*, *60*(5), 742–754. https://doi.org/10.1016/j.molcel.2015.10.032

30. Ferrand, J., Rondinelli, B., & Polo, S. E. (2020). Histone Variants: Guardians of Genome Integrity. *Cells*, *9*(11), 2424. https://doi.org/10.3390/cells9112424

31. Freudenthal, B. D. (2017). Base excision repair of oxidative DNA damage from mechanism to disease. *Frontiers in Bioscience*, *22*(9), 1493–1522. https://doi.org/10.2741/4555

32. Futreal, P., Liu, Q., Shattuck-Eidens, D., Cochran, C., Harshman, K., Tavtigian, S., Bennett, L., Haugen-Strano, A., Swensen, J., Miki, Y., & et, al. (1994). BRCA1 mutations in primary breast and ovarian carcinomas. *Science*, *266*(5182), 120–122. https://doi.org/10.1126/science.7939630

33. Garcia, V., Phelps, S. E. L., Gray, S., & Neale, M. J. (2011). Bidirectional resection of DNA double-strand breaks by Mre11 and Exo1. *Nature*, *479*(7372), 241–244. https://doi.org/10.1038/nature10515

34. Georgoulis, A., Vorgias, C., Chrousos, G., & Rogakou, E. (2017). Genome Instability and γH2AX. *International Journal of Molecular Sciences*, *18*(9), 1979. https://doi.org/10.3390/ijms18091979

35. Hilario, J., Amitani, I., Baskin, R. J., & Kowalczykowski, S. C. (2009). Direct imaging of human Rad51 nucleoprotein dynamics on individual DNA molecules. *Proceedings of the National Academy of Sciences*, *106*(2), 361–368. https://doi.org/10.1073/pnas.0811965106

36. Hiragami-Hamada, K., Shinmyozu, K., Hamada, D., Tatsu, Y., Uegaki, K., Fujiwara, S., & Nakayama, J. -i. (2011). N-Terminal Phosphorylation of HP1 Promotes Its Chromatin Binding. *Molecular and Cellular Biology*, *31*(6), 1186–1200. https://doi.org/10.1128/MCB.01012-10

37. Horn, V., Uckelmann, M., Zhang, H., Eerland, J., Aarsman, I., le Paige, U. B., Davidovich, C., Sixma, T. K., & van Ingen, H. (2019). Structural basis of specific H2A K13/K15 ubiquitination by RNF168. *Nature Communications*, *10*(1), 1751. https://doi.org/10.1038/s41467-019-09756-z

38. Hossain, Md., Lin, Y., & Yan, S. (2018). Single-Strand Break End Resection in Genome Integrity: Mechanism and Regulation by APE2. *International Journal of Molecular Sciences*, *19*(8), 2389. https://doi.org/10.3390/ijms19082389

39. Houtgraaf, J. H., Versmissen, J., & van der Giessen, W. J. (2006). A concise review of DNA damage checkpoints and repair in mammalian cells.

Cardiovascular Revascularization Medicine, *7*(3), 165–172. https://doi.org/10.1016/j.carrev.2006.02.002

40. Huen, M. S. Y., Sy, S. M. H., & Chen, J. (2010). BRCA1 and its toolbox for the maintenance of genome integrity. *Nature Reviews Molecular Cell Biology*, *11*(2), 138–148. https://doi.org/10.1038/nrm2831
41. Islam, T. (2018). *Md Touhidul Islam*. University of Alberta.
42. Jackson, S. P., & Bartek, J. (2009). The DNA-damage response in human biology and disease. *Nature*, *461*(7267), 1071–1078. https://doi.org/10.1038/nature08467
43. Jasin, M., & Rothstein, R. (2013). Repair of Strand Breaks by Homologous Recombination. *Cold Spring Harbor Perspectives in Biology*, *5*(11), a012740–a012740. https://doi.org/10.1101/cshperspect.a012740
44. Johnson, N., Johnson, S. F., Yao, W., Li, Y.-C., Choi, Y.-E., Bernhardy, A. J., Wang, Y., Capelletti, M., Sarosiek, K. A., Moreau, L. A., Chowdhury, D., Wickramanayake, A., Harrell, M. I., Liu, J. F., D'Andrea, A. D., Miron, A., Swisher, E. M., & Shapiro, G. I. (2013). Stabilization of mutant BRCA1 protein confers PARP inhibitor and platinum resistance. *Proceedings of the National Academy of Sciences*, *110*(42), 17041–17046. https://doi.org/10.1073/pnas.1305170110

45. Jones, M. H., Hamana, N., Nezu, J., & Shimane, M. (2000). A Novel Family of Bromodomain Genes. *Genomics*, *63*(1), 40–45. https://doi.org/10.1006/geno.1999.6071

46. Kalb, R., Mallery, D. L., Larkin, C., Huang, J. T. J., & Hiom, K. (2014). BRCA1 Is a Histone-H2A-Specific Ubiquitin Ligase. *Cell Reports*, *8*(4), 999–1005. https://doi.org/10.1016/j.celrep.2014.07.025

47. Kamakaka, R. T. (2005). Histone variants: Deviants? *Genes & Development*, *19*(3), 295–316. https://doi.org/10.1101/gad.1272805

48. Kasai, H., & Nishimura, S. (1984). Hydroxylation of deoxyguanosine at the C-8 position by ascorbic acid and other reducing agents. *Nucleic Acids Research*, *12*(4), 2137–2145. https://doi.org/10.1093/nar/12.4.2137

49. Kim, H., Huang, J., & Chen, J. (2007). CCDC98 is a BRCA1-BRCT domain–binding protein involved in the DNA damage response. *Nature Structural & Molecular Biology*, *14*(8), 710–715. https://doi.org/10.1038/nsmb1277

50. Kinner, A., Wu, W., Staudt, C., & Iliakis, G. (2008). -H2AX in recognition and signaling of DNA double-strand breaks in the context of chromatin. *Nucleic Acids Research*, *36*(17), 5678–5694. https://doi.org/10.1093/nar/gkn550

51. Kolas, N. K., Chapman, J. R., Nakada, S., Ylanko, J., Chahwan, R., Sweeney, F. D., Panier, S., Mendez, M., Wildenhain, J., Thomson, T. M., Pelletier, L., Jackson, S. P., & Durocher, D. (2007). *Orchestration of the DNA-Damage Response by the RNF8 Ubiquitin Ligase*. *318*, 5.

52. Kowalczykowski, S. C. (2015). An Overview of the Molecular Mechanisms of Recombinational DNA Repair. *Cold Spring Harbor Perspectives in Biology*, *7*(11), a016410. https://doi.org/10.1101/cshperspect.a016410

53. Krokan, H. E., & Bjoras, M. (2013). Base Excision Repair. *Cold Spring Harbor Perspectives in Biology*, *5*(4), a012583–a012583. https://doi.org/10.1101/cshperspect.a012583

54. Landschulz, W., Johnson, P., & McKnight, S. (1988). The leucine zipper: A hypothetical structure common to a new class of DNA binding proteins. *Science*, *240*(4860), 1759–1764. https://doi.org/10.1126/science.3289117

55. Langerak, P., Mejia-Ramirez, E., Limbo, O., & Russell, P. (2011). Release of Ku and MRN from DNA Ends by Mre11 Nuclease Activity and Ctp1 Is Required for Homologous Recombination Repair of Double-Strand Breaks. *PLoS Genetics*, *7*(9), e1002271. https://doi.org/10.1371/journal.pgen.1002271

56. Leandro, P., Lechner, M. C., Tavares de Almeida, I., & Konecki, D. (2001). Glycerol Increases the Yield and Activity of Human Phenylalanine Hydroxylase Mutant Enzymes Produced in a Prokaryotic Expression System. *Molecular Genetics and Metabolism*, *73*(2), 173–178. https://doi.org/10.1006/mgme.2001.3172

57. Lee, M. S., Green, R., Marsillac, S. M., Coquelle, N., Williams, R. S., Yeung, T., Foo, D., Hau, D. D., Hui, B., Monteiro, A. N. A., & Glover, J. N. M. (2010).

Comprehensive Analysis of Missense Variations in the BRCT Domain of BRCA1 by Structural and Functional Assays. *Cancer Research*, *70*(12), 4880–4890. https://doi.org/10.1158/0008-5472.CAN-09-4563

58. Li, Z., Pearlman, A. H., & Hsieh, P. (2016). DNA mismatch repair and the DNA damage response. *DNA Repair*, *38*, 94–101. https://doi.org/10.1016/j.dnarep.2015.11.019
59. Lieber, M. R. (2008). The Mechanism of Human Nonhomologous DNA End Joining. *Journal of Biological Chemistry*, *283*(1), 1–5. https://doi.org/10.1074/jbc.R700039200
60. Lindahl, T. (1993). Instability and decay of the primary structure of DNA. *Nature*, *362*(6422), 709–715. https://doi.org/10.1038/362709a0
61. Lindahl, T., & Andersson, A. (1972). Rate of chain breakage at apurinic sites in double-stranded deoxyribonucleic acid. *Biochemistry*, *11*(19), 3618–3623. https://doi.org/10.1021/bi00769a019
62. Lindahl, T., & Nyberg, B. (1974). Heat-induced deamination of cytosine residues in deoxyribonucleic acid. *Biochemistry*, *13*(16), 3405–3410. https://doi.org/10.1021/bi00713a035
63. Liu, Y., & Lu, L.-Y. (2021). BRCA1: A key player at multiple stages of homologous recombination in DNA double-strand break repair. *Genome Instability & Disease*, *2*(3), 164–174. https://doi.org/10.1007/s42764-021-00042-1

64. Lord, C. J., Tutt, A. N. J., & Ashworth, A. (2015). Synthetic Lethality and Cancer Therapy: Lessons Learned from the Development of PARP Inhibitors. *Annual Review of Medicine*, *66*(1), 455–470. https://doi.org/10.1146/annurev-med-050913-022545

65. Lou, Z., Minter-Dykhouse, K., Franco, S., Gostissa, M., Rivera, M. A., Celeste, A., Manis, J. P., van Deursen, J., Nussenzweig, A., Paull, T. T., Alt, F. W., & Chen, J. (2006). MDC1 Maintains Genomic Stability by Participating in the Amplification of ATM-Dependent DNA Damage Signals. *Molecular Cell*, *21*(2), 187–200. https://doi.org/10.1016/j.molcel.2005.11.025

66. Lowary, P. T., & Widom, J. (1998). New DNA sequence rules for high affinity binding to histone octamer and sequence-directed nucleosome positioning. *Journal of Molecular Biology*, *276*(1), 19–42. https://doi.org/10.1006/jmbi.1997.1494

67. Luger, K. (1997). *Crystal structure of the nucleosome core particle at 2.8 A˚ resolution*. *389*, 10.

68. Ma, C. J., Gibb, B., Kwon, Y., Sung, P., & Greene, E. C. (2017). Protein dynamics of human RPA and RAD51 on ssDNA during assembly and disassembly of the RAD51 filament. *Nucleic Acids Research*, *45*(2), 749–761. https://doi.org/10.1093/nar/gkw1125

69. Mailand, N., Bekker-Jensen, S., Faustrup, H., Melander, F., Bartek, J., Lukas, C., & Lukas, J. (2007). RNF8 Ubiquitylates Histones at DNA Double-Strand

Breaks and Promotes Assembly of Repair Proteins. *Cell*, *131*(5), 887–900. https://doi.org/10.1016/j.cell.2007.09.040

70. McGinty, R. K., & Tan, S. (2015). Nucleosome Structure and Function. *Chemical Reviews*, *115*(6), 2255–2273. https://doi.org/10.1021/cr500373h
71. Meza, J. E., Brzovic, P. S., King, M.-C., & Klevit, R. E. (1999). Mapping the Functional Domains of BRCA1. *Journal of Biological Chemistry*, *274*(9), 5659–5665. https://doi.org/10.1074/jbc.274.9.5659
72. Miki, Y., Swensen, J., Shattuck-Eidens, D., Futreal, P., Harshman, K., Tavtigian, S., Liu, Q., Cochran, C., Bennett, L., Ding, W., & et, al. (1994). A strong candidate for the breast and ovarian cancer susceptibility gene BRCA1. *Science*, *266*(5182), 66–71. https://doi.org/10.1126/science.7545954
73. Myler, L. R., Gallardo, I. F., Soniat, M. M., Deshpande, R. A., Gonzalez, X. B., Kim, Y., Paull, T. T., & Finkelstein, I. J. (2017). Single-Molecule Imaging Reveals How Mre11-Rad50-Nbs1 Initiates DNA Break Repair. *Molecular Cell*, *67*(5), 891-898.e4. https://doi.org/10.1016/j.molcel.2017.08.002
74. Nakamura, K., Saredi, G., Becker, J. R., Foster, B. M., Nguyen, N. V., Beyer, T. E., Cesa, L. C., Faull, P. A., Lukauskas, S., Frimurer, T., Chapman, J. R., Bartke, T., & Groth, A. (2019). H4K20me0 recognition by BRCA1–BARD1 directs homologous recombination to sister chromatids. *Nature Cell Biology*, *21*(3), 311–318. https://doi.org/10.1038/s41556-019-0282-9

75. O'Connor, M. J. (2015). Targeting the DNA Damage Response in Cancer. *Molecular Cell*, *60*(4), 547–560. https://doi.org/10.1016/j.molcel.2015.10.040

76. Orthwein, A., Noordermeer, S. M., Wilson, M. D., Landry, S., Enchev, R. I., Sherker, A., Munro, M., Pinder, J., Salsman, J., Dellaire, G., Xia, B., Peter, M., & Durocher, D. (2015). A mechanism for the suppression of homologous recombination in G1 cells. *Nature*, *528*(7582), 422–426. https://doi.org/10.1038/nature16142

77. Ou, H.-L., & Schumacher, B. (2018). DNA damage responses and p53 in the aging process. *Blood*, *131*(5), 488–495. https://doi.org/10.1182/blood-2017-07-746396

78. Panier, S., & Boulton, S. J. (2014). Double-strand break repair: 53BP1 comes into focus. *Nature Reviews Molecular Cell Biology*, *15*(1), 7–18. https://doi.org/10.1038/nrm3719

79. Panigrahi, R., & Glover, J. N. M. (2021). Structural insights into DNA double-strand break signaling. *Biochemical Journal*, *478*(1), 135–156. https://doi.org/10.1042/BCJ20200066

80. Raimundo, L., Calheiros, J., & Saraiva, L. (2021). Exploiting DNA Damage Repair in Precision Cancer Therapy: BRCA1 as a Prime Therapeutic Target. *Cancers*, *13*(14), 3438. https://doi.org/10.3390/cancers13143438

81. Richmond, T. J., & Davey, C. A. (2003). The structure of DNA in the nucleosome core. *Nature*, *423*(6936), 145–150. https://doi.org/10.1038/nature01595

82. Robertson, R. B., Moses, D. N., Kwon, Y., Chan, P., Chi, P., Klein, H., Sung, P., & Greene, E. C. (2009). Structural transitions within human Rad51 nucleoprotein filaments. *Proceedings of the National Academy of Sciences*, *106*(31), 12688–12693. https://doi.org/10.1073/pnas.0811465106

83. Robinett, C. C., Straight, A., Li, G., Willhelm, C., Sudlow, G., Murray, A., & Belmont, A. S. (1996). In vivo localization of DNA sequences and visualization of large-scale chromatin organization using lac operator/repressor recognition. *Journal of Cell Biology*, *135*(6), 1685–1700. https://doi.org/10.1083/jcb.135.6.1685

84. Rodriguez, M., C. (2008). BRCT Domains: Phosphopeptide binding and signaling modules. *Frontiers in Bioscience*, *Volume*(13), 5905. https://doi.org/10.2741/3125

85. Rodriguez, M., Yu, X., Chen, J., & Songyang, Z. (2003). Phosphopeptide Binding Specificities of BRCA1 COOH-terminal (BRCT) Domains. *Journal of Biological Chemistry*, *278*(52), 52914–52918. https://doi.org/10.1074/jbc.C300407200

86. Rossetto, D., Avvakumov, N., & Côté, J. (2012). Histone phosphorylation: A chromatin modification involved in diverse nuclear events. *Epigenetics*, *7*(10), 1098–1108. https://doi.org/10.4161/epi.21975

87. Rouleau, M., Patel, A., Hendzel, M. J., Kaufmann, S. H., & Poirier, G. G. (2010). PARP inhibition: PARP1 and beyond. *Nature Reviews Cancer*, *10*(4), 293–301. https://doi.org/10.1038/nrc2812

88. Rydberg, B., & Lindahl, T. (1982). Nonenzymatic methylation of DNA by the intracellular methyl group donor S-adenosyl-L-methionine is a potentially mutagenic reaction. *The EMBO Journal*, *1*(2), 211–216. https://doi.org/10.1002/j.1460-2075.1982.tb01149.x

89. Samadder, P., Aithal, R., Belan, O., & Krejci, L. (2016). Cancer TARGETases: DSB repair as a pharmacological target. *Pharmacology & Therapeutics*, *161*, 111–131. https://doi.org/10.1016/j.pharmthera.2016.02.007

90. San Filippo, J., Sung, P., & Klein, H. (2008). Mechanism of Eukaryotic Homologous Recombination. *Annual Review of Biochemistry*, *77*(1), 229–257. https://doi.org/10.1146/annurev.biochem.77.061306.125255

91. Sarno, S., Vaglio, P., Marin, O., Issinger, O.-G., Ruffato, K., & Pinna, L. A. (1997). Mutational Analysis of Residues Implicated in the Interaction between Protein Kinase CK2 and Peptide Substrates †. *Biochemistry*, *36*(39), 11717–11724. https://doi.org/10.1021/bi9705772

92. Sato, K., Sundaramoorthy, E., Rajendra, E., Hattori, H., Jeyasekharan, A. D., Ayoub, N., Schiess, R., Aebersold, R., Nishikawa, H., Sedukhina, A. S., Wada, H., Ohta, T., & Venkitaraman, A. R. (2012). A DNA-Damage Selective Role for BRCA1 E3 Ligase in Claspin Ubiquitylation, CHK1 Activation, and DNA Repair. *Current Biology*, *22*(18), 1659–1666. https://doi.org/10.1016/j.cub.2012.07.034

93. Savitsky, K., Sfez, S., Tagle, D. A., Ziv, Y., Sartiel, A., Collins, F. S., Shiloh, Y., & Rotman, G. (1995). The complete sequence of the coding region of the ATM gene reveals similarity to cell cycle regulators in different species. *Human Molecular Genetics*, *4*(11), 2025–2032. https://doi.org/10.1093/hmg/4.11.2025

94. Scharer, O. D. (2013). Nucleotide Excision Repair in Eukaryotes. *Cold Spring Harbor Perspectives in Biology*, *5*(10), a012609–a012609. https://doi.org/10.1101/cshperspect.a012609

95. Schwertman, P., Bekker-Jensen, S., & Mailand, N. (2016). Regulation of DNA double-strand break repair by ubiquitin and ubiquitin-like modifiers. *Nature Reviews Molecular Cell Biology*, *17*(6), 379–394. https://doi.org/10.1038/nrm.2016.58

96. Shibutani, S., Takeshita, M., & Grollman, A. P. (1991). Insertion of specific bases during DNA synthesis past the oxidation-damaged base 8-oxodG. *Nature*, *349*(6308), 431–434. https://doi.org/10.1038/349431a0

97. Shiloh, Y. (2003). ATM and related protein kinases: Safeguarding genome integrity. *Nature Reviews Cancer*, *3*(3), 155–168. https://doi.org/10.1038/nrc1011

98. Singh, N., Basnet, H., Wiltshire, T. D., Mohammad, D. H., Thompson, J. R., Heroux, A., Botuyan, M. V., Yaffe, M. B., Couch, F. J., Rosenfeld, M. G., & Mer, G. (2012). Dual recognition of phosphoserine and phosphotyrosine in histone variant H2A.X by DNA damage response protein MCPH1. *Proceedings of the National Academy of Sciences*, *109*(36), 14381–14386. https://doi.org/10.1073/pnas.1212366109

99. Sneeden, J. L., Grossi, S. M., Tappin, I., Hurwitz, J., & Heyer, W.-D. (2013). Reconstitution of recombination-associated DNA synthesis with human proteins. *Nucleic Acids Research*, *41*(9), 4913–4925. https://doi.org/10.1093/nar/gkt192

100. So, S., Davis, A. J., & Chen, D. J. (2009). Autophosphorylation at serine 1981 stabilizes ATM at DNA damage sites. *Journal of Cell Biology*, *187*(7), 977–990. https://doi.org/10.1083/jcb.200906064

101. Sobhian, B., Shao, G., Lilli, D. R., Culhane, A. C., Moreau, L. A., Xia, B., Livingston, D. M., & Greenberg, R. A. (2007). RAP80 Targets BRCA1 to Specific Ubiquitin Structures at DNA Damage Sites. *Science*, *316*(5828), 1198–1202. https://doi.org/10.1126/science.1139516

102. Soutoglou, E., Dorn, J. F., Sengupta, K., Jasin, M., Nussenzweig, A., Ried, T., Danuser, G., & Misteli, T. (2007). Positional stability of single double-strand breaks in mammalian cells. *Nature Cell Biology*, *9*(6), 675–682. https://doi.org/10.1038/ncb1591

103. Spivak, G. (2015). Nucleotide excision repair in humans. *DNA Repair*, *36*, 13–18. https://doi.org/10.1016/j.dnarep.2015.09.003

104. Stewart, G. S., Wang, B., Bignell, C. R., Taylor, A. M. R., & Elledge, S. J. (2003). MDC1 is a mediator of the mammalian DNA damage checkpoint. *Nature*, *421*(6926), 961–966. https://doi.org/10.1038/nature01446

105. Stucki, M., Clapperton, J. A., Mohammad, D., Yaffe, M. B., Smerdon, S. J., & Jackson, S. P. (2005). MDC1 Directly Binds Phosphorylated Histone H2AX to Regulate Cellular Responses to DNA Double-Strand Breaks. *Cell*, *123*(7), 1213–1226. https://doi.org/10.1016/j.cell.2005.09.038

106. Sun, L. (2017). *Involvement of BRCT Family Proteins in DNA Damage Response*. University of Alberta.

107. Sy, S. M. H., Huen, M. S. Y., & Chen, J. (2009). PALB2 is an integral component of the BRCA complex required for homologous recombination repair. *Proceedings of the National Academy of Sciences*, *106*(17), 7155–7160. https://doi.org/10.1073/pnas.0811159106

108. Syed, A., & Tainer, J. A. (2018). The MRE11–RAD50–NBS1 Complex Conducts the Orchestration of Damage Signaling and Outcomes to Stress in

DNA Replication and Repair. *Annual Review of Biochemistry*, *87*(1), 263–294. https://doi.org/10.1146/annurev-biochem-062917-012415

109. Thorslund, T., Ripplinger, A., Hoffmann, S., Wild, T., Uckelmann, M., Villumsen, B., Narita, T., Sixma, T. K., Choudhary, C., Bekker-Jensen, S., & Mailand, N. (2015). Histone H1 couples initiation and amplification of ubiquitin signalling after DNA damage. *Nature*, *527*(7578), 389–393. https://doi.org/10.1038/nature15401

110. Tubbs, A., & Nussenzweig, A. (2017). Endogenous DNA Damage as a Source of Genomic Instability in Cancer. *Cell*, *168*(4), 644–656. https://doi.org/10.1016/j.cell.2017.01.002

111. Turner, N., Tutt, A., & Ashworth, A. (2004). Hallmarks of "BRCAness" in sporadic cancers. *Nature Reviews Cancer*, *4*(10), 814–819. https://doi.org/10.1038/nrc1457

112. Uribe, S., & Sampedro, J. G. (2003). Measuring solution viscosity and its effect on enzyme activity. *Biological Procedures Online*, *5*(1), 108–115. https://doi.org/10.1251/bpo52

113. Vagenende, V., Yap, M. G. S., & Trout, B. L. (2009). Mechanisms of Protein Stabilization and Prevention of Protein Aggregation by Glycerol. *Biochemistry*, *48*(46), 11084–11096. https://doi.org/10.1021/bi900649t

114. Valko, M., Rhodes, C. J., Moncol, J., Izakovic, M., & Mazur, M. (2006). Free radicals, metals and antioxidants in oxidative stress-induced cancer.

Chemico-Biological Interactions, *160*(1), 1–40. https://doi.org/10.1016/j.cbi.2005.12.009

115. Varma, A. K., Brown, R. S., Birrane, G., & Ladias, J. A. A. (2005). Structural Basis for Cell Cycle Checkpoint Control by the BRCA1−CtIP Complex [†, ‡]. *Biochemistry*, *44*(33), 10941–10946. https://doi.org/10.1021/bi0509651

116. Walser, F., Mulder, M. P. C., Bragantini, B., Burger, S., Gubser, T., Gatti, M., Botuyan, M. V., Villa, A., Altmeyer, M., Neri, D., Ovaa, H., Mer, G., & Penengo, L. (2020). Ubiquitin Phosphorylation at Thr12 Modulates the DNA Damage Response. *Molecular Cell*, *80*(3), 423-436.e9. https://doi.org/10.1016/j.molcel.2020.09.017

117. Wang, B., Matsuoka, S., Ballif, B. A., Zhang, D., Smogorzewska, A., Gygi, S. P., & Elledge, S. J. (2007a). Abraxas and RAP80 Form a BRCA1 Protein Complex Required for the DNA Damage Response. *Science*, *316*(5828), 1194–1198. https://doi.org/10.1126/science.1139476

118. Wang, B., Matsuoka, S., Ballif, B. A., Zhang, D., Smogorzewska, A., Gygi, S. P., & Elledge, S. J. (2007b). Abraxas and RAP80 Form a BRCA1 Protein Complex Required for the DNA Damage Response. *Science*, *316*(5828), 1194–1198. https://doi.org/10.1126/science.1139476

119. Wang, H., Shi, L. Z., Wong, C. C. L., Han, X., Hwang, P. Y.-H., Truong, L. N., Zhu, Q., Shao, Z., Chen, D. J., Berns, M. W., Yates, J. R., Chen, L., & Wu,

X. (2013). The Interaction of CtIP and Nbs1 Connects CDK and ATM to Regulate HR–Mediated Double-Strand Break Repair. *PLoS Genetics*, *9*(2), e1003277. https://doi.org/10.1371/journal.pgen.1003277

120. Ward, J. F. (1988). DNA Damage Produced by Ionizing Radiation in Mammalian Cells: Identities, Mechanisms of Formation, and Reparability. In W. E. Cohn & K. Moldave (Eds.), *Progress in Nucleic Acid Research and Molecular Biology* (Vol. 35, pp. 95–125). Academic Press. https://doi.org/10.1016/S0079-6603(08)60611-X

121. White, E. R., Sun, L., Ma, Z., Beckta, J. M., Danzig, B. A., Hacker, D. E., Huie, M., Williams, D. C., Edwards, R. A., Valerie, K., Glover, J. N. M., & Hartman, M. C. T. (2015). Peptide Library Approach to Uncover Phosphomimetic Inhibitors of the BRCA1 C-Terminal Domain. *ACS Chemical Biology*, *10*(5), 1198–1208. https://doi.org/10.1021/cb500757u

122. Williams, R. S., Green, R., & Glover, J. N. M. (2001). Crystal structure of the BRCT repeat region from the breast cancer-associated protein BRCA1. *Nature Structural Biology*, *8*(10), 838–842. https://doi.org/10.1038/nsb1001-838

123. Williams, R. S., Lee, M. S., Hau, D. D., & Glover, J. N. M. (2004). Structural basis of phosphopeptide recognition by the BRCT domain of BRCA1. *Nature Structural & Molecular Biology*, *11*(6), 519–525. https://doi.org/10.1038/nsmb776

124. Wogan, G. N., Hecht, S. S., Felton, J. S., Conney, A. H., & Loeb, L. A. (2004). Environmental and chemical carcinogenesis. *Seminars in Cancer Biology*, *14*(6), 473–486. https://doi.org/10.1016/j.semcancer.2004.06.010

125. Wright, W. D., Shah, S. S., & Heyer, W.-D. (2018). Homologous recombination and the repair of DNA double-strand breaks. *Journal of Biological Chemistry*, *293*(27), 10524–10535. https://doi.org/10.1074/jbc.TM118.000372

126. Wu, L., Luo, K., Lou, Z., & Chen, J. (2008). MDC1 regulates intra-S-phase checkpoint by targeting NBS1 to DNA double-strand breaks. *Proceedings of the National Academy of Sciences*, *105*(32), 11200–11205. https://doi.org/10.1073/pnas.0802885105

127. Wu, Q., Paul, A., Su, D., Mehmood, S., Foo, T. K., Ochi, T., Bunting, E. L., Xia, B., Robinson, C. V., Wang, B., & Blundell, T. L. (2016). Structure of BRCA1-BRCT/Abraxas Complex Reveals Phosphorylation-Dependent BRCT Dimerization at DNA Damage Sites. *Molecular Cell*, *61*(3), 434–448. https://doi.org/10.1016/j.molcel.2015.12.017

128. Xia, Y., Pao, G. M., Chen, H.-W., Verma, I. M., & Hunter, T. (2003). Enhancement of BRCA1 E3 Ubiquitin Ligase Activity through Direct Interaction with the BARD1 Protein. *Journal of Biological Chemistry*, *278*(7), 5255–5263. https://doi.org/10.1074/jbc.M204591200

129. Xiao, A., Li, H., Shechter, D., Ahn, S. H., Fabrizio, L. A., Erdjument-Bromage, H., Ishibe-Murakami, S., Wang, B., Tempst, P., Hofmann, K., Patel, D. J., Elledge, S. J., & Allis, C. D. (2009). WSTF regulates the H2A.X DNA damage response via a novel tyrosine kinase activity. *Nature*, *457*(7225), 57–62. https://doi.org/10.1038/nature07668

130. Yu, X. (2003). The BRCT Domain Is a Phospho-Protein Binding Domain. *Science*, *302*(5645), 639–642. https://doi.org/10.1126/science.1088753

131. Yu, X., Wu, L. C., Bowcock, A. M., Aronheim, A., & Baer, R. (1998a). The C-terminal (BRCT) Domains of BRCA1 Interact in Vivo with CtIP, a Protein Implicated in the CtBP Pathway of Transcriptional Repression. *Journal of Biological Chemistry*, *273*(39), 25388–25392. https://doi.org/10.1074/jbc.273.39.25388

132. Yu, X., Wu, L. C., Bowcock, A. M., Aronheim, A., & Baer, R. (1998b). The C-terminal (BRCT) Domains of BRCA1 Interact in Vivo with CtIP, a Protein Implicated in the CtBP Pathway of Transcriptional Repression. *Journal of Biological Chemistry*, *273*(39), 25388–25392. https://doi.org/10.1074/jbc.273.39.25388

133. Zelensky, A., Kanaar, R., & Wyman, C. (2014). Mediators of Homologous DNA Pairing. *Cold Spring Harbor Perspectives in Biology*, *6*(12), a016451–a016451. https://doi.org/10.1101/cshperspect.a016451

134. Zeng, X., Herndon, A. M., & Hu, J. C. (1997). Buried asparagines determine the dimerization specificities of leucine zipper mutants. *Proceedings of the National Academy of Sciences*, *94*(8), 3673–3678. https://doi.org/10.1073/pnas.94.8.3673

135. Zhang, F., Ma, J., Wu, J., Ye, L., Cai, H., Xia, B., & Yu, X. (2009). PALB2 Links BRCA1 and BRCA2 in the DNA-Damage Response. *Current Biology*, *19*(6), 524–529. https://doi.org/10.1016/j.cub.2009.02.018

136. Zhao, W., Steinfeld, J. B., Liang, F., Chen, X., Maranon, D. G., Jian Ma, C., Kwon, Y., Rao, T., Wang, W., Sheng, C., Song, X., Deng, Y., Jimenez-Sainz, J., Lu, L., Jensen, R. B., Xiong, Y., Kupfer, G. M., Wiese, C., Greene, E. C., & Sung, P. (2017). BRCA1–BARD1 promotes RAD51-mediated homologous DNA pairing. *Nature*, *550*(7676), 360–365. https://doi.org/10.1038/nature24060

137. Zhao, W., Wiese, C., Kwon, Y., Hromas, R., & Sung, P. (2019). The BRCA Tumor Suppressor Network in Chromosome Damage Repair by Homologous Recombination. *Annual Review of Biochemistry*, *88*(1), 221–245. https://doi.org/10.1146/annurev-biochem-013118-111058

138. Zhou, B.-B. S., & Elledge, S. J. (2000). The DNA damage response: Putting checkpoints in perspective. *Nature*, *408*(6811), 433–439. https://doi.org/10.1038/35044005